https://doi.org/10.15388/vu.thesis.963
https://orcid.org/0000-0002-4599-7444

VILNIUS UNIVERSITY
CENTER FOR PHYSICAL SCIENCES AND TECHNOLOGY

Agnė Minderytė

Integrated Assessment of Long-Range Air Mass Transport Effects on Source-Apportioned Aerosol Black Carbon and Aerosol Properties in Contrasting Environments

DOCTORAL DISSERTATION

Natural Sciences,
Physics (N 002)

VILNIUS 2026

The dissertation was prepared between 2022 and 2026 at the Center for Physical Sciences and Technology. The research was supported by the Research Council of Lithuania, with scholarships granted for academic accomplishments in 2023 and 2024, financial support for participation in the European Aerosol Conference in Tampere (Finland) in 2024, and a research visit to the University of Warsaw (Poland) in 2025.

Academic Supervisor – Dr. Steigvilė Byčenkienė (Center for Physical Sciences and Technology, Natural sciences, Physics – N 002).

This doctoral dissertation will be defended in a public meeting of the Dissertation Defence Panel:

Chairman – Dr. Artūras Plukis (Center for Physical Sciences and Technology, Natural Sciences, Physics – N 002).
Members:
Prof. Dr. Edita Baltrėnaitė-Gedienė (Vilnius Gediminas Technical University, Technological Sciences, Environmental Engineering – T 004),

Prof. Dr. Raimondas Grubliauskas (Vilnius Gediminas Technical University, Technological Sciences, Environmental Engineering – T 004),

Prof. Dr. Tareq Hussein (University of Helsinki / University of Jordan, Natural Sciences, Physics – N 002),

Dr. Evaldas Maceika (Center for Physical Sciences and Technology, Natural Sciences, Physics – N 002).

The dissertation will be defended at a public meeting of the Dissertation Defence Panel at 2 p.m. on September 14, 2026, in meeting room D401 of the Center for Physical Sciences and Technology.

Address: Saulėtekio av. 3, room D401, Vilnius, Lithuania.
Tel. +370 645 15550; e-mail: office@ftmc.lt

https://doi.org/10.15388/vu.thesis.963
https://orcid.org/0000-0002-4599-7444

VILNIAUS UNIVERSITETAS
FIZINIŲ IR TECHNOLOGIJOS MOKSLŲ CENTRAS

Agnė Minderytė

Kompleksinis tolimosios oro masių pernašos poveikio skirtingos kilmės aerozolio juodajai angliai ir aerozolio savybėms vertinimas kontrastingose aplinkose

DAKTARO DISERTACIJA

Gamtos mokslai,
Fizika (N 002)

VILNIUS 2026

Disertacija rengta 2022–2026 metais Fizinių ir technologijos mokslų centre. Mokslinius tyrimus rėmė Lietuvos mokslo taryba: skirtos stipendijos už akademinius pasiekimus 2023 ir 2024 m., finansinė parama dalyvavimui Europos aerozolio konferencijoje Tamperėje (Suomijoje) 2024 m. ir stažuotei Varšuvos universitete (Lenkija) 2025 m.

Mokslinė vadovė – dr. Steigvilė Byčenkienė (Fizinių ir technologijos mokslų centras, gamtos mokslai, fizika – N 002).

Gynimo taryba:
Pirmininkas – dr. Artūras Plukis (Fizinių ir technologijos mokslų centras, gamtos mokslai, fizika – N 002).
Nariai:
prof. dr. Edita Baltrėnaitė-Gedienė (Vilniaus Gedimino technikos universitetas, technologijos mokslai, aplinkos inžinerija – T 004),

prof. dr. Raimondas Grubliauskas (Vilniaus Gedimino technikos universitetas, technologijos mokslai, aplinkos inžinerija – T 004),

prof. dr. Tareq Hussein (Helsinkio universitetas / Jordanijos universitetas, gamtos mokslai, fizika – N 002),

dr. Evaldas Maceika (Fizinių ir technologijos mokslų centras, gamtos mokslai, fizika – N 002).

Disertacija ginama viešame Gynimo tarybos posėdyje 2026 m. rugsėjo mėn. 14 d. 14 val. Fizinių ir technologijos mokslų centro D401 posėdžių salėje.

Adresas: Saulėtekio al. 3, D401, Vilnius, Lietuva.
Tel. +370 645 15550; el. paštas office@ftmc.lt.

CONTENTS

ABBREVIATIONS

AAE – Absorption Ångström Exponent

AAE_{BB} – Absorption Ångström Exponent for Biomass Burning

$AAE_{BB,C}$ – Absorption Ångström Exponent for Biomass and Coal Burning

AAE_{FF} – Absorption Ångström Exponent for Fossil Fuel combustion)

ACSM – Aerosol Chemical Speciation Monitor

ACTRIS – Aerosols, Clouds, and Trace gases Research InfraStructure

BBOA – Biomass Burning Organic Aerosol

BC – Black Carbon

BrC – Brown Carbon

CCN – Cloud Condensation Nuclei

DOM – Domestic Heating sector

eBC – equivalent Black Carbon

eBC_{BB} – Black Carbon originating from Biomass Burning

$eBC_{BB,C}$ – Black Carbon originating from Biomass and Coal Burning

eBC_{FF} – Black Carbon originating from Fossil Fuel combustion

EC – Elemental Carbon

ENE – Energy production sector

FLA – Flaring sector

FLEXPART – FLEXible PARTicle dispersion model

HYSPLIT – Hybrid Single Particle Lagrangian Integrated Trajectory model

ICOS – Integrated Carbon Observation System

IND – Industrial combustion sector

IPCC – Intergovernmental Panel on Climate Change

IR – Infrared (wavelength range)

LDSA – Lung-Deposited Surface Area

MAC – Mass Absorption Cross-section

NOx – Nitrogen Oxides

OA – Organic Aerosol

OOA – Oxidised Organic Aerosol

OC – Organic Carbon

PAHs – Polycyclic Aromatic Hydrocarbons

PMF – Positive Matrix Factorisation

PM – Particulate Matter

PM_1 – Particulate Matter with an aerodynamic diameter of 1 μm or less

$PM_{2.5}$ – Particulate Matter with an aerodynamic diameter of 2.5 μm or less

PM_{10} – Particulate Matter with an aerodynamic diameter of 10 μm or less

POA – Primary Organic Aerosol

RH – Relative Humidity

SAE – Scattering Ångström Exponent

SECA – Sulphur Emissions Control Area

SHP – Shipping sector

SIA – Secondary Inorganic Aerosol

SLCFs – Short-Lived Climate Forcers

SOA – Secondary Organic Aerosol

SSA – Single Scattering Albedo

TRA – Transport sector

UFP – Ultrafine Particles with an aerodynamic diameter of 100 nm or less

UV – Ultraviolet (wavelength range)

VOCs – Volatile Organic Compounds

WHO – World Health Organization

WS – Wind speed

WST – Waste treatment and disposal sector

INTRODUCTION

Relevance of the work

Long-range air mass transport is a significant and well-recognised factor influencing air quality (Atabakhsh et al., 2025; Pappin et al., 2024; Q. Zhang et al., 2017). Air pollutants, once released into the atmosphere, can remain suspended for days to weeks and travel thousands of kilometres from their emission sources (Schneider et al., 2025). Aerosol particles emitted in one region may therefore affect air quality in distant areas, thus research consistently identifies long-range transport as a key driver of atmospheric pollution at continental scales (Yang et al., 2022). The transboundary nature of aerosol pollution also carries direct public health consequences: 3.45 million $PM_{2.5}$-related premature deaths globally have been linked to pollutants transported from distant regions (Q. Zhang et al., 2017), emphasising the importance of understanding long-range transport pathways for both local and regional air quality assessment.

The pollutants most critically shaped by long-range transport are aerosol particles. Their chemical composition and size determine whether they scatter or absorb solar radiation, directly influencing Earth's energy budget, their ability to act as cloud condensation nuclei, modifying cloud properties and the atmospheric water cycle. The IPCC (Intergovernmental Panel on Climate Change) reported in 2013 and later confirmed in 2023 that aerosols exhibit the largest uncertainty in current estimates of Earth's radiative balance (IPCC, 2023), making their accurate characterisation – including the separation of local and transported contributions – a priority for atmospheric and climate research.

Due to rapid urbanisation and economic growth, the majority of aerosol emission sources are concentrated in urban areas. Urban aerosols constitute a complex, dynamic mixture resulting from diverse sources and processes, among which black carbon (BC) is particularly significant. BC is predominantly found in the submicron size range and originates from the incomplete combustion of fossil fuels and biomass (Bond et al., 2013; Savadkoohi et al., 2023). Fossil fuel combustion accounts for the largest share of urban BC emissions, though residential wood burning can become a substantial contributor during the cold season. BC is of particular interest because it is one of the most efficient light-absorbing aerosol species, playing a key role in aerosol-radiation interactions and the broader issue of how urban emissions influence their climate effects across regional scales through long-range transport.

Despite considerable advances in aerosol research, significant uncertainties persist regarding the sources, transformation processes, and transport dynamics of BC, as well as its interactions with other aerosol components. These challenges are especially pronounced when contrasting environments – such as urban and regional background sites – are examined together. Distinguishing between locally emitted and transported aerosols is essential for accurate source attribution, yet remains difficult due to the complex interactions among emission sources and atmospheric processes. Integrated multi-site observational and modelling approaches are therefore needed to advance this understanding.

Although recent studies have examined long-range air mass transport in Lithuania (Kalinauskaitė et al., 2024; Mašalaitė et al., 2024), a comprehensive, integrated assessment of its effects across contrasting environments remains lacking in Central and Northern Europe (Schneider et al., 2025). Quantifying BC at the city level provides a practical means to evaluate how individual urban areas contribute to regional pollution. Characterising submicron aerosol dynamics at regional background sites, in turn, provides observational constraints relevant to climate modelling. This doctoral dissertation addresses these gaps through an integrated approach combining in-situ measurements, source apportionment and atmospheric modelling across environments of contrasting emission characteristics.

Scientific novelty

The novelty lies in the location-specific assessment of the effects of long-range air mass transport on black carbon and PM_1 in urban (Vilnius, Warsaw) and regional background (Preila, Hyltemossa) environments. By combining measured and modelled data, a novel approach is used to separate measured eBC into local and transported components in an urban environment.

The aim of the work

This work aims to investigate the influence of long-range air mass transport on submicron aerosol, with particular emphasis on black carbon concentrations and source contributions in urban environments of Central and North Europe, and on aerosol chemical composition in regional background environments of the southern Baltic Sea region.

Tasks of the work

1. To quantify black carbon mass concentrations in urban environments and to comprehensively characterise their temporal variability across multiple time scales (diurnal, weekly, and seasonal), taking into account the influence of meteorological conditions and emission patterns.
2. To perform source apportionment of black carbon using multi-wavelength optical measurements and to characterise aerosol optical properties, with the aim of interpreting their relationships with aerosol chemical composition, emission sources, and atmospheric processes in the urban environment.
3. To simulate black carbon transport and quantify source contributions using dispersion modelling, and to partition measured black carbon into locally produced and long-range transported components (urban vs. regional background).
4. To analyse the impact of long-range air mass transport on submicron aerosol chemical composition and mass concentrations in regional background environments

Statements to be defended

1. Long-range air mass transport significantly influences black carbon mass concentrations in urban environments, contributing to both pollution enhancement and dilution events, with a stronger impact of air mass transported black carbon during the cold season (on average 46 % in Vilnius and 53 % in Warsaw).

2. A clear seasonal transition in black carbon sources is evident across urban environments in Vilnius and Warsaw, irrespective of concentration levels, with fossil fuel combustion dominating during the warm season (on average 84–86 %) and biomass and coal burning contributing a substantially larger share during the cold season (on average 29–37 %).

3. Seasonal variability in black carbon mass concentrations in urban environments is controlled by a shift in dominant emission sectors, with domestic heating driving increases during the cold season and transport emissions governing variability during the warm season.

4. Aerosol optical properties are highly sensitive to emission sources, with cold season conditions dominated by larger particle mixtures and light-absorbing particles associated with fossil fuel combustion.

5. In regional background environments, the effect of long-range air mass transport on PM_1 is pathway-dependent, with transport over the Baltic Sea causing substantial aerosol removal (-3 %/h) and continental transport leading to aerosol enhancement due to pollution uptake (4 %/h).

Author's contribution

The author conducted data pre-processing, black carbon source apportionment, calculation of aerosol optical properties, and co-developed an application for trajectory threshold-based categorisation and connected-flow event classification using HYSPLIT backward trajectories. The author prepared figures, wrote and revised manuscripts for scientific publications, and presented the findings at national and international conferences.

List of publications

On the dissertation topic

1. **A. Minderytė**, E. A. Ugboma, F. F. Mirza Montoro, I. S. Stachlewska, S. Byčenkienė; Impact of long-range transport on black carbon source contribution and optical aerosol properties in two urban environments; Heliyon; 9, 9, 2023; p. e19652; doi: 10.1016/j.heliyon.2023.e19652.
2. F. M. Hey, **A. Minderytė**, E. A. Ugboma, N. Evangeliou, S. Eckhardt, I. Pisso, S. Byčenkienė, I. S. Stachlewska; City-produced and transported black carbon: Synergy of in-situ optical measurements and modeling; Atmospheric Research; 334, April 2026; 108731; doi: 10.1016/j.atmosres.2025.108731.
3. **A. Minderytė**, J. Pauraite, E. Ahlberg, A. Kristensson, S. Byčenkienė, A. C. Eriksson; Long-Range Transport Influence on Wintertime Submicron Aerosol Chemical Composition from Simultaneous Measurements in Lithuania and Southern Sweden; Atmospheric Environment; 350, March, 2025; 121162; doi: 10.1016/j.atmosenv.2025.121162.

Not included in the dissertation

1. A. Mašalaitė, I. Garbarienė, A. Garbaras, J. Šapolaitė, Ž. Ežerinskis, L. Bučinskas, V. Dudoitis, A. Kalinauskaitė, D. Pashneva, **A. Minderytė**, V. Remeikis, S. Byčenkienė; Dual-isotope ratios of carbonaceous aerosols for seasonal observation and their assessment as source indicators; Science of Total Environment; Vol. 949, 2024; p. 175094; doi: 10.1016/j.scitotenv.2024.175094.
2. D. Pashneva, **A. Minderytė**, L. Davulienė, V. Dudoitis, S. Byčenkienė; Understanding the Dynamics of Source-Apportioned Black Carbon in an Urban Background Environment; Atmosphere; Vol. 15, 2024; p. 0832; doi: 10.3390/atmos15070832.
3. A. Kalinauskaitė, L. Davulienė, J. Pauraite, **A. Minderytė**, S. Byčenkienė; New Year Fireworks Influence on Air Quality in Case of Stagnant Foggy Conditions; Urban Science; 8, 2, 2024; p. 54; doi: 10.3390/urbansci8020054.
4. D. Pashneva, **A. Minderytė**, L. Davulienė, V. Dudoitis, S. Byčenkienė; Variations of black carbon, particulate matter and nitrogen oxides mass concentrations in urban environment with respect to winter heating period and meteorological conditions; Lithuanian Journal of Physics, 64, 3, 2024; p. 189-202; doi: 10.3952/physics.2024.64.3.4.
5. S. Kecorius, L. Madueño, S. Sues, J. Cyrys, M. Lovrić, M. Pöhlker, K. Plauškaitė, L. Davulienė, **A. Minderytė**, S. Byčenkienė; Development of a cost-effective adsorption dryer for high-quality aerosol sampling; Aerosol and Air Quality Research, 24, 3, 2024; p. 230057; doi: 10.4209/aaqr.230057.
6. L. Davulienė, L. Janicka, **A. Minderytė**, A. Kalinauskaitė, P. Poczta, M. Karasewicz, A. Hafiz, D. Pashneva, V. Dudoitis, K. Kandrotaitė, D. Valiulis, C. Böckmann, D. Schüttemeyer, I. S. Stachlewska, S. Byčenkienė; Synergic use of in-situ and remote sensing techniques for comprehensive characterization of aerosol optical and microphysical properties; Science of Total Environment; 906, 2023; p. 167585; doi: 10.1016/j.scitotenv.2023.167585.
7. A. Khan, L. Davulienė, S. Šemčuk, K. Kandrotaitė, **A. Minderytė**, M. Davtalab, I. Uogintė, M. Skapas, V. Dudoitis, S. Byčenkienė; Integrated personal exposure and deposition of black carbon on human lungs; Air Quality, Atmosphere & Health; 17, 2023; p. 35–50; doi: 10.1007/s11869-023-01428-8.

List of conferences

Oral presentations

1. **A. Minderytė**, F. M. Hey, E. A. Ugboma, N. Evangeliou, S. Eckhardt, I. Pisso, S. Byčenkienė ir I.S. Stachlewska. “Local vs. transported black carbon pollution in Vilnius and Warsaw”. Open Readings (2026). Vilnius, Lithuania.
2. **A. Minderytė**, F. M. Hey, E. A. Ugboma, N. Evangeliou, S. Eckhardt, I. Pisso, S. Byčenkienė ir I.S. Stachlewska. “City-produced and transported black carbon: synergy of in-situ optical measurements and modeling”. FizTeCh (2025). Vilnius, Lithuania.
3. **A. Minderytė**, S. Byčenkienė. “Short-term impacts of fireworks and bonfires on urban aerosol characteristics“. EcoBalt 2025. Vilnius, Lithuania.
4. **A. Minderytė**, S. Byčenkienė. “Festive Flares: How Bonfires and Fireworks Shape Urban Aerosol Optical Properties”. Open Readings (2025). Vilnius, Lithuania.
5. **A. Minderytė**, S. Byčenkienė. “Temporal impacts of bonfire and firework events on urban aerosol radiative properties“. 4th International Student Conference – DISC2024 (2024). Virtual conference.
6. **A. Minderytė**, A. Eriksson, E. Ahlberg, S. Byčenkienė, A. Kristensson, J. Pauraite. “The role of the sea transport for submicron aerosol chemical composition“. FizTeCh (2024). Vilnius, Lithuania.
7. **A. Minderytė**, S. Byčenkienė, E. A. Ugboma, I. S. Stachlewska. “Impact of long-range transported biomass burning-related black carbon in two urban environments“. CYSENI (2024). Kaunas, Lithuania.

Poster presentations

1. **A. Minderytė**, J. Pauraite, E. Ahlberg, A. Kristensson, S. Byčenkienė, A. C. Eriksson. “Long-range transport influence on submicron aerosol chemical composition from simultaneous measurements in Lithuania and Southern Sweden“. (Early Career Researchers) ECR online conference (2025). Virtual.
2. **A. Minderytė**, J. Pauraite, E. Ahlberg, A. Kristensson, S. Byčenkienė, A. C. Eriksson. “Influence of long-range transport over the sea on submicron aerosol chemical composition”. European Aerosol Conference (2025). Lecce, Italy. **Received the Best Poster Award.**

3. **A. Minderytė**, F. M. Hey, N. Evangeliou, S. Byčenkienė, I. S. Stachlewska. “Black carbon source apportionment and long-range transport effects in urban areas across warm and cold seasons”. European Aerosol Conference (2025). Lecce, Italy.
4. **A. Minderytė**, A. Eriksson, E. Ahlberg, S. Byčenkienė, A. Kristensson, J. Pauraite. “The role of the sea for aerosol chemical composition: Simultaneous aerosol chemical composition observations at Preila and Hyltemossa during the cold season”. European Aerosol Conference (2024). Tampere, Finland.
5. **A. Minderytė**, A. Eriksson, E. Ahlberg, S. Byčenkienė, A. Kristensson, J. Pauraite. “Physicochemical PM_1 characterization for connected-flow events between Hyltemossa and Preila during winter of 2017-2018”. ACTRIS Science Conference (2024). Renne, France.
6. **A. Minderytė**, A. Eriksson, E. Ahlberg, S. Byčenkienė, A. Kristensson, J. Pauraite. “PM_1 characterization for connected-flow events over the Baltic Sea between Hyltemossa and Preila”. Open Readings (2024). Vilnius, Lithuania.
7. **A. Minderytė**, E. A. Ugboma, F. Mirza Montoro, I. S. Stachlewska, S. Byčenkienė. “Apšviečiant aerozolio daleles miesto aplinkoje: juodosios anglies šaltinių kilmės atskyrimas ir optinis aerozolio dalelių klasifikavimas Vilniuje ir Varšuvoje šiltuoju sezonu 2022”. Lithuanian National Physics Conference (2023). Vilnius, Lithuania.
8. **A. Minderytė**, E. A. Ugboma, F. Mirza Montoro, I. S. Stachlewska, S. Byčenkienė. “Aerosol optical properties and black carbon source apportionment in Vilnius and Warsaw during the warm season of 2022”. FizTeCh (2023) Vilnius, Lithuania.
9. **A. Minderytė**, F. Mirza Montoro, I. S. Stachlewska, S. Byčenkienė. “In situ measured aerosol optical properties in two neighbouring capitals - Vilnius and Warsaw during the warm season of 2022”. European Aerosol Conference (2023). Malaga, Spain.
10. **A. Minderytė**, K. Kandrotaitė, A. Kalinauskaitė, L. Davulienė, L. Janicka, V. Dudoitis, I. S. Stachlewska, S. Byčenkienė. “A case study of extensive biomass burning related black carbon emissions during Midsummer Eve in Vilnius, Lithuania”. Open Readings (2023). Vilnius, Lithuania.
11. **A. Minderytė**, K. Kandrotaitė, A. Kalinauskaitė, L. Davulienė, L. Janicka, V. Dudoitis, I. S. Stachlewska, S. Byčenkienė. “A case study of extensive biomass burning related black carbon emissions during Midsummer Eve in Vilnius, Lithuania” NOSA Symposium (2023). Oslo, Norway.

12. **A. Minderytė**, V. Dudoitis, I. Stachlewska, S. Byčenkienė. “Aerozolio juodosios anglies šaltinių kilmės nustatymas ir aerozolio dalelių optinės savybės 2021-2022 m.”. FizTeCh (2022). Vilnius, Lithuania.

Professional development

1. Secondment at the University of Warsaw, Warsaw, Poland. The effect of extensive biomass burning events in urban environments of Vilnius and Warsaw. 12 – 26 April, 2026. Funded by the Lithuanian Research Council.
2. Secondment at the University of Warsaw, Warsaw, Poland. The quantification of the city-produced and long-range transported black carbon in urban environments of Vilnius and Warsaw. 7 April – 20 June, 2025. Funded by the Erasmus+ programme.
3. International 7th Baltic Earth Winter School for Young Scientists on ‘Earth System Science for the Baltic Sea Region’. Klaipėda, Lithuania. 24 – 28 March 2025.
4. EMME-CARE Autumn School 2023: Atmospheric Measurements Using Miniaturised Sensors and Drones. Nicosia, Cyprus. 30 October – 3 November, 2023.
5. HAAR Summer School: Theory and practice of aerosol chemistry and engineering for climate, air quality, emissions, and health effects. Navarino Environmental Observatory, Greece. 8 – 15 June, 2023.
6. Secondment at Lund University, Lund, Sweden. Investigation of the long-range transport influence on wintertime submicron aerosol chemical composition across Hyltemossa and Preila. 1 March – 31 May, 2023. Funded by the Erasmus+ programme.

1 LITERATURE REVIEW

1.1 Fundamentals of atmospheric aerosol particles

Atmospheric aerosol particles are a complex system consisting of solid or liquid particles suspended in the air. Their importance derives from well-established impacts on human health and a critical role in climate processes. In contrast to gaseous pollutants, aerosols are inherently more complex due to their chemically heterogeneous composition and wide particle-size distribution. Aerosol properties are controlled by environmental conditions, including location, emission intensity, meteorology, and temporal variability (Seinfeld & Pandis, 2006). Among these characteristics, particle size and chemical composition govern aerosol behaviour in the atmosphere and directly reflect their sources of emission. Aerosol particles originate from both natural and anthropogenic sources. Natural sources include sea salt, soil dust, volcanic ash, biogenic aerosols from trees, and soot from biomass burning, whereas anthropogenic sources include transport, energy production, industry, and construction (Putaud et al., 2004; Seinfeld & Pandis, 2006).

Based on their formation mechanisms, aerosol particles are classified as primary or secondary. Primary particles are emitted directly into the atmosphere without undergoing any chemical transformation (Klimont et al., 2017). These include sea salt, volcanic ash, soil dust, and primary organic aerosol emitted by fossil fuel combustion, biomass burning and biological emissions. In contrast, secondary aerosols form when gaseous precursors undergo chemical transformation into low-volatility species, which subsequently partition into the particle phase. Secondary organic aerosols (SOA) form by photooxidation of anthropogenic and natural compounds, oxidation of volatile organic compounds (VOCs), or formation of lower-volatility compounds that subsequently condense onto pre-existing particles (Hu et al., 2019). Secondary inorganic aerosols (SIA) are mainly formed during the oxidation of gaseous SO_2, nitrogen oxides (NOx) and NH_3 (A. U. Lewandowska & Falkowska, 2013a; Sandrini et al., 2016). These precursors undergo reactions that produce particles containing sulphate, nitrate, and ammonium, which either nucleate new particles in the atmosphere or condense onto existing particles, thereby increasing their size.

Overall, the combination of diverse emission sources and continuous physical and chemical transformations in the atmosphere results in a highly dynamic aerosol population whose properties continually change with shifting meteorological conditions and long-range transport (Seinfeld & Pandis, 2006).

1.1.1 Chemical composition of aerosol particles

The chemical composition of aerosol particles varies widely depending on available sources and meteorological conditions, which regulate secondary aerosol formation and ageing (relative humidity, temperature, and available sunlight). Generally, aerosol particle components can be divided into inorganic and organic components, also called carbonaceous components. Carbonaceous aerosols is a broad term for aerosol components containing carbon atoms: black carbon, which is almost pure carbon, and organic aerosol (OA), which may also contain hydrogen and oxygen atoms. OA can be both a primary (POA) or secondary origin (SOA) (Chowdhury et al., 2022; Weagle et al., 2018). OA is a complex collection of light-absorbing organic molecules which can be water-soluble. It can also absorb light efficiently in the ultraviolet and visible wavelengths (Rovira et al., 2025). Exhaust-emitted carbonaceous aerosols, such as BC and POA, are more abundant in close proximity to sources and in urban environments. In contrast, in pristine and natural environments, carbonaceous aerosols are mostly SOA formed from biogenic VOCs (Weagle et al., 2018). Primary carbonaceous aerosols can account for a smaller fraction of PM_1 in background conditions; however, they can represent 60-90 % of the mass in areas heavily affected by traffic or wood burning (Ahlberg et al., 2023; Minderytė et al., 2022; Pauraite et al., 2018; Pirjola et al., 2017). Remote and background locations exhibit a larger fraction of secondary, aged OA (Ahlberg et al., 2023; Schneider et al., 2025).

Inorganic aerosol components such as sulphate, nitrate and ammonium are secondary components in fine PM mass concentration. Sulphate aerosols are formed in the atmosphere by gas-and aqueous-phase oxidation of precursor sulphur gases (SO_2, dimethyl sulphide) emitted from anthropogenic (marine transport, coal-fired power plants) or natural sources (volcanic eruptions) (IPCC, 2023). The major source of reactive nitrogen oxide (NOx) in the atmosphere is emissions from fossil fuel combustion. Nitrate production is favoured by high relative humidity, low temperatures, and elevated levels of fine particles (Sandrini et al., 2016). The main source of ammonia emissions (NH_3) is agriculture and livestock activities. It can be estimated that 98 % of NH_4^+ in $PM_{2.5}$ comes from these sources (Scotto et al., 2021). The emitted NH_3 reacts with nitric acid (HNO_3) and sulphuric acid (H_2SO_4) to form the main secondary inorganic aerosol components: ammonium sulphate ($(NH_4)_2SO_4$) and ammonium nitrate (NH_4NO_3) (A. U. Lewandowska & Falkowska, 2013a; Shrivastava et al., 2017).

Chloride in aerosol particles mainly originates from sea-salt aerosols and is more abundant in marine locations (A. U. Lewandowska & Falkowska,

2013b). Heavy metals are trace components in aerosol particles, with higher mass fractions in areas with industrial activities, such as mining, transport, coal combustion, and iron and steel production (Matei et al., 2025).

Altogether, aerosol chemical composition is a dynamic characteristic that reflects sources and the continuous physical and chemical transformations that occur within the atmosphere, as particles are influenced by co-existing gaseous and particulate species and meteorological conditions.

1.1.2 Physical properties of aerosol particles

While chemical composition reflects the origin and transformation of aerosol particles, their physical properties determine their atmospheric behaviour and impacts. Aerosol particles are rarely uniform in size. Unlike an idealised monodisperse particle population, atmospheric aerosol particles are polydisperse. Their size can range by a factor of 1000 from nanometres to micrometres (Seinfeld & Pandis, 2006). The size of a particle is determined by its formation processes and by the physical and chemical processes it undergoes during atmospheric transport and ageing. Through condensation, evaporation, coagulation, and chemical reactions, the size, number, and composition of ambient aerosol particles constantly change in the atmosphere (Seinfeld & Pandis, 2006; Winkler, 1988). Particle size plays a critical role in determining the transport and deposition behaviour of ambient aerosols. Accordingly, undesirable effects, including respiratory health hazards, visibility reduction, surface deposition, and other effects on regional and global climate, are closely linked to particle size (Birmili et al., 2010; Cappa et al., 2016). Therefore, measuring and characterising atmospheric particle size distributions is essential to understand the origins and effects of aerosol particles.

Particle size distributions can be presented as number, mass, or volume distributions. The volumetric particle size distribution, also known as the Whitby model, reveals three distinct modes: nuclei, accumulation, and coarse, each corresponding to a different formation process and yielding distinct particle properties. The volumetric size distribution provides the fundamental basis for understanding the properties of ambient aerosols. According to Whitby, particles in the nucleation mode range from 0.005 to 0.1 μm, in the accumulation mode from 0.1 to 2 μm, and in the coarse mode are larger than 2 μm in diameter (Jacobson, 2005). The three modes can also be divided into two fractions: fine (diameters < 2 μm) and coarse (diameters > 2 μm). These two fractions differ substantially in their origins and physical and chemical properties. The fine fraction mainly comes from the combustion process,

while the particles in the coarse fraction are generated mechanically. Within the fine fraction, the nuclei mode comprises transient particles formed by coagulation and condensation that rapidly grow and transition to the accumulation mode. In contrast, particles in the coarse fraction most often consist of sea spray, windblown mineral dust, volcanic ash, biological debris, or mechanically made materials such as tyre and brake wear (Manousakas et al., 2017).

Depending on particle size and chemical composition, a particle's ability to absorb or scatter solar radiation varies. Light-scattering properties are common for inorganic species such as nitrate, ammonium, sulphate, and sea salt (Cappa et al., 2016). While the light-absorbing species include mineral dust, BC, which has strong light absorption over a broad spectral range (Bond et al., 2013), and BrC, which has a strong wavelength-dependent light absorption coefficient and therefore strongly absorbs light in the short-wavelength range (Feng et al., 2013; Romano et al., 2019). Therefore, understanding the optical properties can help to identify dominant chemical mixtures by serving as proxies for both the physical size and chemical composition of aerosol particles (Cappa et al., 2016). The two commonly used in-situ instruments for measuring aerosol optical properties are nephelometers (for scattering) and aethalometers (for absorption). Specifically, the Scattering Ångström Exponent (SAE) derived from nephelometer measurements describes how particles scatter light of different wavelengths and therefore serves as a proxy for particle size. SAE values below 1.3 indicate a dominance of coarse particles, such as mineral dust or sea salt, while values above 1.3 indicate fine-mode anthropogenic particles (Cappa et al., 2016). Similarly, Absorption Ångström Exponent (AAE) describes particles' property to absorb light of different wavelengths and provides insights into the chemical composition of aerosol particles: AAE values around 1 are common for BC from fossil fuel combustion, while values around 1.6 and higher suggest BC or BrC from biomass burning or iron oxides in dust (Ealo et al., 2016; Romano et al., 2019). Therefore, the combination of the SAE and AAE allows classification of aerosols into several mixing states based on their optical properties and the extraction of additional information about their chemical composition and size. A classification scheme proposed by Cappa et al. (2016), which is a matrix of SAE plotted against AAE, has been widely employed in several European studies to identify dominant aerosol types (Cazorla et al., 2013; Ealo et al., 2016; Kaskaoutis et al., 2021a; Kaskaoutis et al., 2021b; Pauraite et al., 2022; Romano et al., 2019). Although the method is widely used, it carries its uncertainties, which can be split into classification ambiguity, measurement constraints, and site-specific generalisation. AAE–

SAE combinations do not uniquely identify aerosol type in mixed ambient populations. Generally, estimating the dominant aerosol type via optical properties works best at monitoring locations with a stable and uniform aerosol composition, especially in areas with continental pollution (carbonaceous aerosols), marine pollution (a mix of carbonaceous aerosols and sea salt), and sites affected by continental dust or biomass burning (dust and carbonaceous aerosols) (Schmeisser et al., 2017).

Another commonly used parameter describing aerosol optical properties is the single-scattering albedo (SSA). This parameter describes the ability of aerosol particles to scatter incident light and therefore their radiative effect (Pokhrel et al., 2016). The closer SSA is to 1, the more light is scattered back, while SSA closer to 0 describes particles which tend to absorb more light. In pristine environments, SSA values are close to 0.95. In contrast, in environments with more pollution sources and a high abundance of light-absorbing aerosol components, SSA values tend to be lower (Pandolfi et al., 2018; Rajesh & Ramachandran, 2018). SSA is critical for satellite retrievals; however, SSA uncertainty is among the largest sources of uncertainty in estimating aerosol environmental effects. Both SSA and AAE, which contain information on particles' absorbing characteristics, cannot be directly inferred from fuel type, as they depend strongly on burning conditions (Pokhrel et al., 2016).

The identification of dominant aerosol types and their radiative properties can help interpret remote sensing observations and provide constraints for regional and global models of aerosol flows.

1.1.3 Role of aerosol particles in climate change

Atmospheric aerosol particles significantly influence Earth's radiation budget through their radiative effects and interactions with clouds. These impacts are determined by particle chemical composition and optical properties, which control the balance between light scattering and absorption (IPCC, 2023). Due to their relatively short lifetimes (ranging from a few days to about 1 month (Seinfeld & Pandis, 2006)), aerosols are classified as short-lived climate forcers (SLCFs). As shown in Figure 1, SLCFs are influenced by both natural and anthropogenic sources and affect key environmental parameters, including temperature, hydrological cycle and weather patterns, through radiative effects and feedback processes (IPCC, 2023). Despite their importance, aerosols remain one of the largest sources of uncertainty in the estimates of total radiative forcing, as highlighted by the IPCC Sixth Assessment Report (2023). This uncertainty largely arises from their high

spatial and temporal variability in concentration, chemical composition, size, shape, vertical distribution and hygroscopic properties (Xie et al., 2025). In addition, long-range transport over intercontinental distances further modifies aerosol optical and microphysical properties through mixing and atmospheric processing, resulting in substantial variability in their radiative effects (Cappa et al., 2016; Schneider et al., 2025).

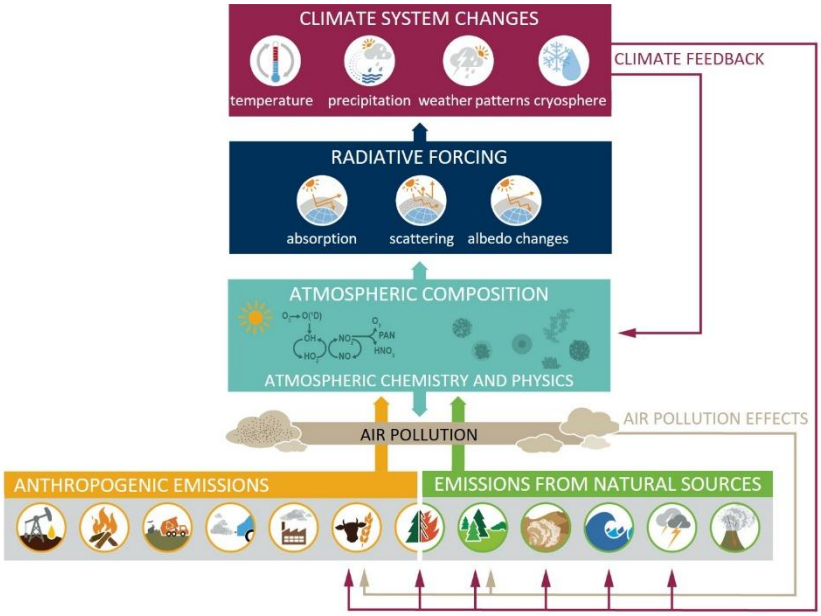

Figure 1. Sources and processes contributing to SLCFs and their effects on the climate system. (IPCC, 2023)

Aerosol radiative effects depend on their optical properties, which can be broadly categorised into light-scattering or light-absorbing. Sulphate-containing particles are strongly light-scattering. Therefore, when transported into the stratosphere, they contribute to negative effective radiative forcing by scattering light and reflecting sunlight back to space (IPCC, 2023). Similarly, NH_4^+ and NO_3^- aerosols produced via gas-to-particle phase reactions constitute a major fraction of fine-mode particles (PM_1) and affect climate through light scattering (IPCC, 2023). However, most of the global nitrate burden resides in coarse-mode particles formed by reactions of nitric acid with dust and sea salt, thus resulting in a relatively weak radiative effect (Bian et al., 2017). Meanwhile, light-absorbing aerosol components such as BC and BrC contribute to positive radiative forcing. The light-absorbing species affect radiative fluxes through direct absorption of shortwave radiation and semi-direct effects associated with changes in atmospheric temperature distribution.

In addition, absorption in the UV range can alter photochemical processes, with implications for tropospheric ozone concentrations (Jacobson, 1998).

In addition to their radiative effects, aerosols also influence the climate system through interactions with clouds. Anthropogenic emissions from combustion processes significantly increase the number of cloud condensation nuclei (CCN) on which the water vapour can condense, thus increasing the number of cloud-forming droplets (Spracklen et al., 2011). These droplets are smaller than naturally formed cloud droplets and form brighter, more reflective clouds with higher albedo. The brighter clouds reflect solar radiation, preventing it from penetrating deeper into the atmosphere and reaching the bottom of the cloud layer. This effect, called the indirect cloud albedo effect, describes the cooling of Earth's surface beneath brightly scattering clouds. Furthermore, because cloud droplets have smaller radii, they take longer to grow large enough to precipitate and be removed from the atmosphere. Thus, increasing the lifetime of the clouds and changing precipitation patterns (IPCC, 2023; Khadir et al., 2023).

1.2 Black carbon as a key climate-relevant aerosol component

1.2.1 Physicochemical properties of black carbon

BC is an aerosol component formed during the combustion of organic material. The name "black carbon" is used because the particles appear black and strongly absorb light across the ultraviolet (UV), visible, and infrared (IR) wavelength ranges (Bond et al., 2013).

BC is a general term for a variety of carbonaceous materials of hydrophobic and aromatic origin, ranging from partially charred plant residues to highly graphitised (i.e., highly ordered molecular carbon structures, as found in graphite) soot. The wide variety of carbonaceous materials forms as products of incomplete combustion, which occurs when oxygen is insufficient, and the temperature is not high enough for complete oxidation to CO_2 (Bond et al., 2013). There is no universally accepted chemical definition of BC; thus, it can be referred to as soot, graphitic carbon, or elemental carbon (EC). However, despite their chemical similarities, EC and BC are measured by different methods: EC is determined by thermogravimetric analysis, whereas BC is determined by the increase in light absorption through a filter as the amount of deposited aerosol particles increases (Long et al., 2013).

During combustion, released BC particles are nanometre-sized and immediately aggregate into larger and fractal particles of various shapes. BC

particles exist in the form of aggregates, consisting of hundreds or even thousands of monomers (Liu et al., 2018). In a study by Reddington et al. (2013), it was found that black carbon mass distribution peaks at 200 nm, whereas the numerical contribution is dominated by particles 100 nm in diameter.

During combustion, BC particles are always co-emitted with other combustion by-products, which can be gaseous or particulate matter. After emission, atmospheric processing can lead to the absorption or deposition of the by-products onto the highly absorbing surfaces of BC particles (Bond et al., 2013). The formation of coatings on BC particles can alter the morphology, light-absorbing characteristics, and chemical interactions with other species, thereby influencing their environmental fate and impacts. Moreover, BC particles can carry and internally mix with toxic contaminants, including heavy metals and polycyclic aromatic hydrocarbons (PAHs), during combustion, posing significant risks to human health (Chowdhury et al., 2022; Janssen et al., 2012). Therefore, the chemical composition and physical properties of particles containing BC are determined by the properties of burning fuel (e.g. carbon content, moisture, and density) and combustion conditions (e.g. duration and temperature) (Bond et al., 2013; Long et al., 2013).

1.2.2 Sources and source apportionment of black carbon

Although BC can form naturally (e.g., through volcanic eruptions and the open burning of forests and savannas), the dominant source of BC pollution globally is anthropogenic activities. Anthropogenic sources include mobile and stationary diesel engines and, to a lesser extent, petrol engines, fossil fuel-powered power plants and other energy sources, industrial and commercial boilers, domestic devices (i.e., fire stoves, boilers), biomass burning for heating and cooking purposes or leisure activities (Bond et al., 2013; Helin et al., 2018).

eBC (equivalent Black Carbon) mass concentration and source contributions can vary significantly depending on a region due to different climatic conditions, the nature of the activities carried out, and pollution sources (Rovira et al., 2025; Savadkoohi et al., 2023). For example, in cities and other populated areas, a seasonal increase in eBC mass concentration is observed and is associated with the heating season. In areas where domestic heating is still dominated by biomass burning, increased contribution of eBC originating from biomass burning (eBC_{BB}) is observed, whereas in areas where energy generation relies on other renewable energy sources, eBC is

dominated by contributions from fossil fuel combustion (Fourtziou et al., 2017; Helin et al., 2018; Savadkoohi et al., 2023). A distinct seasonal characteristic observed in some rural areas during spring is elevated eBC_{BB} concentrations associated with annual open field grass fires resulting from agricultural waste burning (Pauraite et al., 2021; Ulevicius et al., 2016). Although open field fires are prohibited in some regions or countries (e.g., the EU, Norway, Ukraine, China, and during the high-risk season in Australia (European Commision, 2022; Hall et al., 2021; Hyde et al., 2017; Rafaqat et al., 2025; Tu et al., 2026)), long-range transport of air masses can carry pollutants from regions with lower air quality and weaker environmental regulations. Thus, determining the origin of aerosol BC pollution in individual regions is a critical step toward understanding the main sources of pollution and developing targeted emission-reduction strategies to improve ambient air quality.

BC originating from fossil fuel combustion and biomass burning exhibits different optical characteristics. In particular, BC particles from biomass burning contain a higher amount of co-emitted particulate matter, PAHs, NOx, and carbon monoxide (CO). The co-emitted organic compounds exhibit strong UV absorption. In contrast, high combustion temperatures in vehicle engines favour the formation of NOx through reactions between atmospheric nitrogen (N_2) and oxygen (O_2), resulting in a lower CO/NOx emission ratio associated with exhaust BC aerosol particles (Sandradewi et al., 2008). As a result, the ratio of absorption coefficients at 370 nm to 880 nm for eBC_{BB} is higher than for eBC originating from fossil fuel combustion (eBC_{FF}) (Kirchstetter et al., 2004; Sandradewi et al., 2008). The distinct spectral absorption signatures of emissions from biomass and fossil-fuel combustion enable source apportionment of eBC measured by multi-wavelength photometers. Among these, the aethalometer, which measures light absorption from 370 to 950 nm, allows estimation of contributions from the two source types: fossil fuel combustion (FF) and biomass or wood burning (BB) (Sandradewi et al., 2008). In the aerosol community, this method is also known as the Aethalometer model. It does not require any auxiliary measurements, which is beneficial, as only the 7-wavelength aethalometer measurements are sufficient.

Furthermore, assessing local source contributions enables evaluation of the effectiveness of air quality improvement measures, providing insights beyond changes in total eBC mass concentration by revealing the relative effectiveness of reducing emissions from distinct source types (Minderytė et al., 2022; Savadkoohi et al., 2023). Although there are no set air quality guidelines or limits for ambient eBC concentrations, in the EU, BC emissions

are indirectly regulated and mitigated through stricter limits on exhaust particle emissions, cleaner fuels, and technologies such as fabric filters, electrostatic precipitators, and other filters (European Commision, 2022). In 2021, the World Health Organization (WHO) recommended systematic eBC measurements and the development of BC emissions inventories to implement mitigation strategies, address health and environmental concerns associated with eBC and improve understanding of urban emissions (WHO, 2021).

1.2.3 Climate and environmental impacts of black carbon

The environmental effects of BC are mainly determined by its light-absorbing properties. The strong light absorption across the entire solar spectrum plays a crucial role in the radiative balance of the Earth's system (Fu et al., 2020; Rajesh & Ramachandran, 2018). The thermal balance of the atmosphere is disrupted by particles' ability to absorb thermal energy from the Sun or from the reflected surface. The result is a warming atmosphere, while the Earth's surface receives less solar energy (IPCC, 2023). Moreover, another negative effect is observed when such light-absorbing particles deposit on planetary surfaces, thereby reducing the albedo (i.e., the fraction of incident light reflected by a surface) of light-coloured surfaces (i.e., snow and ice) (IPCC, 2023). This process enhances snow and ice melting and promotes regional atmospheric warming. Eventually, as snow and ice melt, a smaller fraction of the energy received from the Sun is reflected from their surfaces, further enhancing warming (Li et al., 2022).

The environmental and climate impacts of BC significantly rely on the mixing of BC with non-BC components and are substantially different from those of pure BC particles. While pure BC particles are inactive as CCN due to their hydrophobic surface, BC-containing particles are able to act as CCN under very low supersaturations (~0.1 %) (Kuwata et al., 2009). BC particles form coatings of soluble materials, such as sulphate and organic carbon (OC), and become more hygroscopic as the plume ages. At some point, this ageing and associated accumulation of soluble mass allows these particles to form or become part of a water droplet through a process called activation. Although the BC contribution to aerosol mass is small, it significantly influences CCN concentrations (Spracklen et al., 2011). Light absorption is further enhanced by approximately 50 % or more when BC is internally mixed with other chemical components and embedded into cloud droplets, thereby affecting the indirect climatic effect (Bond et al., 2013). When a BC-containing particle is in a water droplet, it can affect the droplet's size and albedo, while also inducing a semi-direct effect where atmospheric heating causes cloud

evaporation and determines the optical properties and lifetime of clouds (Bond et al., 2013; G. Zhang et al., 2024).

Due to their long-term persistence in the atmosphere, these particles can be transported to higher atmospheric layers and form clouds that would not form there naturally (Bond et al., 2013). Due to the variety of processes involved and their simultaneous occurrence, the total long-term impact of the interaction between BC and clouds has not yet been precisely assessed and remains uncertain (IPCC, 2023).

1.3 Variability of aerosol particles across environments

1.3.1 Urban environment

Spatial distribution and local sources are primary determinants of aerosol particle characteristics in urban areas, with particle concentrations typically decreasing along a gradient from kerbside and traffic sites to urban background environments (Kutzner et al., 2018; Pauraite et al., 2023; Savadkoohi et al., 2023). These environments are heavily influenced by local anthropogenic emissions. In urban environments, road transportation – particularly diesel engine emissions – is a major source of both BC and ultrafine particles (UFP). Another major contributor is residential combustion, where burning wood, coal, and biomass for heating and cooking releases significant amounts of carbonaceous aerosols (Kaskaoutis et al., 2021a; Kutzner et al., 2018). Furthermore, industrial activities and energy production contribute primary particles and gaseous precursors, which, alongside secondary aerosol formation, further define the local aerosol mixture (Pirjola et al., 2017; Rönkkö et al., 2023). Due to rapid urban growth, the major sources of coarse crustal particles are construction and demolition activities. The wide variety of emission sources results in an aerosol particle size distribution ranging from the finest, freshly emitted exhaust particles to coarse particles transported from distant regions or locally emitted crustal particles (Birmili et al., 2010; Hu et al., 2019; Pirjola et al., 2017). Geographical location also influences trends, as urban areas in southern Europe often exhibit higher mass concentrations than those in northern regions due to variations in regional climate patterns and emission densities (Contini et al., 2018; Savadkoohi et al., 2023; Scotto et al., 2021). Furthermore, urban air quality is not solely a product of local activity but is also frequently affected by the long-range transport of aged continental air masses (Ahlberg et al., 2023; Hu et al., 2019; Janicka et al., 2017; Yuan et al., 2024).

Meteorological factors and boundary-layer dynamics are critical drivers of the temporal variability of urban aerosols (Birmili et al., 2010; Wang et al., 2019). Cities experience pronounced seasonal variations, with significantly elevated aerosol concentrations during winter months (Jafar & Harrison, 2021; Kaskaoutis et al., 2021b; Savadkoohi et al., 2023). The observed wintertime pollution increases are also influenced by more frequent atmospheric inversions and reduced mixing layer heights, which trap pollutants near the surface, alongside higher residential heating emissions. Diurnal patterns in urban environments typically reflect these dynamics and human activity, characterised by distinct concentration peaks during morning and evening rush hours (Birmili et al., 2010; Jafar & Harrison, 2021; Kaskaoutis et al., 2021a; Minderytė et al., 2022; Savadkoohi et al., 2023).

Recent long-term observations indicate a consistent decreasing trend in anthropogenic eBC mass concentration across many urban areas in Europe and China over the past decade (Cao et al., 2021; Davulienė et al., 2019; Savadkoohi et al., 2023). These reductions are primarily linked to the effective implementation of air quality policies and emissions standards, such as the mandatory fitting of diesel particle filters and the establishment of low-emission zones in Europe. In Beijing, for example, eBC concentrations fell by 60–80 % from 2013 to 2021 due to China's Air pollution action plans, stricter coal-to-gas conversion and stricter traffic and industrial controls (Xie et al., 2025). However, while traffic-related emissions have notably declined, the relative contribution from residential and commercial combustion sources has remained fairly constant or increased slightly in some locations (Savadkoohi et al., 2023).

Aerosol particles in urban environments are a major focus of scientific and policy concern due to their profound impacts on human health and air quality, as more than 70 % of the population nowadays lives in cities and is therefore closely exposed to air pollution. Increased PM concentrations are associated with increased mortality (Chowdhury et al., 2022; Janssen et al., 2012). Fine particles ($PM_{2.5}$), especially UFP, can easily deposit in the lungs, leading to a range of negative health outcomes (e.g., reduced lung function, asthma, cardiovascular and respiratory diseases, lung cancer and stroke) (WHO, 2021). Air pollution will remain a persistent and growing threat to human health as populations continue to migrate to urban areas. A comprehensive understanding of air pollutant sources in urban environments is crucial to mitigate and control urban air quality and its associated health risks.

1.3.2 Marine environment

In marine environments, sea salt aerosols are primarily generated by the whitecaps, where bursting air bubbles emit seawater droplets into the atmosphere (O'Dowd & De Leeuw, 2007). The chemical composition of marine aerosols varies with latitude, distance from the coastline and seawater salinity (A. U. Lewandowska & Falkowska, 2013b). A significant fraction of marine aerosols formed at the sea surface consists of chlorides and sulphates, which account for nearly 99 % of their mass. In addition to natural marine emissions of dimethyl sulphide from seawater, anthropogenic sulphur dioxide from fossil fuel combustion is an important precursor of submicron aerosols in the marine atmosphere. In urbanised coastal regions, anthropogenic emissions further modify the composition of marine aerosols. For example, nitric acid reacts with sea salt to form coarse sodium nitrate ($NaNO_3$) particles. Across Europe, particulate nitrate (NO_3^-) is largely anthropogenic, produced by the oxidation of nitrogen oxides (NO and NO_2) emitted during high-temperature combustion in vehicle engines and industrial activities (A. U. Lewandowska & Falkowska, 2013b; Seinfeld & Pandis, 2006).

The influence of shipping emissions on aerosol particle properties in marine and coastal environments has also been widely investigated, particularly in the Baltic Sea region. Previous studies indicate that shipping is a major contributor to regional NO_2 concentrations, accounting for up to 50 %, whereas its contribution to $PM_{2.5}$ mass is comparatively small (5–10 %) (Jonson et al., 2019). A consistent finding across observational studies is the strong impact of ship emissions on particle number concentration, especially within the ultrafine size range (Ausmeel et al., 2019, 2020; Kecorius et al., 2016; Plauškaitė et al., 2017). Ship exhaust is characterised by BC-containing particles with diameters typically below 100 nm (Kaskaoutis et al., 2023; Kecorius et al., 2016). Owing to their small size, these particles contribute substantially to number concentrations but only weakly to particle mass. Reported contributions to $PM_{0.15}$ range from 9–18 % with dominant particle sizes near 41 nm (Kivekäs et al., 2014), while wintertime observations indicate minimal contributions to $PM_{0.15}$ and $PM_{0.5}$ mass concentrations (Ausmeel et al., 2020).

Chemical transport modelling supports these observations, estimating shipping contributions of 3.2–5.7 % to $PM_{2.5}$ in Baltic coastal regions (Karl et al., 2019). Emissions control measures, including reduced fuel sulphur content in Sulphur Emissions Control Area (SECA) regions, have further decreased particle number concentrations and particle mass (Seppälä et al., 2021). Seasonal processes may also influence aerosol formation, as interactions

between ship emissions and agricultural ammonia enhance $PM_{2.5}$ formation in spring (Jonson et al., 2020), whereas long-range-transported industrial pollutants may dominate air quality impacts in some regions (Ahlberg et al., 2023).

Overall, marine environments are dominated by sea salt aerosols and shipping emissions, which mostly affect ultrafine particle number concentrations (diameter < 100 nm), while their contributions to submicron particle mass, including PM_1 and $PM_{2.5}$, remain limited. Their influence, however, is relevant for specific aerosol components, such as sulphate, nitrate and organic species, although contributions to eBC at coastal sites are generally low (Ausmeel et al., 2020).

1.3.3 Regional background and rural environment

Regional background and rural sites are defined primarily by their distance from significant anthropogenic emission sources: rural sites are typically located 10–50 km away, while regional background sites are located more than 50 km from large pollution sources (Van Dingenen et al., 2004). These environments generally exhibit lower annual average concentrations of PM_{10} and $PM_{2.5}$ than their urban counterparts. There is a pronounced spatial gradient in which total particle number concentrations and lung-deposited surface area (LDSA) decrease significantly as one moves from urban or kerbside locations toward more remote background areas (Kecorius et al., 2025; Putaud et al., 2018; Van Dingenen et al., 2004). Despite lower mass loadings, the presence of BC even at natural background sites confirms that these areas are consistently affected by long-range transport of combustion-related pollutants (Cavalli et al., 2016; Savadkoohi et al., 2024).

The chemical composition of aerosols at regional and rural sites is dominated by secondary aerosol components rather than local primary emissions (Putaud et al., 2010; Schneider et al., 2025). In these regions, SOA and SIA, specifically sulphates, nitrates and ammonium, comprise the majority of the submicron particulate mass (Manousakas et al., 2017; Putaud et al., 2010; Schneider et al., 2025). Moreover, biogenic sources from vegetation and soils contribute a larger fraction to the organic aerosol budget in rural environments than in densely populated cities (Schneider et al., 2025; Van Dingenen et al., 2004). As aerosol particles are transported from urban centres to the regional background environments, they undergo physical transformations such as coagulation and dilution, which tend to remove smaller nuclear-mode particles while shifting the mass toward the accumulation mode (Putaud et al., 2010; Van Dingenen et al., 2004).

Broad regional similarities exist across Europe, yet specific chemical gradients are observed based on site classification and geographical location (Putaud et al., 2010; Van Dingenen et al., 2004). Seasonal variation at rural and regional background sites is driven by changes in source strengths, such as more active biogenic aerosol formation through photochemical reactions during summertime and increased heating demand and residential wood burning during winter. Overall, the concentrations of aerosol particles in regional background and rural environments are highly sensitive to large-scale meteorological patterns, with air masses from clean oceanic sectors providing dilution, while continental air flows from industrialised regions can trigger significant pollution episodes (Ahlberg et al., 2023; Ovadnevaite et al., 2014; Putaud et al., 2010).

1.4 Long-range air mass transport as a driver of aerosol variability

Long-range air mass transport significantly influences the composition and mass concentrations of aerosol particles, particularly in regions with limited local emission sources. Atmospheric aerosol particles can travel vast distances, extending far beyond their original emission points and affecting regions remote from their sources (Schneider et al., 2025). Long-range transport can cause peaks in particulate matter concentration when air masses from regions with high emissions of particles and/or precursor gases arrive during weak atmospheric mixing. (Tang et al., 2026). During these events, the aerosol mass is frequently dominated by secondary components – including oxygenated organic aerosol (OOA) and inorganic species like sulphates – which are formed through the physical and chemical ageing of pollution plumes during transport (Pirjola et al., 2017; Van Dingenen et al., 2004). In many European regions, these secondary species, particularly sulphates, serve as distinct markers for long-range transport episodes (Ahlberg et al., 2023; Juda-Rezler et al., 2020; Manousakas et al., 2017).

There is a pronounced spatial gradient in the mass concentrations of carbonaceous aerosol constituents, which generally increase from Northern Europe toward Central and Southern Europe (Cavalli et al., 2016). This variability is heavily influenced by large-scale meteorological patterns; for example, air masses transported from the Atlantic Ocean can significantly improve air quality in Central France, whereas air masses arriving from Eastern Europe can trigger heavy pollution episodes (Hu et al., 2019). As aerosols undergo long-range transport, physical processes such as coagulation and dilution typically remove smaller nucleation-mode particles while shifting the mass toward the accumulation mode (Chowdhury et al., 2022; Van

Dingenen et al., 2004). During such long-range transport events, these transformed particles may pose significant health risks even in areas far away from their emission sources, including rural background regions (WHO, 2021).

1.5 Modelling of atmospheric aerosol transport and source contribution

1.5.1 HYSPLIT model for aerosol transport analysis

The Hybrid Single-Particle Lagrangian Integrated Trajectory (HYSPLIT) model is a versatile tool extensively used in the atmospheric sciences to compute air parcel trajectories and simulate the transport, dispersion, and deposition of various pollutants (Draxler & Hess, 1998). Developed by the Air Resources Laboratory of the National Oceanic and Atmospheric Administration (NOAA), it employs a hybrid approach combining Lagrangian and Eulerian methodologies to establish source-receptor relationships (Rolph et al., 2017; Stein et al., 2015). Within the European context, the model has been instrumental in tracking diverse aerosol types, including wildfire smoke, mineral dust, allergens, and volcanic ash (Rolph et al., 2017; Stein et al., 2015). For instance, studies in the Western Mediterranean have utilised HYSPLIT to determine that North African dust sources contribute up to 10 $\mu g/m^3$ to annual PM_{10} in the Eastern Mediterranean and 2–4 $\mu g/m^3$ in the Western Mediterranean (Escudero et al., 2011). Furthermore, the model has been used to analyse the fate and transport of mercury emissions specifically across the European continent (Stein et al., 2015).

In the Baltic Sea region and Northern Europe, HYSPLIT has been essential for quantifying the impact of long-range transport on local air quality. Research conducted in Vilnius, Lithuania, found that elevated particle number concentrations and eBC levels often originate from heavily industrialised areas in Poland, Germany, and the Czech Republic, as well as from biomass-burning products transported from Ukraine and Russia (Byčenkienė et al., 2013, 2014). A specific 2022 study in Vilnius used 72-hour backward trajectories to categorise air mass episodes, finding that clean air masses from the mid-Atlantic decreased columnar pollution, while slow easterly air masses from Belarus and Russia significantly increased eBC concentrations (Davulienė et al., 2019). Similarly, in Central Europe, HYSPLIT trajectory clustering linked high wintertime concentrations of submicron aerosols to eastern continental transport from Poland (Arora et al., 2026).

The model has also been uniquely applied to evaluate aerosol transformation above the Baltic Sea, providing evidence for the significant

contribution of maritime activities and natural processes (Kecorius et al., 2016). Additionally, multi-wavelength lidar studies in Poland, combined with HYSPLIT trajectories, confirmed that aerosol properties depend heavily on advection direction, with strong northerly winds from the open sea significantly increasing the aerosol effective radius through sea spray emissions (Makuch et al., 2021). Ultimately, the HYSPLIT model's robust analytical features provide the empirical foundation necessary for effective transboundary air quality research and management.

1.5.2 FLEXPART model for aerosol dispersion

The FLEXible PARTicle dispersion model (FLEXPART) is a Lagrangian tool widely used to calculate the long-range, multi-scale dispersion of atmospheric tracers, including BC, mineral dust and radionuclides (Bakels et al., 2024). Originally developed to simulate the transport of hazardous substances from point sources, such as nuclear accidents, it has evolved into a community model for diverse applications in air pollution and climate research (Pisso et al., 2019; Stohl et al., 2005). FLEXPART, being fully open source and easily integrated with models such as WRF and ERA5, is continuously validated against real observations. Its ability to connect with emission inventories provides detailed output data, enabling it to assign modelled BC to various source categories (Source Spectrum) and to determine contributions from related source regions (Continent Spectrum).

FLEXPART has repeatedly demonstrated strong skill in reproducing observed eBC concentrations at background and remote sites, including the European Arctic – a region predominantly influenced by long-range transport with correlations of approximately 0.89 (Winiger et al., 2016). The model has demonstrated excellent performance when compared to eBC measurements from ship- and aircraft-based campaigns in remote regions (Evangeliou et al., 2018; O. B. Popovicheva et al., 2017), as well as ground-based monitoring stations across Europe (Eckhardt et al., 2015; Evangeliou et al., 2021; O. Popovicheva et al., 2025; Winiger et al., 2019; Yttri et al., 2024) and Asia (Dasari et al., 2020; M. Jia et al., 2021). Moreover, FLEXPART has been used to capture eBC variability during episodic pollution events (Evangeliou et al., 2019).

The model's reliability for European regional dispersion has been validated through large-scale experiments such as the European Tracer Experiment (ETEX), which involved a controlled release in France and subsequent measurements at 168 stations across Europe (Bakels et al., 2024; Forster et al., 2007). Results from these experiments confirm FLEXPART's ability to

accurately simulate the transport of air masses across national borders. By coupling Lagrangian trajectories with high-resolution emission inventories, the model identifies that pollution plumes from Central Europe often reach the Nordic countries and the Arctic, proving that the atmospheric composition at the target region is a product of both local activities and international-scale transport (Pisso et al., 2019; Zhu et al., 2020).

2 METHODOLOGY

2.1 Measurement sites

In this work, measurement data from 4 sites were investigated. Two of the sites were located in urban environments – Vilnius (Lithuania, North Europe) and Warsaw (Poland, Central Europe), while the remaining two sites were located in rural background environments – Preila (Lithuania) and Hyltemossa (Sweden, Northern Europe) (Figure 2). The sampling periods and instrumentation equipped in each station are presented in Table 1.

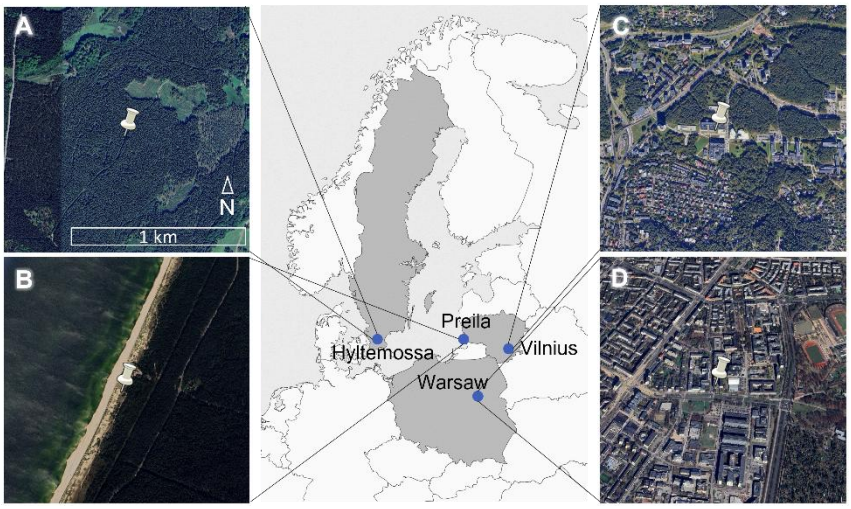

Figure 2. Map of the measurement sites: A – Hyltemossa, B – Preila, C – Vilnius, D – Warsaw. All subfigures (A-D) are shown in uniform scale.

Vilnius is the largest city in Lithuania, with a population of 0.6 million residents and an area of about 400 km² (~1500 residents per km²). The larger conurbation comprising the city and the districts of Vilnius and Trakai has approximately 0.75 million residents (~1360 residents per km²) (*Lithuanian State Enterprise Centre of Registers*, accessed on 4 June 2025). The measurement site in Vilnius is located on the roof of the Centre for Physical Sciences and Technology (54°42′50.474″ N, 25°15’9.808″ E; 131 a.s.l.) building, approximately 6 km northeast of the city centre. The site is situated in a mixed-use environment surrounded by private residential houses, a university campus, and forested areas. The building is screened from the nearest highway (0.6 km) and other low-traffic streets (0.3 km) by a forested area. Therefore, this site represents an urban background environment

influenced by distributed sources and by some nearby roads, without direct impact from strong, active pollution sources.

Warsaw has a population of 1.9 million residents and is therefore the largest city in Poland. The municipal area of the city is about 520 km^2 (3600 residents/km^2) (in 2022–2023) (*Statistics Poland*, accessed on 24 April 2023). It is important to note that Warsaw is surrounded by many satellite towns with over 1 million residents, which border directly on the Warsaw municipality area. This large conurbation is referred to as the Warsaw metropolitan area (4200 km^2). Daily traffic from the satellite towns to Warsaw and back is an important factor when describing the site, as it is a significant source of transport exhaust emissions in the city. The measurement site in Warsaw is located on the roof of the Faculty of Physics at the University of Warsaw (52°12′45.047″ N, 20°58′57.762″ E; 112 a.s.l.), about 3 km southwest of the city centre. The site is classified as urban, as it is surrounded by residential buildings, the University Campus Park, a large hospital area with a large parking lot, and green municipal parks. The main pollution sources at the site are residential and transport activities (Stachlewska et al., 2018).

Table 1. General information about performed studies: the sampling time, locations, their types, and the instruments used.

	Sampling time	**Location 1**	**Location 2**
Study No. 1	2022.05.01–2022.08.18	Vilnius (Urban background site)	Warsaw (Urban site)
		Aethalometer AE33	Aethalometer AE33
		Nephelometer TSI 3563	Aurora4000
Study No. 2	2022.05.01–2022.08.18 and 2022.11.01–2023.02.28	Vilnius (Urban background site)	Warsaw (Urban site)
		Aethalometer AE33	Aethalometer AE33
		Nephelometer TSI 3563	Aurora4000
Study No. 3	2017.12.01–2018.03.28	Preila (Marine background)	Hyltemossa (Rural background)
		Aethalometer AE31	Aethalometer AE33
		Q-ACSM	ToF-ACSM

The measurement site in Preila (55°22′ N, 21°1′ E, 1 m a.s.l.) is located in the south-eastern part of the Baltic Sea, the Curonian Spit, west of Lithuania.

The station is situated 40 km from the closest large city, Klaipėda, and 80 km from Kaliningrad (the Russian Federation), with some industrial activity. This site is therefore considered a marine background environment due to its large proximity to any local pollution sources and is mainly influenced by long-range transported pollution.

The Hyltemossa site is a research station of Aerosols, Clouds, and Trace gases Research InfraStructure (ACTRIS) and Integrated Carbon Observation System (ICOS) networks located in southern Sweden (56°5′N, 13°25′E, 118 m a.s.l.). The closest urban areas are: Helsingborg (Sweden), 25 km to the west; Malmö (Sweden), 50 km to the southwest; and Copenhagen (Denmark), 60 km to the southwest. The Hyltemossa site is surrounded by forests and is therefore considered a rural background site. There are no direct pollution sources in proximity; thus, the site is very suitable for background observations of long-range transported pollution, as its dynamics are not influenced by rapid changes typical of an urban environment with many active, direct sources.

2.2 Instrumentation and methods

2.2.1 Aethalometers

Aerosol light absorption measurements were taken using 7-wavelength (370, 470, 520, 590, 660, 880, and 950 nm) aethalometers, which measure all wavelengths simultaneously and continuously.

The main principle of the instrument is to measure light transmission through a filter spot where aerosol particles are deposited and through a control spot where none are deposited. Controlled airflow deposits aerosol particles onto a filter tape. Over time, as light-absorbing aerosol particles accumulate on the filter spot, the detected light transmission decreases. Light attenuation is used to calculate the absorption coefficient (b_{abs}), which is proportional to the mass of optically absorbing material deposited on the filter. Mass concentration is then calculated using wavelength-specific mass absorption cross-section (MAC).

In Vilnius, Warsaw, and Hyltemossa, aethalometers AE33 (Magee Scientific, model AE33, Berkeley, CA, USA) were used, while an aethalometer AE31 (Magee Scientific, model AE31 Spectrum, manufactured by Aerosol d.o.o., Slovenia) was used in Preila. The measurement time resolution was 1 minute for A33 and 2 minutes for AE31, and the flow rate was 5.0 L/min for both AE33 and AE31. The lower detection limit is 0.01 μg/m^3 for both AE33 and AE31 (Sedlacek, 2016).

In the case when mass concentration is measured indirectly (i.e., converted from b_{abs}), the term eBC should be used instead of BC, as a proxy of the measurement method. eBC mass concentration was calculated from the b_{abs} at 880 nm, as BC is the main light-absorbing aerosol component at this wavelength. For calculating eBC mass concentrations at the wavelength, the wavelength-specific MAC value was 7.77 m^2/g for AE33 data (set by the manufacturer (Aerosol d.o.o, 2018)) and 16.6 m^2/g for AE31 data (set by the manufacturer (Sedlacek, 2016)):

$$eBC = \frac{b_{abs\ 880\ nm}}{MAC_{880\ nm}} \quad (1)$$

For the accuracy of eBC mass concentration determination, measurement data should be corrected for artefacts of filter-based measurement techniques, such as the particle loading effect. The AE33 aethalometer, which is a newer generation instrument, uses a real-time loading effect compensation algorithm proposed by Drinovec et al. (2015). To ensure comparability, the data measured with AE31 were corrected offline using the method of Weingartner et al. (2003). An intercomparison study by Drinovec et al. (2015) showed a very good agreement between data compensated by both methods proposed by Drinovec and Weingartner. The AE33 data were processed using a harmonised methodology: the b_{abs} were recalculated using a harmonisation factor (H* is 1.76 when C_0 is 1.39) (Savadkoohi et al., 2023).

Uncertainties in aethalometer measurements of eBC mass concentration arise from two main sources: the measurement uncertainty in attenuation/absorption (including instrumental variability and cross-sensitivity to scattering, each estimated at 10 % (Drinovec et al., 2015)), and the conversion of absorption to mass concentration (due to the assumed fixed MAC and multiple scattering correction factor C_0) (Drinovec et al., 2015; Zanatta et al., 2016; Zotter et al., 2017). AE33 measurements rely on detecting small relative changes in optical transmission rather than on absolute calibration of detector response signals. Zero-noise tests using a HEPA filter indicated an optical/electrical system stability of 0.11 $\mu g/m^3$ for hourly means (Allerton et al., 2022).

2.2.2 Black carbon source apportionment

BC source apportionment was performed using the method proposed by Sandradewi et al. (2008). The Aethalometer model is based on the differences in the light absorption of BC originating from different sources and source-specific AAE values (Zotter et al., 2017). The AAE defines how the light

absorption coefficient varies across the measured wavelength range (370–950 nm). The relationship between b_{abs} and AAE is expressed in equation (2):

$$b_{abs}(\lambda) \sim \lambda^{-AAE} \quad (2)$$

Here, $b_{abs}(\lambda)$ marks absorption at a wavelength λ. A more detailed explanation of the method can be found in the original paper of Sandradewi et al. (2008).

The source-apportioned b_{abs} of eBC_{FF} and eBC_{BB} were calculated as follows:

$$b_{abs\,FF} = \frac{b_{abs}(470\ nm) - b_{abs\,FF}(950nm) * \left(\frac{470}{950}\right)^{-AAE_{BB}}}{\left(\frac{470}{950}\right)^{-AAE_{FF}} - \left(\frac{470}{950}\right)^{-AAE_{BB}}} \quad (3)$$

$$b_{abs} = b_{abs\,FF} + b_{abs\,BB} \quad (4)$$

where b_{abs}(470 nm) marks the total eBC light absorption coefficient at 470 nm and b_{abs}(950nm) at 950 nm, respectively, AAE_{BB} is the source-specific AAE value for eBC from biomass burning emissions, and AAE_{FF} – eBC from fossil fuel combustion. Equation (4) shows that the total light absorption at a selected wavelength is composed of $b_{abs\,FF}$ (absorption coefficient of eBC_{FF}) and of $b_{abs\,BB}$ (absorption coefficient of eBC_{BB}).

Source-specific AAE values can vary across regions depending on the fuels most commonly used, their origins, the transport fleet, and meteorological conditions (Garg et al., 2016; Zotter et al., 2017). In the present study, a previously determined combination of AAE_{FF} and AAE_{BB} for Vilnius (0.9 and 2.2, respectively) for the warm season measurements in Vilnius (Minderytė et al., 2022). For the warm season in Warsaw, the AAE_{FF} and AAE_{BB} values were 1.0 and 2.0, respectively, as recommended by the manufacturer (Aerosol d.o.o, 2018). For the cold season, the value selection had to account for the increased influence of coal burning during the cold season, which is typical of Poland. Therefore, values from a winter study in north Poland (Kristensson et al., 2020) were applied to the cold season data. The coal combustion contribution was combined with the biomass burning contribution: 1.03 (AAE_{FF}) and 1.93 ($AAE_{BB,C}$) for both sites. The wavelength pair in this study was chosen as 470 and 950 nm, which is the most commonly used wavelength pair in this field (Liu et al., 2018; Saarikoski et al., 2021; Sandradewi et al., 2008; Zotter et al., 2017).

2.2.3 Nephelometers

Aerosol light-scattering for Studies No.1 and 2 was measured using nephelometers. A nephelometer measures the light-scattering coefficient (b_{scat}) of aerosol particles. The main measurement principle is to measure the intensity of light scattered by aerosol particles suspended in air as they pass through the light beam. The use of nephelometers is widespread because the method is simple and makes no assumptions about particle composition, size, or shape.

In Vilnius, an integrating nephelometer TSI, model 3563 (TSI Inc, St. Paul, MN, USA) was used to measure light scattering at 3 wavelengths (450, 550, 700 nm) for total scattering angles from 7° to 170°. The lower detectable limit was 0.5 $Mm^{-1,}$ and the instrument precision is about 3 % (Anderson & Ogren, 1998). The sample flow was 23 L/min. Due to technical issues, the cold season measurements in Vilnius were available from 20 January to 28 February.

In Warsaw, a polar nephelometer Aurora 4000 (Ecotech Pty, Ltd, Knoxfield, Australia) was used. It measures light scattering at 3 wavelengths (450, 525, 635 nm) at angles from 9° to 170°. The instrument detection limit was 0.3 Mm^{-1}, and the sampling flow rate was approximately 5 L/min.

Both instruments at the two sites were set to have the same sampling frequency of 30 s. Scattering coefficients from both instruments were corrected for truncation error using the method suggested by Müller et al. (2011). This method applies the truncation error to each wavelength, using a wavelength-specific factor defined for each instrument.

2.2.4 Calculation of derived aerosol optical properties

For aerosol optical classification, a scheme suggested by Cappa et al. (2016) was used. The approach apportions general aerosol types and mixing states based on their absorption and scattering properties: AAE and SAE. The scheme consists of thresholds for $AAE_{532/660}$ plotted against $SAE_{450/550}$. To follow the original approach to get precise results for aerosol classification, the b_{abs} value at 532 nm had to be interpolated (Eq. 5) to calculate $AAE_{532/660}$ at wavelengths 532 and 660 nm (Eq. 6). This was performed using the method by Zhuang et al. (2015) and b_{abs} at 520 nm measured using the aethalometer:

$$b_{abs}(532\ nm) = b_{abs}(520\ nm) \cdot \left(\frac{532}{520}\right)^{-AAE_{590/520}} \quad (5)$$

$$AAE_{532/660} = -\frac{ln\left(\frac{b_{abs}(532\ nm)}{b_{abs}(660\ nm)}\right)}{ln\left(\frac{532}{660}\right)} \quad (6)$$

The same interpolation approach was applied to calculate b_{scat} at 550 nm (Eq. 7) to then calculate $SAE_{450/550}$ (Eq. 8):

$$b_{scat}(550\ nm) = b_{scat}(525\ nm) \cdot \left(\frac{550}{525}\right)^{-SAE_{450/635}} \quad (7)$$

$$SAE_{450/550} = -\frac{ln\left(\frac{b_{scat}(450\ nm)}{b_{scat}(550\ nm)}\right)}{ln\left(\frac{450}{550}\right)} \quad (8)$$

The SSA_{550} was calculated using b_{abs} from an aethalometer and b_{scat} from a nephelometer at a wavelength of 550 nm:

$$SSA = \frac{b_{scat}(550\ nm)}{b_{scat}(550\ nm) + b_{abs}(550\ nm)} \quad (9)$$

The uncertainties of the derived optical parameters – AAE, SAE, and SSA – were estimated analytically from the instrumental measurement uncertainties. The b_{abs} measured by the AE33 aethalometers carry an instrumental uncertainty of 10 %, accounting for the dual-spot loading correction and multiple scattering correction factor (Drinovec et al., 2015). The b_{scat} from nephelometer measurements carries an instrumental uncertainty of ±3 %, with an additional ±3 % uncertainty introduced by the truncation correction (Müller et al., 2011), yielding a combined scattering uncertainty of approximately ±4 % (propagated using standard error). For both parameters AAE and SAE, the uncertainty was propagated as follows:

$$\sigma = \frac{\sqrt{2} \cdot u}{\left|\ln(b_{\lambda_1} / b_{\lambda_2})\right|} \quad (10)$$

where u is the relative instrumental uncertainty of the respective coefficient. This yields typical relative uncertainty of approximately ±12–15 % for AAE and ±10–12 % for SAE. The SSA at 550 nm was derived from independently measured b_{abs} and b_{scat}, and the absolute uncertainty was propagated as:

$$\sigma_{SSA} = \frac{1}{(b_{scat} + b_{abs})^2}\sqrt{b_{abs}^2\sigma_{scat}^2 + b_{scat}^2\sigma_{abs}^2} \quad (11)$$

yielding a typical absolute uncertainty of approximately ±0.05 in SSA.

2.2.5 Aerosol Chemical Speciation Monitors

The ambient non-refractory submicron aerosol chemical composition and concentration were measured using aerosol chemical speciation monitors

(ACSM). In the instrument, the flow of aerosol particles is focused by aerodynamic lenses and directed into a vacuum chamber, where the particle beam impacts a heated (600 °C) tungsten plate. Shortly thereafter, the non-refractory aerosol components (nitrate (NO_3^-), sulphate (SO_4^{2-}), ammonia (NH_4^+), chloride (Chl), and OA) are flash-evaporated and ionised by 70 eV electron impact. In a Quadrupole ACSM (Q-ACSM), the ionised molecular fragments of the aerosol components are detected and characterised by a quadrupole mass spectrometer and sorted by the mass-to-charge ratio (m/z). A newer type of ACSM, Time-of-flight ACSM (ToF-ACSM), sorts molecular fragments based on their time-of-flight to the detector: lighter ions reach the detector faster, while heavier ions take longer.

The site in Preila was equipped with a quadrupole ACSM (Q-ACSM, Aerodyne Research Inc., USA). The measurement time resolution was 30 minutes. The instrument has a sensitivity of 0.012 μg/m^3 for nitrate, 0.024 μg/m^3 for sulphate, 0.284 μg/m^3 for ammonia, 0.011 μg/m^3 for chloride, and 0.148 μg/m^3 for organics (as reported by Ng et al. (2011)). The site in Hyltemossa was equipped with a ToF-ACSM (Aerodyne Research Inc., USA), which operated at a 10-minute time resolution and a sensitivity on the order of <0.03 μg/m^3 for a time resolution of 30 min. The collection efficiency for both sites was evaluated by the composition-dependent approach suggested by Middlebrook et al. (2012).

2.2.6 Organic aerosol source apportionment

OA sources were investigated using the Positive Matrix Factorisation (PMF) method to unit mass resolution data, following the technique described by Paatero (1997). In the study, organic and error matrices were generated for *m/z* signals from 12 to 120 for both datasets from Preila and Hyltemossa. PMF analysis was carried out using SofiPro (version 6.8), with the initial setup guided by the recommendations of Paglione et al. (2020).

After a detailed evaluation of mass spectral profiles, residuals, time series, diurnal patterns, and temporal residuals, a three-factor solution was selected for both locations. Four-factor solutions resulted in non-physical splits in factor profiles, whereas the three-factor solution demonstrated strong stability. Scaled residuals ranged from -0.2 to 0.2, indicating an appropriate model fit for all mass spectra.

Solutions were generated through 100 iterative runs. Based on the highest contribution of *m/z* to the biomass-burning-related factor, 15 runs were retained and averaged. Factor similarity was assessed using the theta angle calculations (Kostenidou et al., 2009), where $\theta < 15°$ indicates strong

similarity, $15° < \theta < 30°$ indicates partial similarity, and $\theta > 30°$ indicates no similarity.

2.3 Meteorological parameters

For Vilnius, meteorological data, including temperature (T), wind speed (WS), wind direction (WD), precipitation, and relative humidity (RH), were obtained via API access to the Lithuanian Hydrometeorological Service archives for the Vilnius weather station, situated 17.8 km southwest of the aerosol measurement site (*Meteo.Lt API*, n.d.). The distance is considered acceptable, as the site represents an urban background environment with a relatively large spatial footprint, making it representative of the conditions at the aerosol measurement location.

Measurements of meteorological parameters were conducted at the University of Warsaw site in Warsaw, co-located with the aerosol instrumentation.

At the Hyltemossa site, meteorological measurements were performed continuously by ICOS Sweden along with aerosol measurements (Heliasz & Biermann, 2024).

The meteorological parameters for Preila were measured at a meteorological station in the nearby town of Nida by the Lithuanian Hydrometeorological Service and were obtained via API access to the archives (*Meteo.Lt API*, n.d.).

The meteorological data are reported at the precision provided by the respective measuring agencies, without uncertainty assessment.

2.4 Data processing and statistical analysis

To ensure consistency between datasets of different instruments and meteorological parameters, all data were averaged to a 1-hour time resolution. Before that, the aethalometer data were quality-controlled to remove perturbed values: negative absorption values, spontaneous short-term spikes, zero values during the instrument warm-up or clean-up, and flowmeter calibration.

Statistical significance was evaluated using the Kruskal-Wallis test, and a critical value of $p = 0.05$ was selected. Spearman's rank correlation test was used to assess correlations among parameters.

Measured or derived parameter values are reported with their standard deviations to indicate dataset variability.

2.5 Long-range air mass transport modelling

The modelling of long-range air mass transport backward trajectories and territories where the air mass has passed over was done using software based on Lagrangian and Eulerian methodologies: Hybrid Single Particle Lagrangian Integrated Trajectory model HYSPLIT (Studies No. 1 and No. 3) and FLEXible PARTicle (FLEXPART) dispersion model (Study No. 2). This section will present the details of the models and how the modelling was performed.

2.5.1 HYSPLIT

HYSPLIT was used to model 72-hour backward air-mass trajectories using the Global Data Assimilation System (GDAS) meteorological databases at the NOAA Air Resources Laboratory's web server (Draxler & Rolph, 2003).

For Study No. 1, 72-hour backward air mass transport trajectories were calculated, ending at 500 m a.s.l. at the precise coordinates of the measurement sites in Vilnius and Warsaw at 12:00 UTC for each day of the measurement campaign (from May 1, 2022, to August 18, 2022).

In Study No. 3, 72-hour backward air mass transport trajectories arriving at the receptor sites (Hyltemossa and Preila) were modelled at hourly intervals throughout the measurement campaign (from December 12, 2017, to March 28, 2018). To narrow down the calculations, the following criteria were introduced: the backward trajectory must pass the upwind site within a 50 km radius and arrive at the downwind site at 100 m a.s.l.

2.5.2 FLEXPART

The FLEXPART model was driven by hourly ERA5 reanalysis meteorological fields from the European Centre for Medium-Range Weather Forecasts (ECMWF), using 137 vertical levels and horizontal resolutions of $0.5° \times 0.5°$ and $0.1° \times 0.1°$ (Hersbach et al., 2020). In FLEXPART, computational particles were released from heights between 0 and 100 m a.g.l. at the receptor sites (Vilnius and Warsaw) and tracked backwards over 30 days. This integration period is sufficient to capture the majority of BC emissions reaching the stations, given the typical atmospheric lifetime of BC is approximately one week (Bond et al., 2013). The tracking encompasses gravitational settling of spherical particles, dry and wet deposition, turbulence, unresolved mesoscale motions, and deep convection. The model output is the footprint emission sensitivity, which indicates the probability that emissions

from each grid cell reach the receptor site. When combined with gridded emission inventories, it is directly translated into modelled concentrations at receptor sites. The FLEXPART output used in this work has a temporal resolution of 3 hours. A more detailed description of the model framework can be found in Pisso et al. (2019).

In this work, the anthropogenic emissions at a horizontal resolution of 0.5° × 0.5° were taken from ECLIPSE (Evaluating the CLimate and Air Quality ImPacts of Short-livEd Pollutants) version 6b inventory (Klimont et al., 2017). This dataset includes the following emission sectors: domestic heating (DOM), energy production (ENE), gas flaring (FLA), industrial combustion (IND), shipping (SHP), waste treatment and disposal (WST), and transport (TRA).

To better resolve city-scale contributions, higher-resolution emission data (0.1° × 0.1°) over Europe was adopted from Winiwarter et al. (2024). In this inventory, emission sectors were defined as: (A) public power, (B) industrial, (C) other stationary combustion sources, (D) fugitives, (E) solvents, (F) road transport, (G) shipping, (H) aviation, (I) off-road transport, and (J) waste management emissions. To keep consistent sector division with ECLIPSE 6b sector definitions, the following approach was applied: DOM was set to be equal to (C), IND was defined as the sum of (A), (B), (D), and (E), SHP corresponded to (G) shipping, and TRA was defined as the sum of (F), (H), and (I), WST corresponds to (J). Emission sectors ENE and FLR were not provided as separate categories in the high-resolution dataset and were therefore set to zero. Wildfire emissions at both resolutions (0.1° × 0.1° and 0.5° × 0.5°) were taken from the Copernicus Global Fire Assimilation System (CAMS GFAS; (Kaiser et al., 2012)). The dataset provides plume rise and subsequent dispersion simulations.

The uncertainty of the model was assessed by evaluating FLEXPART's sensitivity to the spatial resolution of the meteorological input fields. Two FLEXPART simulations, utilising meteorological data with horizontal resolutions of 0.1° × 0.1° and 0.5° × 0.5°, were employed. The uncertainty was quantified as the standard deviation of the modelled concentrations obtained from these simulations, thereby providing an estimate of the variability in the simulated concentrations attributable to differences in input resolution. All other model configurations and parameterisations were maintained constant.

2.6 Diagnostic analyses based on modelled air mass transport

2.6.1 Threshold-based categorisation of backward air mass trajectories

The obtained 72-hour backward air mass trajectories starting at Vilnius and Warsaw for Study No. 1 were inspected in terms of their uniformity based on thresholds:

- The directional threshold. Trajectories were defined as arriving from the same direction if they were centred within ±30 ° of the receptor sites (Vilnius and Warsaw).
- The horizontal threshold (H-threshold), which was defined as a horizontal 430 km distance between the trajectories (considering the air distance between Vilnius and Warsaw is 430 km).
- The vertical threshold (V-threshold), which is defined as a difference in the altitude of a trajectory.

After inspecting the backward trajectories, they were assigned to predefined categories, based on their characteristics:

- Category A – trajectories have similar or overlapping air mass transport pathways; therefore, one aerosol origin or source is expected.
- Category B – trajectories arrived at the sites from different directions and pathways; therefore, there is a possibility of one aerosol origin or source region.
- Category C – contains all cases that could not be categorised into „overlapping“ (Category A) or „strictly different“ (Category B).

A representative example is presented in the Supplementary material (Figure 29).

2.6.2 Pollution boost and dilution calculation

In Study No. 1, days with air mass trajectories categorised as Category A were analysed to evaluate eBC pollution boosts or dilution events. The impact on eBC mass concentrations was assessed by comparing the mean concentrations of consecutive 6-hour periods before and after the arrival of each trajectory at the receptor site:

$$\Delta eBC = \frac{\overline{eBC_{t+1\ldots t+6}} - \overline{eBC_{t-6\ldots t-1}}}{\overline{eBC_{t-6\ldots t-1}}} \quad (12)$$

Here, $\overline{eBC_{t+1\ldots t+6}}$ represents the mean eBC concentration over the following six hours after the arrival of the Category A trajectory, while $\overline{eBC_{t-6\ldots t-1}}$ represents the mean eBC concentration over the six hours prior to its arrival at the receptor site. In cases when ΔeBC is negative, it is considered a

decrease, while when ΔeBC is positive, it is considered a boost in eBC mass concentration. A 6-hour averaging period was chosen as it is long enough to smooth out short-term spikes and local variability in eBC concentrations, yet short enough to capture changes associated with the arrival of the air mass at the receptor site and the immediate influence of long-range transport.

2.6.3 BC emission source regions

To evaluate the contribution of transported BC, derived from modelling, to the measured eBC concentrations at the receptor measurement sites in Study No. 2, potential source region maps were generated using 3-hour-averaged measured eBC mass concentrations, consistent with the temporal resolution of the FLEXPART output. For each site, the dataset was separated into high- and low-concentration episodes. High-concentration episodes were defined as 3-hour intervals with measured eBC exceeding the 80th campaign percentile, while the low-concentration episodes correspond to values below the 20th campaign percentile. For both high- and low-concentration episodes, the corresponding FLEXPART footprints were averaged to identify the dominant source sectors of BC reaching the receptor sites.

2.6.4 Partition of BC into city-produced and transported components

To quantify the relative contributions of local BC emissions in the city and the transported BC, the measured eBC mass concentration was partitioned into transported and city-produced components, following the equation:

$$BC_{measured} = BC_{city-produced} + BC_{transported} \quad (13)$$

Here, $BC_{measured}$ denotes the eBC mass concentration measured by the aethalometers, the city-produced component, $BC_{city-produced}$, represents the fraction of BC attributable to emissions within the city boundaries, and $BC_{transported}$ corresponds to the BC concentration at the receptor site modelled using FLEXPART. $BC_{transported}$ was obtained by subtracting the contribution of emission grid cells within the administrative boundaries of Warsaw and Vilnius from the FLEXPART modelled BC. At the 0.1° × 0.1° spatial resolution, this corresponds to 8 grid cells for Warsaw and 6 grid cells for Vilnius. The normalised FLEXPART-modelled BC therefore represents exclusively BC transported from outside the city borders, with no contribution from local city emissions.

In addition to excluding emissions within the administrative city boundaries, sensitivity analyses were performed by progressively excluding emissions within circular areas of 20 km and 50 km radius around the

measurement sites. This approach enables the assessment of the influence of near-city sources on the estimated contribution of transported BC. Spatial maps illustrating the regions excluded from the modelled BC contributions are provided in Figure 30 in the Supplementary material.

2.6.5 Selection of connected flow long-range air mass transport events

For study No. 3, 72-hour backward trajectories exhibiting sharp bends or looping structures between the receptor sites (Hyltemossa and Preila) were excluded from the analysis in order to avoid inaccuracies. After manual revision, consecutive hourly trajectories that met the predefined selection criteria (section 2.5.1) were grouped into connected flow events (hereafter referred to as events for brevity). For statistical significance, only events comprising three or more consecutive hourly trajectories were investigated.

Events of westerly air masses (starting upwind in Hyltemossa and arriving at Preila) were more frequent (14 events consisting of 102 hourly trajectories in total) than events from the east (starting upwind in Preila and arriving at Hyltemossa) (6 events consisting of 62 hourly trajectories in total). The latter were excluded from further statistical analysis due to the limited sample size. The events of westerly air masses were labelled using the abbreviation HP (from Hyltemossa to Preila) and a given number in the chronological order of occurrence.

The identified events were further classified into three classes based on modelled meteorological conditions and spatial data along the trajectory pathway (Table 2): Class A represents trajectories extending from west to east with no notable bends over the Baltic Sea and arriving at the downwind site; Class B includes trajectories extending from west to east with no notable bends over the Baltic Sea and arriving at the downwind site with precipitation along the path; Class C comprises trajectories extending either north or south, passing over a continental region before arriving at the downwind site, with precipitation occurring along its pathway.

In the context of the current study, there were no events without precipitation in which the trajectory extended either north or south and passed over a continental region before arriving at the downwind site.

Table 2. Overview of available emission sources and sinks in the proposed event classes.

Sources and sinks	Class A	Class B	Class C
Sea transport (dry deposition/ chemistry effects/ cloud or fog activation)	+	+	+
Wet deposition	−	+	+
Land emissions	−	−	+
Shipping emissions	+	+	+

2.6.6 Aerosol mass concentration change assessment

In study No. 3, to assess changes in PM_1 mass concentration during transport across Hyltemossa and Preila, trajectory duration was taken into consideration. As described in the previous section (2.5.1), backward trajectories were calculated on an hourly basis. Thus, knowing the exact arrival time at the site in Preila enabled determining when each trajectory passed over Hyltemossa by calculating backwards duration from the arrival time. This way, aerosol composition and chemical concentration data points were assigned to the start and end of each trajectory. To calculate the PM_1 concentration and composition in the air mass departing from Hyltemossa, an average was calculated for the entire duration of the event from the first to the last hourly trajectory leaving the site. The same approach was applied to Preila: an average was calculated over the first-to-last hourly trajectories arriving at the site. Then the aerosol concentration change was estimated for a component *i* during an event *j*, using equation (14):

$$\Delta M_{i,j} = \left[\frac{M_{i,j\ Preila} \cdot 100\ \%}{M_{i,j\ Hyltemossa}} - 100\ \%\right] / t_j \qquad (14)$$

Here $M_{i,j\ Preila}$ and $M_{i,j\ Hyltemossa}$ mark the mean mass concentrations of component *i* during event *j* in Preila and Hyltemossa, accordingly. The mean duration of event *j* is marked as t_j [h] and is determined by averaging all the consecutive hourly trajectory durations of event *j*.

The influence of different factors (sea transport, wet deposition processes, and potential emissions over land) and their combinations on the PM_1 concentration was calculated for each aerosol component and event class:

$$\Delta M_{i,Class\ A\ /\ B\ /\ C} = \frac{\sum \Delta M_{i,j}}{n} \qquad (15)$$

Here n marks the number of events in the corresponding Class A, B, or C. Class A is characterised by air masses influenced by the sea transport, whereas

Class B shows the combined influence of sea transport and wet deposition processes. Class C additionally includes the effects of potential emissions over land. The combination of processes aerosol particles undergo over the sea is represented by the sea transport effect, which is observed in Class A ($\Delta M_{i,Class\ A}$) as the wet deposition processes or other factors do not play a role in this class:

$$Sea\ transport\ effect_i = \Delta M_{i,Class\ A} \quad (16)$$

Then, the effects of wet deposition processes and land-atmosphere interactions on the mass of component i were calculated using the following equations:

$$Wet\ deposition\ processes_i = \Delta M_{i,Class\ B} - \Delta M_{i,Class\ A} \quad (17)$$

$$Land - atmosphere\ interactions_i = \Delta M_{i,Class\ C} - \Delta M_{i,Class\ B} \quad (18)$$

2.6.7 Total accumulated precipitation evaluation per event

To evaluate the total accumulated precipitation during a long-range transport event, the following approach was applied. The arithmetic mean of the precipitation was calculated for each hour of the event, because the modelled precipitation values from GDAS at NOAA varied across calculated hourly trajectories. To obtain the total precipitation amount during the event, the hourly mean values were summed. A visual representation of the approach is presented in Figure 3. To minimise uncertainty caused by modelled rather than directly measured precipitation, the data were not normalised based on precipitation amount.

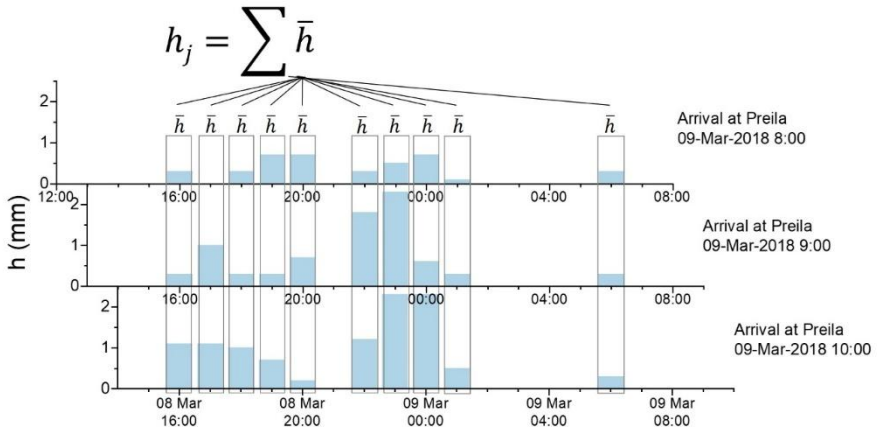

Figure 3. Schematic representation of the calculation for the total precipitation during the long-range transport event of 3 consecutive hourly trajectories.

3 RESULTS

The chapter consists of two parts that reflect the aerosol characteristics of the environment under investigation. Urban environments are evaluated using eBC concentrations: focusing on eBC rather than the entire aerosol mixture isolates the combustion emission signal within a highly complex source environment. In contrast, regional background and marine environments are examined through the entire submicron aerosol matrix, since eBC in these settings is typically aged and spatially remote from its sources, limiting its effectiveness as a standalone transport tracer.

3.1 Impact of long-range air mass transport on eBC levels in urban environments (Studies No. 1 and 2)

In this chapter, the results of eBC mass concentrations and source apportionment in the North and Central European capitals of Vilnius and Warsaw are presented. The analysis covers two distinct seasons - the warm season of 2022 and the cold season of 2022–2023.

Aerosol optical properties are examined in relation to eBC source apportionment results and eBC mass concentrations to better characterise the dominant aerosol mixture. The role of long-range air mass transport is then investigated.

Study No. 1 focuses on the impact of long-range air mass transport on pollution boosts and dilution of eBC mass concentration at both sites during the warm season. Study No. 2 extends the analysis to both warm and cold seasons and quantifies the contributions of city-produced and long-range-transported BC to urban environments in Vilnius and Warsaw.

3.1.1 eBC mass concentration analysis in Vilnius and Warsaw

3.1.1.1 Campaign overview

The time series of eBC mass concentrations for the warm and cold seasons are presented in Figure 4 and Figure 5, respectively. Overall, eBC mass concentration in Warsaw was consistently higher than in Vilnius for 1-hour and 72-hour running means during both seasons ($p < 0.05$). The high short-term resolution (1-hour data) captures short-term variability associated with local emission sources, such as traffic-related peaks during rush hour. In contrast, the 72-hour running mean reflects broader temporal patterns influenced by meteorological conditions and long-range air mass transport. A

comparison of seasonal mean eBC mass concentrations for both cities is provided in Table 3.

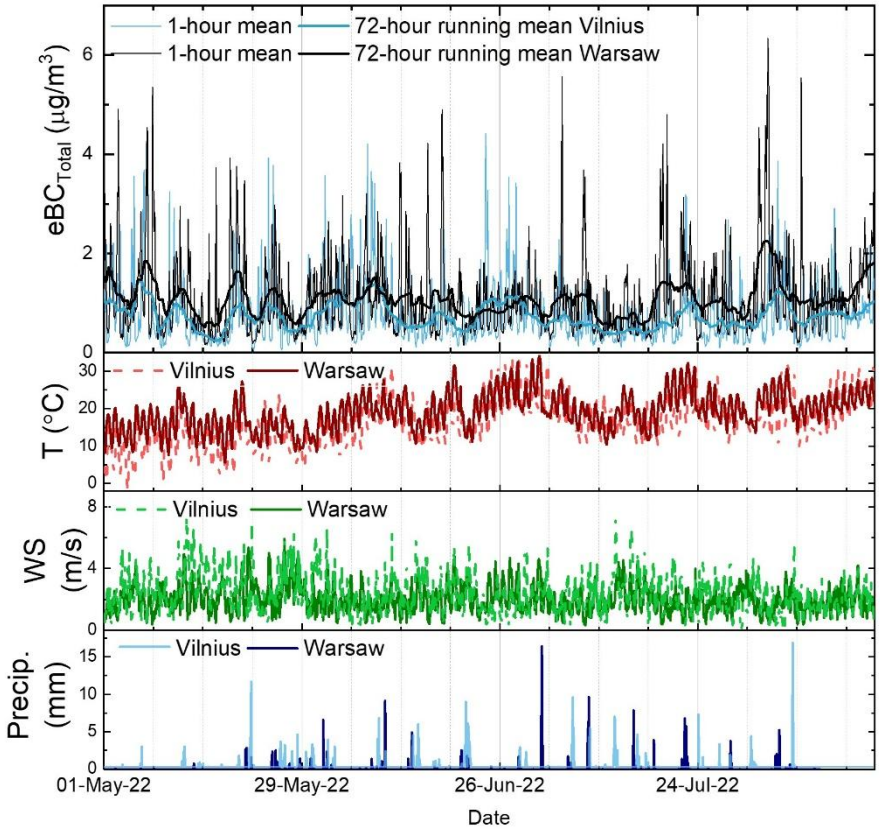

Figure 4. Time series of eBC mass concentrations and meteorological parameters in Vilnius and Warsaw during the warm season of 2022.

The mean eBC mass concentration in Warsaw was 1.07 µg/m^3 during the warm season and 2.02 µg/m^3 during the cold season. These values were 39 % higher than those observed in Vilnius (0.77 µg/m^3) during the warm season and 82 % higher during the cold season (1.11 µg/m^3). The elevated concentrations in Warsaw can be partly attributed to the substantially larger population (2.7 times that of Vilnius), higher population density (approximately double that of Vilnius, according to the Central Statistical Office of Poland and the Lithuanian State Enterprise Center of Registers), and extensive transit traffic within and through the metropolitan area and the city, which contributes to traffic congestions and increased exhaust traffic emissions.

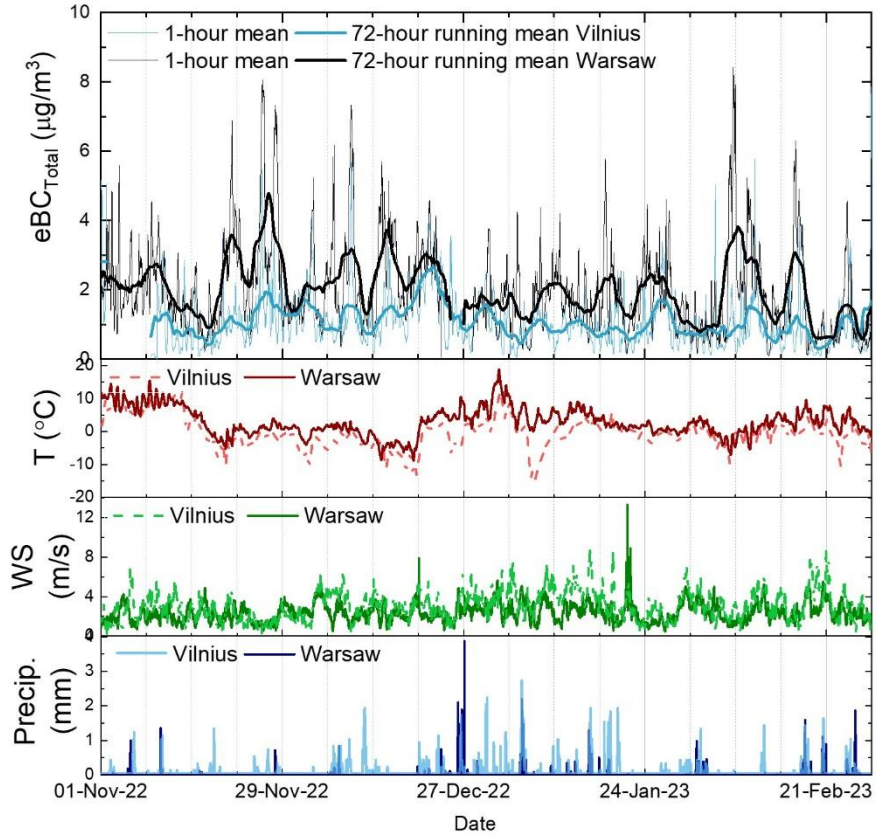

Figure 5. Time series of eBC mass concentrations and meteorological parameters in Vilnius and Warsaw during the cold season of 2022-2023.

The observed eBC mass concentrations are comparable to, or lower than, those reported for other urban background sites in northern and central Europe, including Helsinki (Helin et al., 2018), London (Jafar & Harrison, 2021), and Zurich-Kaserne (Grange et al., 2020). The values also align with findings from earlier studies conducted in Vilnius (Garbarienė et al., 2022; Minderytė et al., 2022). However, comparable long-term observations for the cold season have not yet been reported for Warsaw.

An intriguing feature in the 72-hour data for both seasons is that eBC mass concentration generally follows a similar trend in Warsaw and Vilnius. This pattern cannot be attributed solely to local factors; therefore, large-scale influences on both cities need to be considered. Meteorology is one of the influencing factors, as wind speed, temperature, and precipitation all affect aerosol concentrations, including eBC (Kumar et al., 2023).

Table 3. Overview and comparison of the warm and cold seasons in Vilnius and Warsaw. Average values with standard deviation values (± SD) to show the data variability are presented for eBC mass concentrations, source apportionment results, aerosol optical characteristics, temperature, WS, and RH. Meteorological data are presented with such precision as was provided.

	Warm season		Cold season	
	Vilnius	Warsaw	Vilnius	Warsaw
BC (μg/m^3)	0.77 ± 0.63	1.07 ± 0.8	1.11 ± 0.86	2.02 ± 1.33
eBC_{FF} (μg/m^3)	0.64 ± 0.52	0.92 ± 0.68	0.76 ± 0.57	1.25 ± 0.8
eBC_{BB} (μg/m^3)	0.13 ± 0.14	0.15 ± 0.15	0.34 ± 0.33	0.77 ± 0.61
eBC_{FF} (%)	84 ± 5	86 ± 5	71 ± 9	63 ± 10
$SAE_{450/550}$	1.75 ± 0.35	1.62 ± 0.35	1.48 ± 0.38	1.20 ± 0.27
$AAE_{532/660}$	1.26 ± 0.09	1.3 ± 0.07	1.42 ± 0.1	1.53 ± 0.10
SSA_{550}	0.81 ± 0.08	0.81 ± 0.07	0.83 ± 0.07	0.84 ± 0.05
Temperature (°C)	16.2 ± 5.9	19.2 ± 5.0	-0.5 ± 4.7	2.8 ± 4.3
Wind speed (m/s)	2.3 ± 1.2	2.0 ± 0.9	3.0 ± 1.5	2.4 ± 1.0
RH (%)	70.1 ± 19.8	55.3 ± 16.8	89.2 ± 8.0	78.1 ± 9.5
Accumulated precipitation (mm)	367.0	222.1	89.2	68.1

Between 20 and 30 November, Warsaw experienced a pronounced episode of elevated eBC mass concentration, while no comparable increase occurred in Vilnius. The episode in Warsaw was likely associated with stagnant meteorological conditions: wind speed was below 4 m/s, and there was only a single day with precipitation (less than 2 mm). Such conditions favour the retention of pollutants within the urban environment, leading to higher pollution levels. Similar pollution build-up events under stagnant atmospheric conditions have been reported by Fourtziou et al. (2017), Kalinauskaitė et al. (2024), and Pauraite et al. (2022).

To further investigate the influence of meteorology, polar plots were generated to illustrate the relationship of wind speed, wind direction, and the corresponding mass concentrations of eBC_{FF} and eBC_{BB} ($eBC_{BB,C}$ in the cold season) in Warsaw. In the cold season, a pronounced directional dependence became clear. However, in the warm season (Figure 6A, B), eBC_{FF} and eBC_{BB} exhibited very similar patterns: the highest mean concentrations occurred under low wind speed conditions, and no substantial dependence on wind direction was observed.

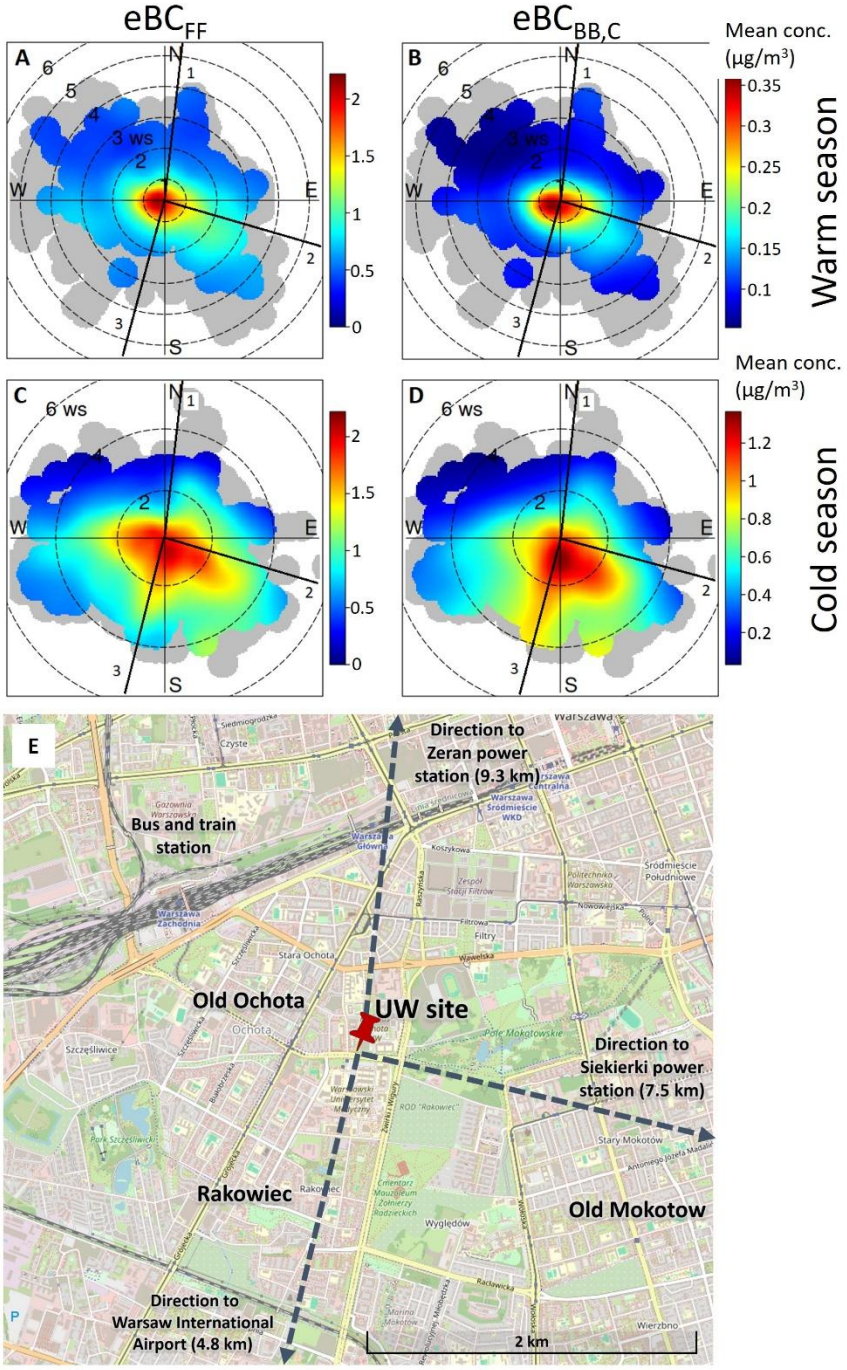

Figure 6. Polar plots of mean eBC_{FF} and $eBC_{BB,C}$ mass concentrations as a function of wind speed and wind direction for the warm season (A, B) and the cold season (C, D) in Warsaw, along with a map of the UW site (E).

During the cold season, a more pronounced directional dependence was observed (Figure 6C, D). Winds from the west, south, and southeast were associated with elevated mean eBC_{FF} concentrations. In contrast, the directional pattern for $eBC_{BB,C}$ differed notably from that of eBC_{FF}. Winds from the west did not result in increased $eBC_{BB,C}$ levels, whereas southerly winds had a substantially stronger effect. Elevated $eBC_{BB,C}$ concentrations were recorded even at wind speeds up to 4 m/s, indicating the presence of a strong $eBC_{BB,C}$ source south of the measurement site. Conversely, a source located west of the station appears to be dominated by eBC_{FF}. Generally, during the cold season, increased eBC concentrations occurred over a wider range of wind speeds than in the warm season, likely reflecting more active and diverse eBC sources within the urban area.

To facilitate the interpretation of potential eBC sources in Warsaw, directional lines were plotted for possible major sources in the city (Figure 6). The three principal sources considered were the Zeran power station (distance 9.3 km; direction: north; line 1 in Figure 6), the Siekierki power station (distance: 7.5 km; direction: east; line 2), and Warsaw International Airport (distance: 4.8 km; direction: south; line 3). Neither the Siekierki nor the Zeran power station contributed significantly to eBC mass concentrations at the measurement site.

Meanwhile, aircraft operations are known to emit up to 1 g of eBC per kilogram of burned fuel (Timko et al., 2014), leading to elevated eBC concentrations in the immediate vicinity of airports (Herndon et al., 2008). Additional airport-related eBC sources include ground support equipment and vehicular traffic associated with passenger and cargo transportation. However, in Warsaw, enhanced eBC concentrations from the airport direction were observed only during the cold season, indicating that the observed signal is not solely attributable to airport emissions but also seasonal emissions from the residential areas, e.g., Rakowiec. A similar enhancement is evident from the south-eastern sector, corresponding to the Old Mokotów district, characterised by dense urban development, narrow streets, older private houses and apartment buildings. Street canyon effects and associated small-scale airflow patterns can further influence eBC accumulation. In Warsaw, major roadways were planned and built to function as urban ventilation corridors, which can help dilute local pollutant concentrations but can also allow pollution to be transported into the city. This mechanism may partly explain the elevated eBC concentrations observed during the cold season under southerly wind directions.

All the above-mentioned sources remain possible; however, a higher level of confidence in source attribution would require the application of a

triangulation approach involving multiple measurement locations, as described by Carslaw et al. (2006).

Notably, when considering the relatively strict WHO guideline for $PM_{2.5}$ (daily mean of 15 μg/m^3 (WHO, 2021)), and assuming that eBC contributes no more than 15 % to $PM_{2.5}$ (2.25 μg/m^3), the results suggest that neither Warsaw nor Vilnius experienced exceedances during the warm season. During the cold season, only a limited number of high-pollution events were observed in Vilnius, whereas such events occurred more frequently in Warsaw.

3.1.1.2 Monthly variation of eBC

The monthly variability of eBC mass concentrations and differences in source contributions are presented in Figure 7. Beyond the generally higher mean eBC mass concentrations, eBC in Warsaw also exhibited greater variability, as indicated by the interquartile range (0.56–1.36 μg/m^3, 25th–75th percentile), compared to Vilnius (0.34–0.93 μg/m^3). The level of variability is comparable to that reported for other European suburban or urban background sites, including Bern and Zurich in Central Europe and Bucharest in Eastern Europe (Savadkoohi et al., 2023).

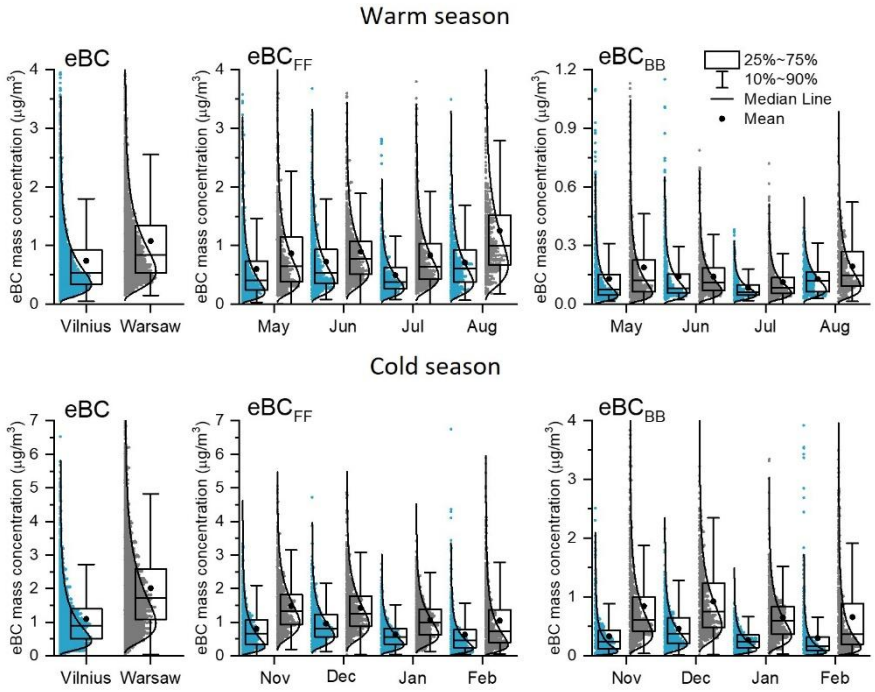

Figure 7. Box-and-whisker plots of eBC, eBC_{FF}, and eBC_{BB} mass concentrations in Vilnius and Warsaw during the warm and cold seasons.

During the warm season, the relative contribution of eBC_{BB} was similar in Warsaw (11–16 %, 25^{th}–75^{th} percentile range) and Vilnius (13–19 %) and remained substantially lower than that of eBC_{FF} in both cities (Table 3). In Vilnius, monthly eBC_{FF} concentrations were higher in June and August, whereas in Warsaw, an increase was observed only in August. The eBC_{BB} contribution followed a comparable pattern at both sites, with minimum values occurring in July.

During the cold season, variability in eBC mass concentration remained stronger in Warsaw (1.07–2.62 μg/m^3, 25^{th}–75^{th} percentile range) than in Vilnius (0.53–1.41 μg/m^3). Source contributions changed markedly compared to the warm season, with a substantially higher contribution of $eBC_{BB,C}$ accounting for 29–43 % in Warsaw and 24–33 % in Vilnius. Elevated $eBC_{BB,C}$ levels in Warsaw may be partly attributed to air mass transport from surrounding rural regions, where biomass and coal burning for residential heating are more prevalent than in large cities like Warsaw or Vilnius. In comparison, other Northern European cities typically experience lower eBC_{BB} contributions (25–34 %) than Warsaw, while urban background sites in Central Europe report even lower fractions, ranging from 24 % to 27 % (Helin et al., 2018; Savadkoohi et al., 2023). The higher $eBC_{BB,C}$ contribution observed in Warsaw suggests a more extensive use of solid fuels, such as coal and wood, for residential heating in Poland. Polish households account for approximately 87 % of all household coal consumption in the European Union (Macuk, 2019), a pattern that is significantly less pronounced in Lithuania.

3.1.1.3 Weekly variation of eBC

The weekly variation of eBC mass concentration for both seasons is presented in Figure 8. During the warm season, a consistent pattern was observed in both cities, characterised by higher eBC concentrations on weekdays and lower values during the weekends. In the cold season, the weekly cycle becomes more complex, with stronger day-to-day variability.

In both seasons and at both sites, eBC_{BB} and $eBC_{BB,C}$ contributions increase during weekends, whereas eBC_{FF} contributions are highest on working days. Elevated eBC_{FF} levels on weekdays could be influenced by increased traffic activities and more distinguishable traffic rush hours. In contrast, the enhanced weekend contribution of eBC_{BB} and $eBC_{BB,C}$ can be attributed to two main factors: (i) reduced eBC_{FF} emissions due to lower traffic intensity and limited industrial activity, and (ii) increased eBC_{BB} and $eBC_{BB,C}$ emissions. The latter arises from recreational activities such as bonfires and barbeques during the

warm season, as well as from greater residential heating demand during weekends in the cold season, when more time is spent indoors.

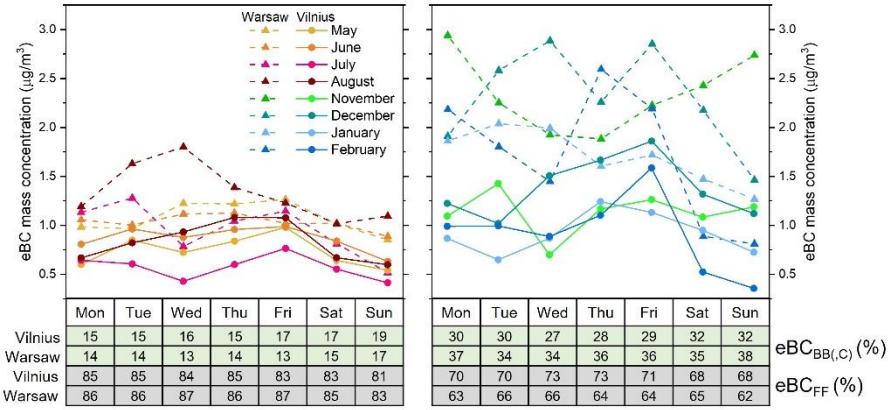

	Mon	Tue	Wed	Thu	Fri	Sat	Sun
Vilnius	15	15	16	15	17	17	19
Warsaw	14	14	13	14	13	15	17
Vilnius	85	85	84	85	83	83	81
Warsaw	86	86	87	86	87	85	83

	Mon	Tue	Wed	Thu	Fri	Sat	Sun
	30	30	27	28	29	32	32
	37	34	34	36	36	35	38
	70	70	73	73	71	68	68
	63	66	66	64	64	65	62

$eBC_{BB(,C)}$ (%)

eBC_{FF} (%)

Figure 8. Mean weekly eBC mass concentration by month for warm (left) and cold (right) seasons in Vilnius and Warsaw. Below are shown the mean daily contributions of $eBC_{BB,C}$ and eBC_{FF}.

3.1.1.4 Diurnal variation of eBC

The diurnal cycles of source-apportioned eBC mass concentrations are presented in Figure 9. In both seasons and both cities, eBC_{FF} exhibited a similar bimodal pattern, with the highest concentrations occurring on working days. The first peak appeared in the morning hours, followed by a second peak during the evening and continuing into the nighttime. The morning eBC_{FF} peak in both Vilnius and Warsaw reflects the strong influence of traffic exhaust emissions during rush hour. Concentrations subsequently decreased as temperature and mixing layer height increased, processes that promote atmospheric dilution (Yassin et al., 2018).

The evening peak shifted toward the evening rush hour (approximately 4–7 p.m., local time) and is linked to decreasing temperature and a corresponding reduction in mixing layer height. The shallower mixing layer enhances near-surface eBC accumulation, leading to elevated nighttime concentration, despite reduced traffic intensity. A clear seasonal difference in the timing of the evening peak was observed. During the warm season, elevated eBC_{FF} concentrations occurred mainly between 9 p.m. and 11 p.m., whereas in the cold season, they occurred earlier, between approximately 4 p.m. and 10 p.m. This shift was likely related to the earlier and more pronounced reduction in boundary layer height under colder conditions. In addition, domestic heating, including oil- and gas-based systems that

contribute to eBC_{FF} emissions, likely broadened and prolonged the evening peak during the cold season compared with warm season conditions.

The diurnal cycle of eBC_{BB} exhibited a slightly different cycle from eBC_{FF}. During the warm season, eBC_{BB} displayed a consistent bimodal pattern, whereas in the cold season, $eBC_{BB,C}$ concentrations showed low variability, particularly in Vilnius. The highest $eBC_{BB,C}$ concentrations were observed during the evening hours – especially on working days (between 6 p.m. and 11 p.m.) reaching up to 1.32 $\mu g/m^3$ in Warsaw, followed by a gradual decline overnight. In Warsaw, the lowest $eBC_{BB,C}$ concentrations (approximately 0.45 $\mu g/m^3$) occurred during daytime hours. In contrast, in the warm season, $eBC_{BB,C}$ in Vilnius exhibited a more complex diurnal behaviour, with minimum concentrations occurring at varying times, either during the day or at night. The generally elevated evening and nighttime concentrations were consistent with enhanced domestic heating activity and a reduction in boundary-layer height (Diapouli et al., 2017; Saarikoski et al., 2021). The more irregular patterns observed in Vilnius may be attributed to the smaller urban scale and a relatively stronger influence of air mass transport on local pollution levels. It should also be noted that isolated strong emission events can influence time-averaged eBC concentrations, as reflected in the monthly, weekly, and diurnal statistics; however, the analysis of such events is beyond the scope of the study.

Following the assessment of eBC mass concentrations and source apportionment results, the next section focuses on the optical properties of the aerosol particles.

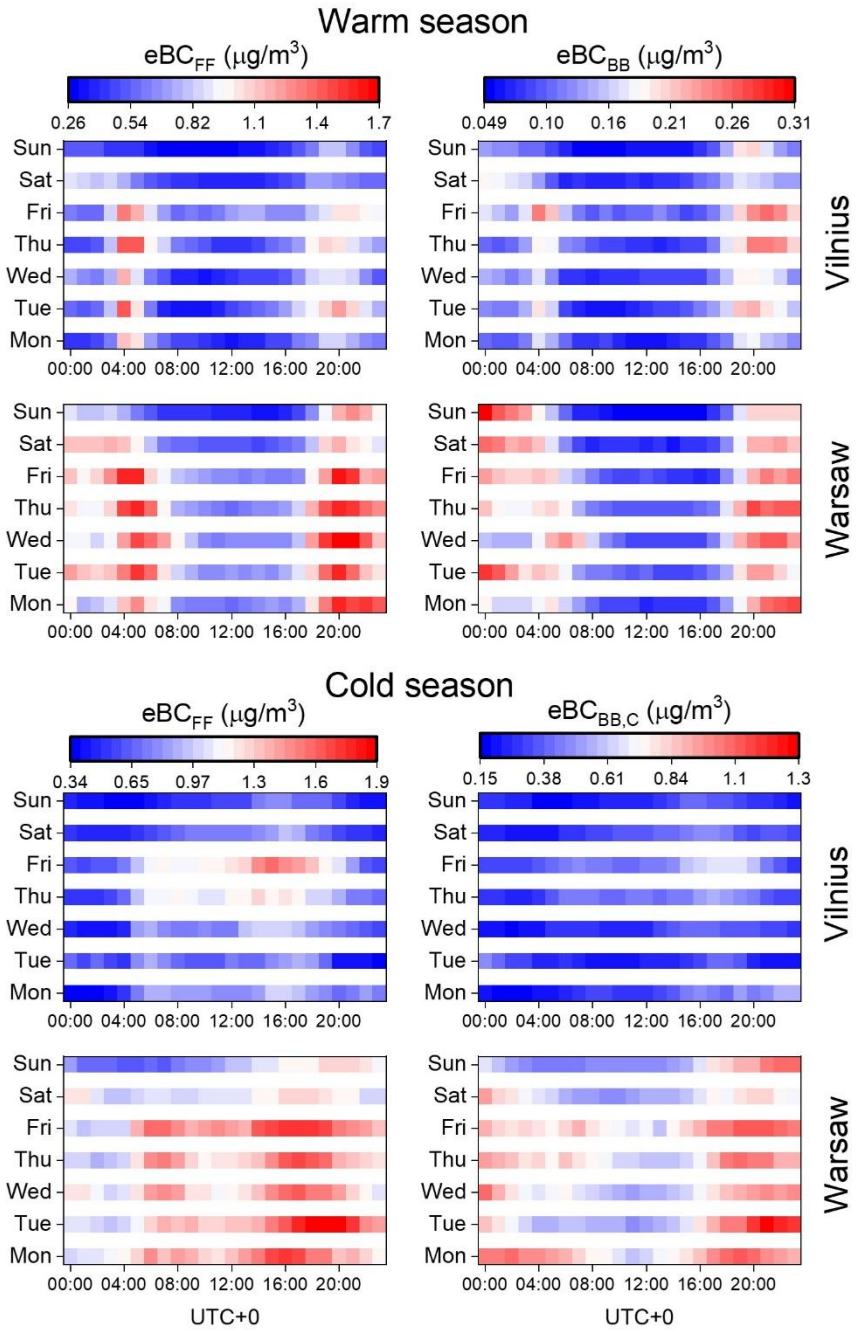

Figure 9. Diurnal cycles of source-apportioned eBC_{FF}, eBC_{BB} and $eBC_{BB,C}$ for the warm and cold seasons in Vilnius and Warsaw. Note the different scales.

3.1.2 Optical properties of aerosol particles

The AAE, SAE, and SSA were analysed to characterise optical properties in relation to eBC source contribution and mass concentration, and to compare these properties across seasons.

3.1.2.1 Aerosol light absorption

$AAE_{532/660}$ is a qualitative characteristic of carbonaceous aerosol particles, reflecting their origin and chemical composition. Results from the current study indicate that both Vilnius and Warsaw exhibited lower AAE values during the warm season (1.30 ± 0.07 in Warsaw and 1.26 ± 0.09 in Vilnius) compared to the cold season (1.53 ± 0.1 in Warsaw and 1.42 ± 0.1 in Vilnius; $p < 0.05$). Therefore, the source apportionment results (Section 3.1.1.1), which indicate higher $eBC_{BB,C}$ contributions, are consistent with the observed increase in AAE values, confirming a greater presence of biomass- and coal-burning-related carbonaceous aerosols during the cold season.

3.1.2.2 Aerosol light scattering

SAE is indicative of particle size, with lower values indicating a greater presence of larger particles predominating the aerosol mixture in the air. The mean $SAE_{450/550}$ values in Warsaw and Vilnius were lower during the cold season (1.20 ± 0.27 and 1.48 ± 0.38, respectively) compared to the warm season (1.62 ± 0.35 and 1.75 ± 0.35, respectively). Thus, the lower SAE values in the cold season at both sites imply an increased presence of larger particles, in contrast to the warm season when smaller particles predominated the aerosol mixture. This seasonal shift in particle size distribution could be influenced by a variety of factors, including meteorological conditions, atmospheric processes, and emission sources. A study by Pandolfi et al. (2018) in Central and Eastern Europe reported that the spring and summer months are characterised by higher concentrations of smaller particles and more frequent new particle formation events, leading to higher SAE values. Additionally, the higher relative humidity in the cold season (Table 3) provides more water vapour in the air, which can condense onto existing aerosol particles, promoting the particle growth to larger sizes. The lower boundary layer height and increased humidity during the cold season help keep aerosol particles closer to the ground, allowing the formation of water coatings on particles and the coagulation of smaller particles into larger ones (Winkler, 1988). Moreover, temperature inversions, which are common during the cold season, trap pollutants near the surface, reducing atmospheric dispersion. Combined with higher emissions from heating and traffic sources, this results in an

increased particle number concentration and enhanced coagulation of smaller particles into larger ones (Birmili et al., 2010).

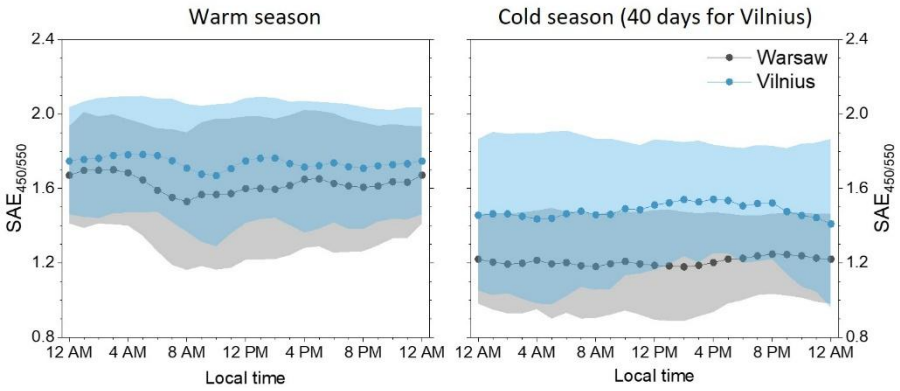

Figure 10. Diurnal cycles of SAE in Vilnius and Warsaw for the warm and cold seasons. The shaded area represents 1 standard deviation.

In addition, the diurnal cycles of SAE were examined. During the warm season at both sites, the SAE exhibited a pronounced diurnal minimum shortly after the morning rush hour (Figure 10), with the SAE values of 1.53 in Warsaw at 8 a.m. and 1.67 in Vilnius at 10 a.m. This behaviour may indicate particle growth following the morning rush hour and enhanced transport-related emissions (i.e., exhaust and non-exhaust traffic emissions, organic aerosol formation) (Alshetty & Nagendra, 2022).

In contrast, during the cold season in both Warsaw and Vilnius, the SAE diurnal cycles were comparatively flat, showing much weaker temporal variability than in the warm season. This suggests that SAE alone may not adequately capture diurnal changes in aerosol particle size distribution under cold season conditions, or that such changes are less pronounced throughout the day. The relatively uniform diurnal cycle may be influenced by emission sources such as domestic heating, which operates continuously throughout the day to maintain indoor temperatures, thereby leading to a more consistent influence on SAE. Nevertheless, the specific factors driving the weak diurnal variability during the cold season cannot be conclusively identified based on the available data.

3.1.2.3 Relationship between aerosol light absorption and scattering

The relationship between aerosol light absorption and scattering was investigated using the aerosol classification scheme proposed by Cappa et al. (2016), which derives dominant aerosol types and mixing states from combined absorption and scattering properties. Figure 11 illustrates the relationships of aerosol optical properties, eBC mass concentration, and the relative contributions of biomass and coal burning each month during both measurement campaigns in Vilnius and Warsaw.

During the cold season in Warsaw, the data points were distributed across four categories in decreasing order of occurrence: „Mixed dust/BC/BrC“ (the most prevalent, 55.3 %), followed by “Large particle/ eBC mix,” “BC dominated,” and “Mixed BC/BrC” (the least prevalent, 4.1 %) (Table 4). In Vilnius during the cold season, the dominant aerosol type was “BC dominated” (57.6 %), followed by mixed aerosol types in decreasing order: “Large particle/BC mix,” “Mixed BC/BrC,” and “Mixed dust/BC/BrC”.

In contrast, during the warm season, the “BC dominated” category was significantly prevalent in both Warsaw (83.7 %) and Vilnius (88.8 %). This indicates that aerosol particles are more frequently internally mixed during the cold season than in the warm season, with a higher occurrence of mixed aerosol types such as “Mixed dust/BC/ BrC,” “Large particle/BC mix,” and “Mixed BC/BrC.” This behaviour is consistent with the enhanced contribution of biomass- and coal-burning emissions (i.e., $eBC_{BB,C}$, and BrC) during the cold season, as discussed in the previous section and reported in previous studies (Kaskaoutis et al., 2021c; Kumar et al., 2023; Liakakou et al., 2020). The increased presence of BrC during the cold season in Poland, particularly from residential heating sources, is in agreement with findings by Kristensson et al. (2020).

Table 4. Contributions of the identified aerosol types in Vilnius and Warsaw during the warm and cold seasons.

		Mixed dust, BC/ BrC	Mixed BC/ BrC	Large particle/BC mix	BC dominated
Warm season	Vilnius	0.4 %	1.8 %	9.0 %	88.8 %
	Warsaw	0.3 %	1.0 %	15.1 %	83.6 %
Cold season	Vilnius	8.4 %	10.0 %	24.0 %	57.6 %
	Warsaw	55.3 %	4.1 %	34.3 %	6.3 %

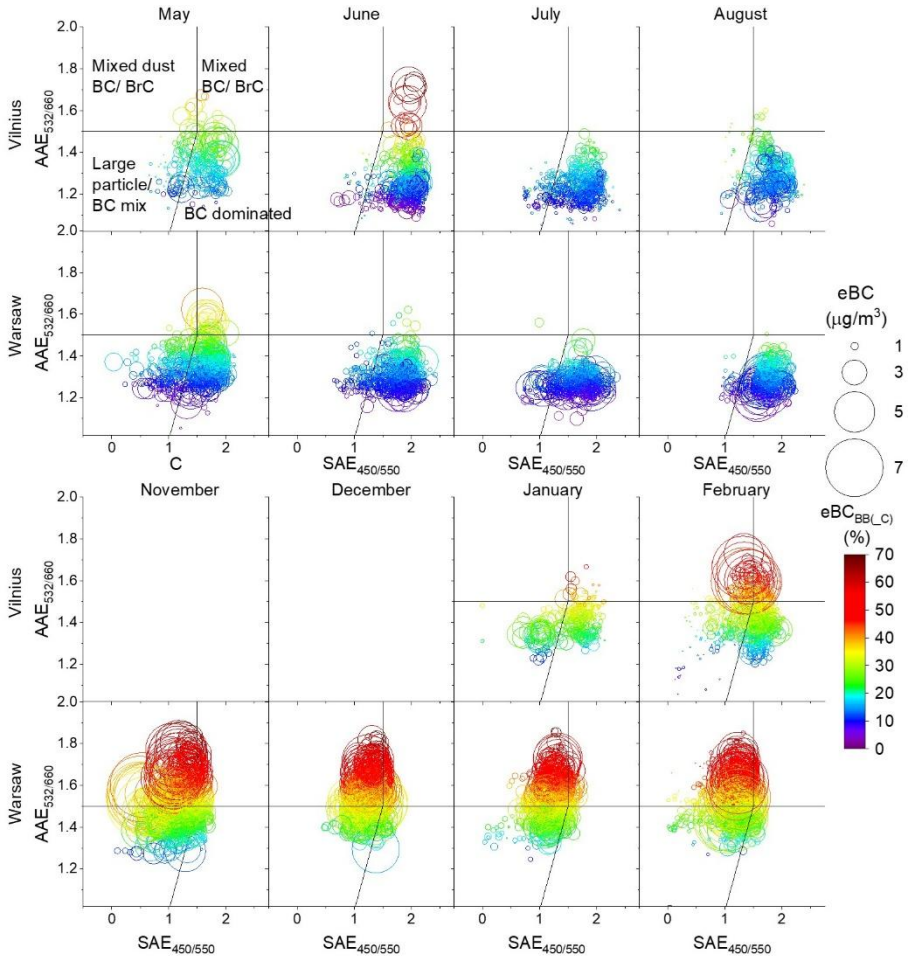

Figure 11. Relationship between AAE, SAE, eBC mass concentration, and biomass- and coal-burning contribution in the warm and cold seasons. The classification scheme is proposed by Cappa et al. (2016).

During the warm season, monthly variability was generally low, particularly during June–August in Warsaw and July–August in Vilnius. However, distinct deviations were observed in May in Warsaw and in June in Vilnius, when a higher fraction of data points fell within the "Large particle/ BC mix" and "Mixed BC/BrC" types. These episodes coincide with major national holidays – May Day celebrations in Warsaw (1–3 May) and Midsummer in Vilnius (24 June).

During the May Day celebrations, a national holiday period in Poland, including Labour Day, Flag Day, and Constitution Day, a significant increase in the biomass burning contribution (42 %) was observed. Temporary regulations during this period allowed barbecuing in designated public areas,

including the municipal park Pole Mokotowskie, located only a few hundred metres from the measurement site. These activities likely contributed to the observed enhancements in eBC mass concentration (up to 4.0 μg/m^3) and eBC_{BB} contribution.

A similar feature was observed in Vilnius in June, where the data points within the "Mixed BC/BrC" region exhibited the highest eBC mass concentrations during the warm season (hourly mean up to 4.4 μg/m^3) and highest biomass burning contribution (up to 43 %). During this episode, the increase in eBC mass concentration was threefold, while the eBC_{BB} contribution increased sevenfold compared to the monthly average. This episode was observed on Midsummer night, which is traditionally celebrated with bonfires and outdoor festivities. The pronounced biomass-burning signal observed during this night can therefore be attributed to leisure-related activities rather than residential heating. Due to cultural differences, no comparable event occurred in Warsaw in June.

Although these episodes are not prominently reflected in the eBC time series (Figure 4), they are clearly distinguishable in the aerosol optical properties and, consequently, in the aerosol classification scheme (Figure 11). The shifts associated with widespread barbecuing and bonfire burning differ from typical warm season aerosol mixtures and therefore stand out against the otherwise homogeneous warm season background.

Similarly, during the cold season, monthly variability in aerosol type distribution was relatively low from December to February, indicating broadly consistent aerosol mixing states. In contrast, the November dataset showed a stronger influence of larger particles, with an increased occurrence of the „Mixed dust/BC/BrC" and „Large particle/BC mix" types. Notably, the data points coincide with the episode when the highest eBC mass concentration (8.43 μg/m^3) during the cold season was recorded in Warsaw. Between 20 and 30 November, when eBC mass concentration and AAE values were elevated, while the SAE values were lower. This combination suggests that the aerosol particle mixture during the days was dominated by larger, supermicron particles, which also contained substantial amounts of light-absorbing eBC and BrC. The atmospheric conditions that favour the accumulation of pollution during this episode are discussed in Section 3.1.1.1.

Since SSA is the key parameter describing the influence of aerosol particles on atmospheric radiative transfer, it was examined in both cities and seasons. In Warsaw, the mean SSA during the cold season (0.84 ± 0.05) was comparable to that observed in the warm season (0.81 ± 0.07), although the difference between seasons was statistically significant ($p < 0.05$). A similar seasonal pattern was observed in Vilnius, where the mean SSA was higher

during the cold season (0.83 ± 0.07) than during the warm season (0.81 ± 0.08), with the difference also being statistically significant ($p < 0.05$).

During the warm season, hourly eBC_{FF} concentrations in both cities exhibited moderate negative correlation with SSA, with correlation coefficients ranging from -0.48 in Vilnius to -0.54 in Warsaw. In contrast, $eBC_{BB,C}$ showed weaker correlations with SSA (-0.36 in Vilnius and -0.35 in Warsaw). During the cold season, the correlations weakened for both eBC_{FF} and $eBC_{BB,C}$. The relationship between eBC_{FF} and SSA decreased to -0.10 in Vilnius and -0.18 in Warsaw, while correlations between $eBC_{BB,C}$ and SSA were -0.10 and -0.13, respectively.

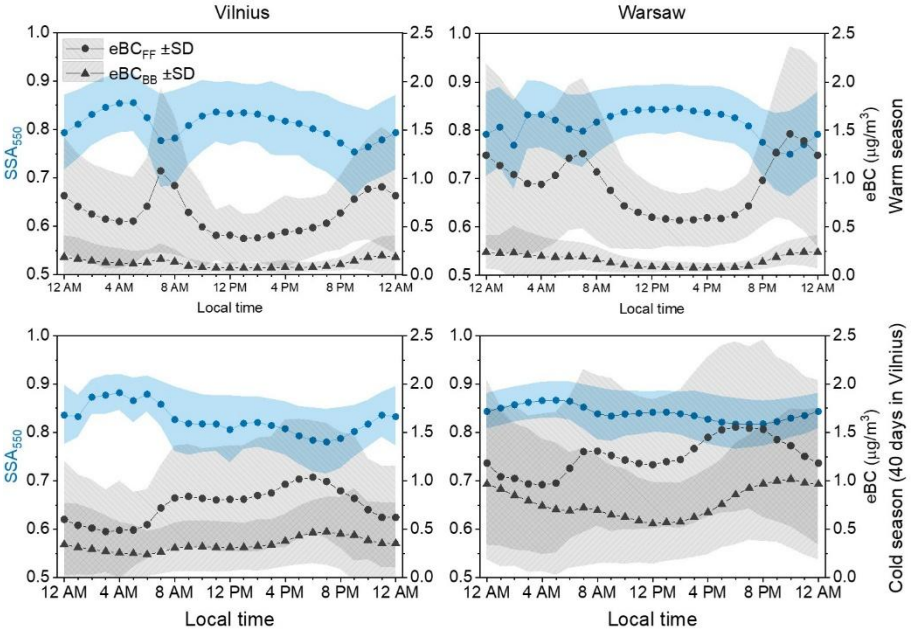

Figure 12. Diurnal cycles of SSA, eBC_{FF}, and $eBC_{BB,C}$ in the warm and cold seasons for Vilnius and Warsaw. The shaded area represents 1 standard deviation.

However, analysis of the diurnal cycles (Figure 12) revealed substantially stronger correlations between eBC_{FF} and SSA during both seasons, with values ranging from -0.69 (warm season in Vilnius) to -0.97 (cold season in Warsaw). The use of diurnal averages reduces the influence of short-term local fluctuations and highlights the underlying relationship between the parameters. As shown in Figure 12, increases in eBC_{FF} concentrations during traffic rush hours were accompanied by decreases in SSA, whereas higher SSA values occurred during periods of lower eBC_{FF} concentrations. This

behaviour reflects the enhanced light absorption associated with elevated eBC_{FF} levels, which leads to a reduction in SSA.

In contrast, correlations between $eBC_{BB,C}$ and SSA remained weaker across both cities and seasons, ranging from -0.07 (cold season in Warsaw) to -0.22 (cold season in Vilnius), suggesting no direct or weaker influence on SSA. Overall, the results prove a clear and direct relationship between fossil fuel combustion emissions and the aerosol radiative characteristic SSA.

3.1.3 Role of long-range air mass transport

3.1.3.1 Impact of long-range air mass transport on eBC pollution boosts or dilution

Further, the extent to which long-range air mass transport influences the boosting or dilution of eBC mass concentration and source contributions was assessed (Study No. 1). The study was conducted for the warm season campaign at the two sites. The analysis focused on the relationship between measured eBC and backward air-mass trajectories arriving at receptor sites, calculated using HYSPLIT. A total of 112 backward trajectories were classified into three main categories based on similarities in transport pathways and vertical structure, as described in Section 2.6.1.

The majority of cases (47) were assigned to Category A, characterised by overlapping trajectories with similar transport directions and comparable horizontal and/or vertical thresholds, suggesting coherent mesoscale transport conditions. Within this category, short-duration uniform trajectories (overlapping for less than 12 hours) were more frequent (25 cases), accounting for more than half of the cases. Semi-uniform trajectories, parallel in horizontal direction, occurred less often (15 cases). Long uniform trajectories, which overlapped for at least 36 hours, were comparatively rare (7 cases), indicating that prolonged stable transport conditions occurred infrequently during the warm season of 2022.

Category B, characterised by distinctly different transport pathways in both horizontal and vertical directions, represented a substantially smaller fraction of cases (17 cases). The remaining trajectories (48 cases) were assigned to Category C, encompassing cases with complex or transitional transport characteristics that could not be clearly categorised. Overall, the predominance of overlapping trajectories highlights the importance of regional-scale transport and mesoscale meteorology in shaping eBC variability, while distinctly divergent air mass pathways appear to play a secondary role.

For Category A, when trajectories arriving at the receptor sites were overlapping for 12 hours or more, eBC mass concentration behaviour was evaluated by distinguishing between pollution boosts or dilution by comparing consecutive 6-hour periods before and after the trajectory arrived at the receptor site. Simultaneous decreases in eBC mass concentration were observed at both sites in 20 cases, whereas concurrent increases were observed in 18 cases. Only 9 cases exhibited no clear trend. This pattern indicates that air masses following overlapping trajectories and arriving simultaneously at both sites exert a strong influence on local eBC mass concentration levels.

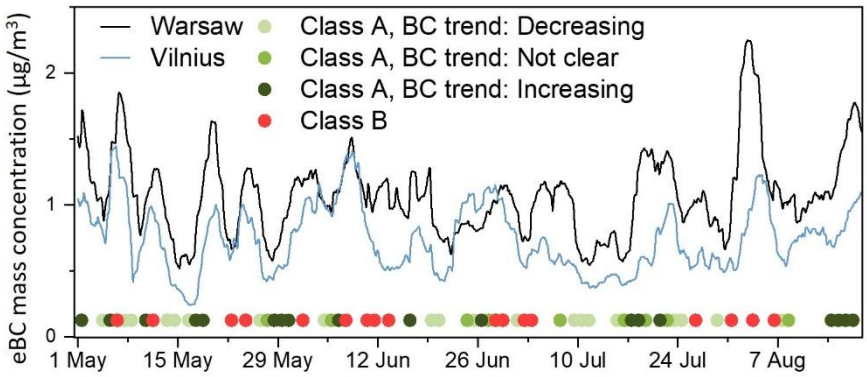

Figure 13. eBC mass concentration time series of 72-hour running mean for the warm season of 2022, together with circles marking air mass trajectory categories and simultaneous eBC mass concentration behaviour at the two sites.

Figure 13 illustrates the 72-hour running mean of eBC mass concentrations in Vilnius and Warsaw, with symbols indicating the air mass transport categorisation. Uniform air mass transport (Category A, green dots) with overlapping backward trajectories affecting both sites accounted for 42 % of the dataset. In contrast, distinctly non-uniform air mass pathways accounted for only 16 % of cases (Category B, red dots).

Within Category A, uniform air mass transport was associated with coherent eBC variability at both sites, manifested as either simultaneous decreases (20 cases, light green dots) or simultaneous increases (18 cases, dark green dots) in eBC mass concentration. Concurrent decreases can be explained by the ventilation effect, whereby cleaner air masses – often originating from northern regions – dilute pollution at both locations. On the contrary, simultaneous increases likely reflect the advection of polluted air masses from regions with elevated emissions, such as Western or Eastern Europe.

Long-range air mass transport is known to affect aerosol properties within the boundary layer over long distances. Previous studies have documented anthropogenic pollution intrusions from Germany to Warsaw (Stachlewska et al., 2017) and biomass burning intrusions from Ukraine (Stachlewska et al., 2018), both of which can alter aerosol optical properties.

To assess potential similarities at each site, when air mass trajectories were uniform or distinctly different, the results are presented as the diurnal cycles of eBC_{FF} and eBC_{BB} in consecutive rows (Figure 14). As expected, no clear patterns were observed for Category B, reflecting the different sources and inconsistent pathways of air masses, which prevented the trajectories from encountering one another or passing over similar regions. Any apparent similarities in this category are therefore considered accidental. In contrast, Category A exhibits more coherent patterns, reflecting either ventilation-driven decreases in eBC concentration (dilution) or eBC pollution enhancements (boosts) due to air mass transport.

Overall, the dilution of eBC was comparable at both sites (42 % in Warsaw and 50 % in Vilnius), whereas pollution boosts were more prominent in Vilnius (64 %) than in Warsaw (30 %). When considering eBC sources, pollution boosts were more significant for eBC_{FF} (27 % in Warsaw and 50 % in Vilnius) than for eBC_{BB} (7 % in Warsaw and 11 % in Vilnius). Similarly, dilution effects were stronger for eBC_{FF} in Vilnius (51 %) than in Warsaw (34 %), while eBC_{BB} dilution was comparable between the two sites (5 % in Vilnius and 8 % in Warsaw).

These findings suggest that biomass-burning-related eBC from long-range transport had a limited influence compared to local sources, as observed during national celebrations (e.g., May Days in Warsaw and Midsummer in Vilnius). In contrast, eBC_{FF} was substantially affected by long-range transport, resulting in both significant pollution dilution and enhancement events at both sites.

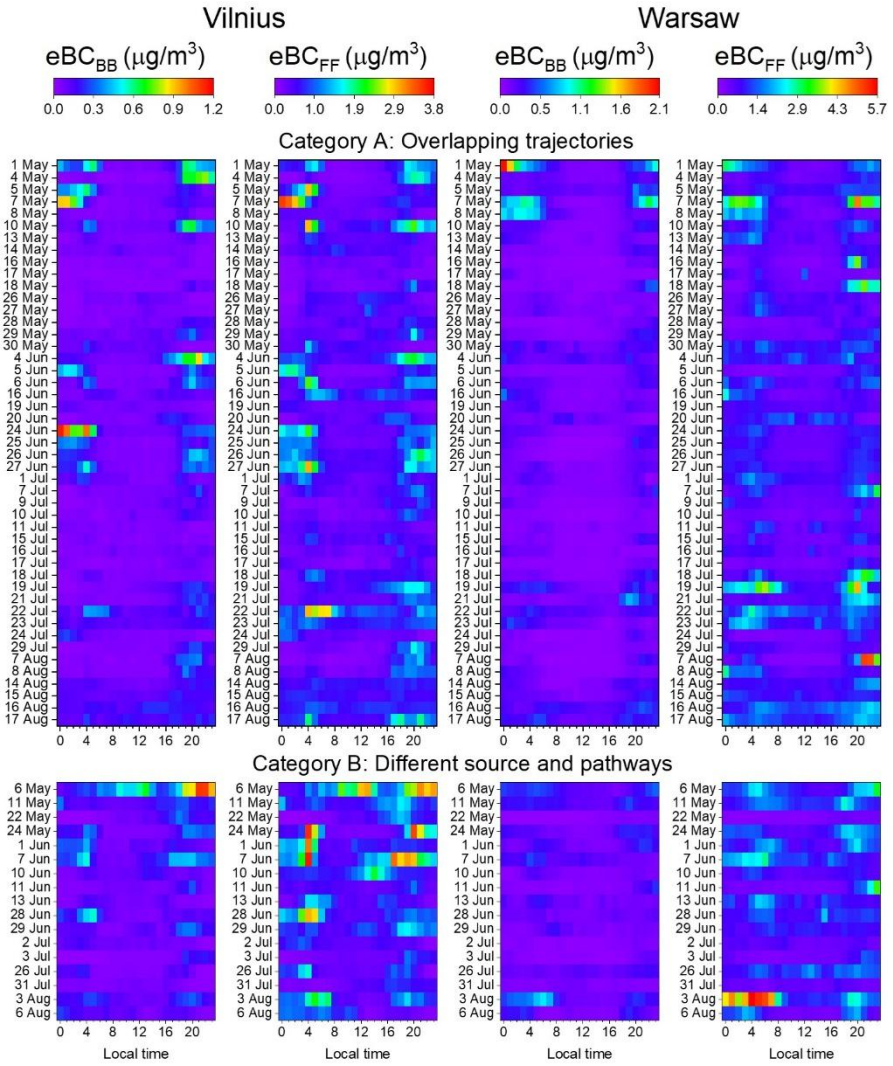

Figure 14. Heat maps of the diurnal cycles of eBC_{FF} and eBC_{BB} in Vilnius and Warsaw, presented for days when air mass trajectories were assigned to Categories A and B.

3.1.3.2 Comparison of measured eBC and modelled BC concentrations

For Study No. 2, the influence of air mass transport on eBC mass concentrations in both cities was investigated using FLEXPART model simulations for the warm and cold seasons. Comparisons between modelled and measured eBC mass concentrations are presented in Figure 15 for the warm season and Figure 16 for the cold season. eBC concentrations were simulated at two horizontal resolutions (0.5° × 0.5° and 0.1° × 0.1°), with the

finer resolution intended to better capture urban-scale transport. During the warm season, the agreement between modelled and measured eBC was moderate, with correlation coefficients ranging from 0.53 to 0.56 in both cities for both spatial resolutions.

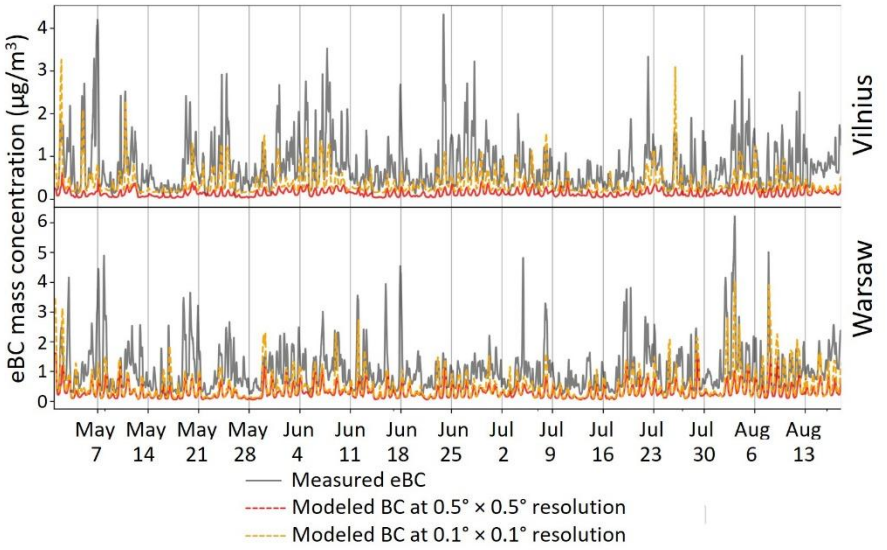

Figure 15. Time series of measured eBC and modelled BC mass concentrations in Vilnius and Warsaw during the warm season.

Notably, modelled BC concentrations were generally lower than the measured eBC mass concentrations in both cities. This discrepancy was expected given the relatively coarse spatial resolution of the FLEXPART model, which has mainly been applied in studies at background sites, where good agreement between modelled BC and measured eBC has been reported. At such sites, measured eBC largely reflects transported contributions, given the absence of strong local sources. In contrast, the measured eBC at the urban sites considered here represents a superposition of transported and locally produced BC. A clear difference was nevertheless observed between simulations performed at the two spatial resolutions, with higher BC concentrations obtained using the finer 0.1° × 0.1° resolution.

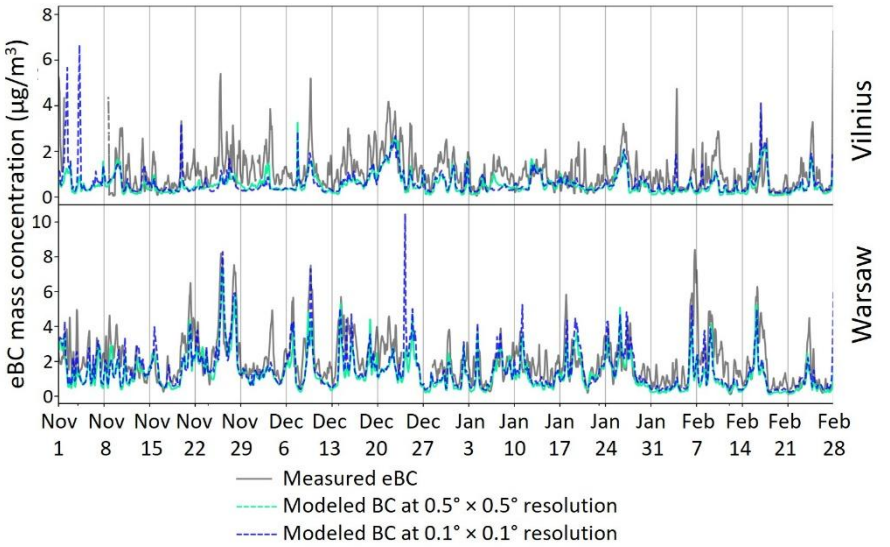

Figure 16. Time series of measured eBC and modelled BC mass concentrations in Vilnius and Warsaw during the cold season.

During the cold season, a moderate to strong correlation was observed between modelled BC and measured eBC concentrations. Correlation coefficients ranged from 0.61 in Vilnius to 0.70 in Warsaw for the 0.5° × 0.5°resolution and from 0.59 in Vilnius to 0.69 in Warsaw for the 0.1° × 0.1° resolution. Overall, the agreement between modelled BC and measured eBC was better in the cold season than in the warm season. Also, the absolute concentration of the modelled BC was closer to the measured eBC concentration in the cold season. In contrast, during the warm season, differences between the modelled BC concentrations obtained at 0.5° × 0.5° and 0.1° × 0.1° resolution were more pronounced (Figure 15).

In general, FLEXPART reproduces the observed eBC concentrations to a satisfactory degree. The overall temporal variability is primarily driven by long-range transport of BC from remote regions, while smaller-scale variations in the modelled concentrations reflect the influence of local (urban) emission sources.

To investigate the relationship between measured eBC and its source regions, contribution maps were calculated and averaged for each city, separately for high-concentration episodes (mean 3-hour eBC mass concentration above the 80th percentile of the season) and low-concentration episodes (mean 3-hour eBC mass concentration below the 20th percentile of the season). For brevity, only the contribution maps for Warsaw during the cold season on high-concentration episodes are presented in Figure 17, as this

site and season showed the highest eBC mass concentrations. The maps, generated using the 0.1° × 0.1° resolution data, display the contribution of BC from each model grid cell to the receptor site. Contribution maps for both seasons and sites, and both high- and low-concentration episodes, are provided in the Supplementary material (Figure 31 and Figure 32).

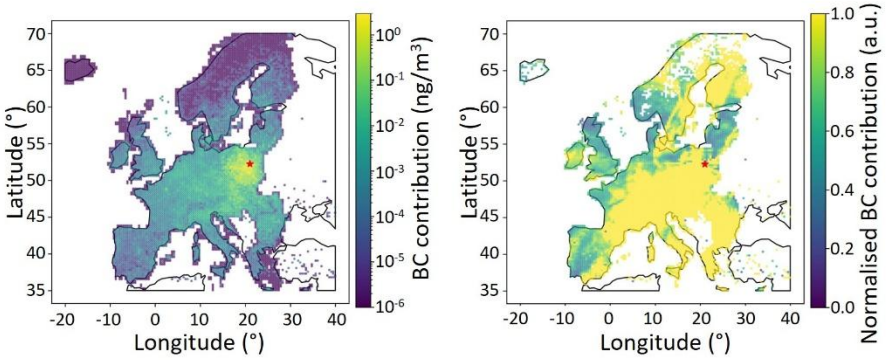

Figure 17. Absolute BC concentration and normalised BC concentration contribution maps for Warsaw during high-concentration episodes in the cold season.

For the warm season, the BC contribution maps revealed a general distinction between high- and low-concentration episodes. During high-concentration episodes, no clear dependence on specific emission regions was evident. In contrast, low-concentration episodes showed higher contributions from air masses originating in areas to the northwest of the cities, particularly Scandinavia.

The pattern is also evident during the cold season. During high-concentration episodes, BC predominantly originated from regions southwest of the cities, encompassing parts of Southern and Central Europe. In contrast, during low-concentration episodes, regions contributing to BC are more diverse, including Scandinavia and areas from Western and Southern Europe. These observations indicate that air mass transport can either dilute or enhance eBC concentrations measured in the city, depending on the amount of BC accumulated along the transport path, which is influenced by both the trajectory and the emissions along it.

In addition to identifying the source regions of BC emissions, modelled sector contributions were investigated and are presented in Figure 18 with numerical values provided in Table 5. Across both cities and seasons, the two dominant sectors contributing to BC mass concentration are domestic heating (DOM) and transportation (TRA).

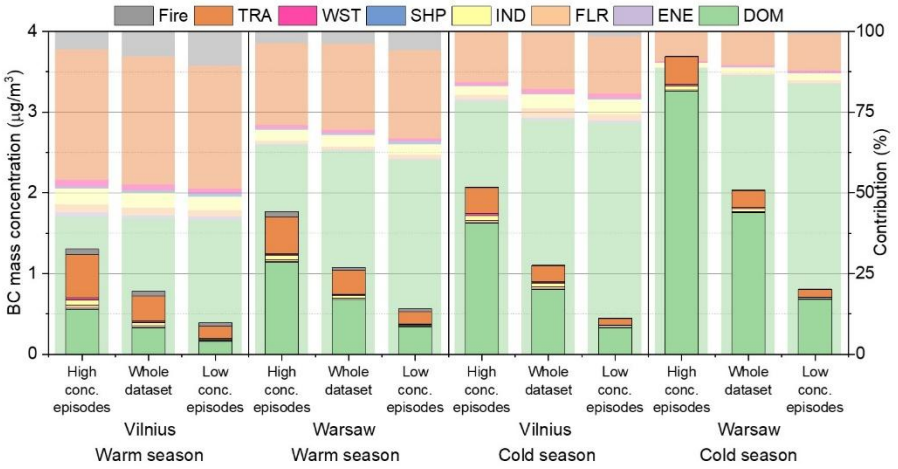

Figure 18. Stacked column graph of BC source sector contributions obtained with FLEXPART in Vilnius and Warsaw for high-concentration episodes, the whole dataset of a season, and low-concentration episodes.

During the warm season, DOM was the largest contributor in Vilnius, accounting for up to 43 % of BC during high-concentration episodes, while BC from TRA showed comparable contributions, reaching a maximum of 41 % on high-concentration episodes. In Warsaw, DOM accounted for the major fraction of BC (65 %), followed by the transport sector (27 %). During the cold season, DOM became the dominant source sector in both cities, contributing up to 78 % in Vilnius and 88 % in Warsaw during high-concentration episodes. The transport sector remained the second-largest contributor, with TRA contributions ranging from 11 % in Warsaw to 18 % in Vilnius during low-concentration episodes.

Comparing the two seasons, it is evident that DOM contributes more during the cold season than during the warm season in both cities, in both absolute and relative terms. The modelled sector contributions indicate that a larger fraction of BC in Vilnius originates from TRA compared to Warsaw. It is important to note that the source apportionment results presented in Section 3.1.1.1 quantify BC contributions by source (fossil fuel combustion, biomass- and coal-burning), while the FLEXPART results discussed here attribute BC to emission sectors. Although absolute eBC_{FF} mass concentrations were higher in Warsaw than in Vilnius, the results of sectoral analysis suggest that fossil fuel combustion in Warsaw contributes substantially to BC not only through transport but also through other sectors. In contrast, in Vilnius,

transport-related BC emissions account for a comparatively large share of total BC emissions, despite similar relative eBC_{FF} contributions in the two cities.

Table 5. BC source sector contributions obtained using FLEXPART in Vilnius and Warsaw for high-concentration episodes, the whole season dataset, and low-concentration episodes for the warm and cold seasons.

					Vilnius				
	Sector (%)	DOM	ENE	FLR	IND	SHP	WST	TRA	Fire
Warm season	Whole campaign	42	1	2	5	1	2	40	8
	High conc. episodes	43	1	3	5	1	2	41	6
	Low conc. episodes	42	1	2	4	1	1	38	11
Cold season	Whole campaign	73	1	3	4	0	1	17	1
	High conc. episodes	78	1	1	3	0	1	16	0
	Low conc. episodes	72	1	2	5	0	1	18	1.5
					Warsaw				
	Sector (%)	DOM	ENE	FLR	IND	SHP	WST	TRA	Fire
Warm season	Whole campaign	63	0	1	4	0	1	27	4
	High conc. episodes	65	0	1	3	0	1	26	4
	Low conc. episodes	60	0	1	3	1	1	28	6
Cold season	Whole campaign	86	0	1	2	0	1	10	0
	High conc. episodes	88	0	0	2	0	1	9	0
	Low conc. episodes	84	0	1	2	0	1	12	1

For this analysis, the 0.5° × 0.5° ECLIPSEv6b source contributions were used because of their clearly defined emission categories (Section 2.5.2). In addition to the sensitivity to spatial resolution (Figure 15 and Figure 16), the model results also depend on the choice of emission inventory. The sensitivity of FLEXPART-modelled concentrations to different inventories has been extensively evaluated in previous studies (Evangeliou et al., 2018; H. Jia et

al., 2021; M. Jia et al., 2023; Tichý et al., 2023), showing generally small differences. Bottom-up emission inventories tend to provide consistent spatial and temporal emission patterns at regional scales. Variations among inventories mainly arise from differences in sectoral allocation and assumptions about emission factors. However, it typically causes only modest differences in long-range transported BC concentrations.

Consequently, for applications focusing on synoptic-scale source-receptor relationships, such as in the present study, the choice among commonly used BC emission inventories has a relatively minor impact on source-receptor patterns compared to uncertainties related to transport, wet scavenging, and other meteorological processes (Sauvage et al., 2017; Zhu et al., 2020).

After characterising the properties of transported BC and its influence on urban BC concentrations, the following section introduces a novel approach to partition the measured eBC into locally produced and transported components.

3.1.3.3 BC partition into transported and city-produced components

The results of the BC source partitioning, separating the city-produced and transported contributions, were derived following the methodology described in Section 2.6.2 and are presented in Figure 19. The relative contributions of transported and locally produced BC differ substantially between the warm and cold seasons (Table 6). During the warm season, the 0.1° × 0.1° resolution model results indicate that BC in Vilnius was predominantly city-produced, accounting for 87 % on average (81–95 %, 25th–75th percentile range), while the transported BC contributed a minor part (13 % on average). A similar pattern was observed in Warsaw, where city-produced BC accounted for 77 % (65–90 %, 25th–75th percentile range) and transported BC for 23 % of the total measured eBC.

In the cold season, the relative importance of transported BC increased markedly in both cities (Table 6). In Vilnius, transported BC contributed 36 % on average (20–52 %, 25th–75th percentile range), with the remaining 64 % originating within the city, whereas in Warsaw, transported BC accounted for 53 % on average (39–70 %) and city-produced BC accounted for 47 %.

Increasing the excluded emission area from the city limits to radii of 20 km and 50 km resulted in a greater contribution of city-produced BC. This is due to the inclusion of emissions from adjacent towns and villages within the wider metropolitan area, which are then counted as part of the city-related BC rather than as long-range transported contributions.

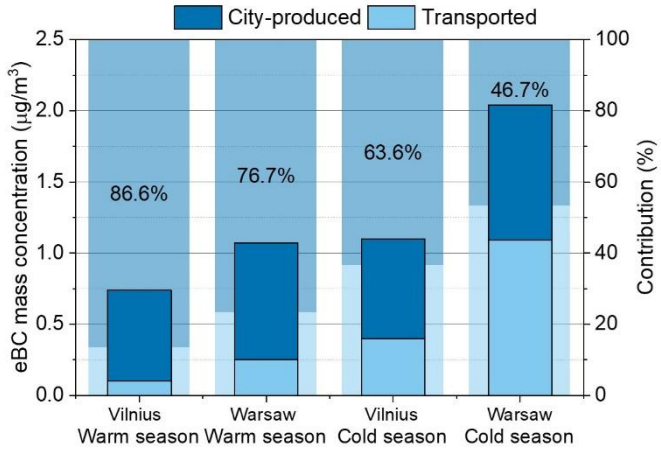

Figure 19. Stacked column graph of city-produced and transported BC contributions in Vilnius and Warsaw during the warm and cold seasons.

Table 6. Results of BC partitioning into transported and city-produced components, presented in both percentage and absolute mass concentration.

		Vilnius				**Warsaw**			
		Transported		City-produced		Transported		City-produced	
Removed contributions	Season	%	μg/m^3	%	μg/m^3	%	μg/m^3	%	μg/m^3
City limits	Warm	13	0.13	87	0.64	23	0.25	77	0.82
	Cold	36	0.40	64	0.71	53	1.09	47	0.95
20 km radius	Warm	11	0.08	89	0.66	20	0.22	80	0.85
	Cold	35	0.39	65	0.72	48	0.98	52	1.06
50 km radius	Warm	9	0.07	91	0.67	15	0.16	85	0.92
	Cold	33	0.37	67	0.74	39	0.79	61	1.25

Since the city-produced component of BC is calculated as the difference between measured eBC and modelled BC at the stations, the source partitioning results are strongly dependent on the FLEXPART simulations. Several factors may therefore contribute to uncertainties and potential errors:

- Biased wind direction. Although there could be biases in wind direction, this is highly unlikely, as the measurement campaigns lasted from 3 to 4 months, and therefore any biases should be smoothed out when investigating the campaign average.
- Horizontal resolution of the wind and transport model output. Beyond the grid size, spatial allocation plays a critical role, particularly for urban emissions, which are often represented using parameterisations developed for

long-range transport and spatially diffuse sources distributed across multiple grid cells. When emissions originate from many contributing grid cells, statistical robustness increases, and errors associated with numerical noise can be approximated as Gaussian, allowing small uncertainties to partially cancel out. In contrast, localised emission hotspots are much more sensitive to modelling uncertainties, and their representation can be strongly affected by resolution-related errors. In this study, the horizontal resolution of the FLEXPART simulations had a notable influence on the results. Increasing the resolution from $0.5° \times 0.5°$ to $0.1° \times 0.1°$ led to a substantial increase in modelled BC concentrations during the warm season (Figure 15), whereas the corresponding increase during the cold season was negligible (Figure 16).

- Vertical resolution and mixing layer height in the model. In the model, horizontal transport across neighbouring grid cells is most efficient within the mixing layer, i.e., below the modelled mixing-layer top. A lower mixing layer height facilitates the rapid escape of particles to higher altitudes, where they are transported away by horizontal advection. Once lifted above the mixing layer, the likelihood of particles descending back into the near-surface layer is reduced. Consequently, strong vertical mixing combined with a shallow mixing layer can lead to lower modelled BC concentrations at the receptor site. In contrast, a higher mixing layer height tends to retain particles in the lower atmosphere for longer, resulting in higher modelled concentrations. The influence of changes in the model's vertical resolution was not assessed within the scope of this study. However, the modelled mixing layer heights were compared with independent observations in Warsaw, derived from Doppler lidar measurements, and found to be in good agreement with those reported by Carneiro et al. (2024).
- Uncertainties in the emission inventories. FLEXPART estimates BC concentrations and source contributions at the receptor sites using bottom-up emission inventories, namely ECLIPSEv6b (Klimont et al., 2017) at $0.5° \times 0.5°$ resolution and GAINS emissions at $0.1° \times 0.1°$ resolution (Winiwarter et al., 2024). Overestimation of emission fluxes would result in elevated modelled BC concentrations at the receptor sites and, consequently, an underestimation of the city-produced BC fraction. Conversely, underestimation of emission fluxes would lead to lower modelled BC concentrations and an apparent increase in the derived city-produced BC contribution. In addition, discrepancies between the spatial distributions of emission hotspots in the inventories and their actual locations may introduce further uncertainties into the modelled BC concentrations and source-sector contributions.

Overall, air mass transport plays a significant role in affecting the eBC mass concentrations in both cities and across seasons, with a particularly strong influence during the cold season. A clear dependence of measured eBC mass concentrations in Vilnius and Warsaw on the spatial distribution of BC emission regions was observed. Moreover, source-sector analysis results indicate a pronounced dominance of BC from the DOM and TRA sectors in both cities and seasons, with domestic heating as the primary contributor during the cold season.

3.1.4 Chapter conclusions

Black carbon mass concentrations in urban environments (Vilnius and Warsaw) showed pronounced seasonal and spatial variability. Mean eBC mass concentrations were consistently higher in Warsaw than in Vilnius, reaching 1.07 μg/m³ and 0.77 μg/m³ in the warm season, and increasing to 2.02 μg/m³ and 1.11 μg/m³ in the cold season, respectively. Therefore, compared with the warm season, concentrations increased by about 89 % in Warsaw and 44 % in Vilnius during the cold season.

Concentration variability was largely driven by fossil-fuel-related emissions, which controlled both diurnal and weekly patterns. During the warm season, fossil-fuel-related eBC accounted for 86 % in Warsaw and 84 % in Vilnius on average, while in the cold season its contribution decreased to 63 % and 71 %, respectively, as the influence of biomass and coal burning increased. In the cold season, the contribution of biomass- and coal-burning-related eBC increased to 29–43 % in Warsaw and 24–36 % in Vilnius (25^{th}–75^{th} percentile range), indicating a stronger effect of residential heating emissions, especially in Warsaw.

Aerosol optical properties exhibited clear seasonal contrasts. Optical aerosol classification based on AAE and SAE indicated a substantially higher occurrence of larger particle mixtures containing mineral dust, BC, and BrC during the cold season, accounting for 94 % in Warsaw and 42 % in Vilnius. The AAE increased from 1.3 to 1.53 in Warsaw and from 1.26 to 1.42 in Vilnius, while the SAE decreased from 1.62 to 1.20 and from 1.75 to 1.48, respectively. Mean SSA values were comparable across seasons and cities, with the cold season showing slightly higher values (0.84 ± 0.05 in Warsaw and 0.83 ± 0.07 in Vilnius) than the warm season (0.81 ± 0.07 in Warsaw and 0.81 ± 0.08 in Vilnius). Despite similar seasonal averages, pronounced diurnal variability in SSA was observed, with a strong negative correlation with eBC_{FF} in both seasons (from -0.69 in Vilnius during the warm season to -0.97 in Warsaw during the cold season). The pronounced influence of fossil-fuel

combustion-related eBC on SSA underscores the role of these emissions in enhancing aerosol light absorption and thereby amplifying atmospheric warming.

Long-range air mass transport played a significant role in controlling eBC variability in both urban environments. Uniform long-range air masses arriving from similar directions caused comparable eBC dilution at both sites (42 % in Warsaw and 50 % in Vilnius). In contrast, pollution enhancements were markedly stronger in Vilnius (64 %) than in Warsaw (30 %). These effects were primarily driven by fossil-fuel-related black carbon, with substantially stronger responses in Vilnius (increases of 50 % and decreases of 51 %) compared to Warsaw (27 % and 34 %). In contrast, biomass burning-related black carbon showed only minor, comparable changes in both urban environments, with increases of 11 % and decreases of 5 % in Vilnius and increases of 7 % and decreases of 8 % in Warsaw.

FLEXPART modelling confirmed that domestic heating and transport are the dominant sources of BC. Domestic heating increased markedly from 63 % to 86 % in Warsaw and from 42 % to 73 % in Vilnius from the warm season to the cold season, indicating a strong influence of residential heating. In contrast, transport contributions decreased from 27 % to 10 % (Warsaw) and from 40 % to 17 % in Vilnius, emphasising the significant role of traffic emissions during the warm season. Despite the influence of air mass long-range transport, locally emitted black carbon remained dominant, contributing 77–87 % in the warm season and 47–64 % in the cold season, while the transported fraction increased during the cold season, reaching up to 53 % in Warsaw. Expanding the area of excluded city-produced emissions to include a 50 km radius around the measurement sites substantially increased the local contribution. Under this broader spatial definition, city-produced BC represented 85 % and 91 % of the measured eBC during the warm season, and 61 % and 67 % during the cold season in Warsaw and Vilnius, respectively.

3.2 Long-range transport influence on wintertime submicron aerosol chemical composition across Hyltemossa and Preila (Study No. 3)

In this chapter, the results of modelled long-range transport events across the two sites, Hyltemossa and Preila, are presented first. Then follows a comprehensive overview of the measurement campaigns at both stations, where differences between Hyltemossa and Preila are examined. In the later subsection, aerosol mass concentration changes are investigated for each event class as absolute and relative changes per event, and later scaled by air mass transport duration to account for differences in event duration. The last subsection considers and discusses the impacts of quantitatively assessed sea transport effects, wet deposition processes, and land-atmosphere interactions on PM_1 concentration and chemical composition.

3.2.1 Modelled connected-flow events

Using the HYSPLIT model in backward mode, 14 connected-flow air-mass transport events across Hyltemossa and Preila were calculated for the measurement campaign (from 1st December 2017 to 28th March 2018). Based on the classification presented in Section 2.6.5, the events were assigned to the event classes shown in Table 7.

Events consisted of 3 to 21 hourly trajectories. On average, the connected-flow event between Hyltemossa and Preila lasted 21 hours (± 11 hours). However, event durations ranged from 7 to 53 hours, as some trajectories turned south or north after passing over Hyltemossa (Figure 20). The trajectory height along the pathway ranged from 8 to 665 m a.s.l., with an average of 130 (± 103) m a.s.l. The altitudes indicate that the investigated air masses were transported within the marine boundary layer for most of the time, given that the modelled boundary layer height on average was 465 (± 255) m a.s.l. Also, observations from previous studies indicate that the marine boundary layer height in the North Sea and the southern Baltic Sea typically exceeds 400 m during roughly three-quarters of the winter period (Gryning & Batchvarova, 2003; Krogsæter & Reuder, 2015), consistent with the modelled values obtained here.

Precipitation occurred during eight events. The approach for determining the total accumulated precipitation for events with multiple trajectories is described in Section 2.6.7 and illustrated in Figure 3.

Table 7. The descriptive statistics of events. Number of hourly trajectories constituting an event (traj. no.), duration of trajectory (t), trajectory height (h), pressure (p), air temperature (T), relative humidity (RH), and accumulated precipitation (prec.) obtained from the GDAS archive at NOAA for each long-range transport event between Hyltemossa and Preila. The duration of the trajectory and meteorological parameters are presented as average values with standard deviation values (± SD). Precipitation is depicted as a cumulative total over the entire event duration.

Class	Event	Traj. No.	t [h]	h [m]	p [hPa]	T [°C]	RH [%]	Prec. [mm]
A	HP7	3	23 ± 0	70 ± 32	994 ± 8	4 ± 0	84 ± 2	-
	HP8	3	12 ± 1	107 ± 66	1014 ± 12	1 ± 1	68 ± 3	-
	HP9	6	24 ± 1	125 ± 50	1017 ± 10	2 ± 1	87 ± 2	-
	HP10	4	22 ± 3	128 ± 68	1004 ± 12	3 ± 1	92 ± 3	-
	HP11	10	10 ± 1	92 ± 24	999 ± 4	4 ± 1	85 ± 4	-
	HP12	5	14 ± 1	88 ± 42	1003 ± 8	3 ± 1	83 ± 3	-
B	HP1	4	11 ± 1	93 ± 62	990 ± 13	3 ± 1	71 ± 6	2.3
	HP2	4	22 ± 1	55 ± 38	992 ± 9	4 ± 1	79 ± 6	1.6
	HP5	14	8 ± 0	59 ± 27	995 ± 7	8 ± 1	86 ± 3	3.2
	HP6	21	14 ± 3	101 ± 45	989 ± 10	7 ± 1	91 ± 4	7.4
C	HP3	12	49 ± 3	181 ± 129	994 ± 20	1 ± 1	82 ± 6	0.7
	HP4	11	35 ± 5	96 ± 77	1008 ± 17	2 ± 1	91 ± 2	0.4
	HP13	5	27 ± 4	99 ± 41	1005 ± 7	-2 ± 2	70 ± 3	0.7
	HP14	12	24 ± 3	216 ± 135	978 ± 20	1 ± 0	90 ± 4	0.3

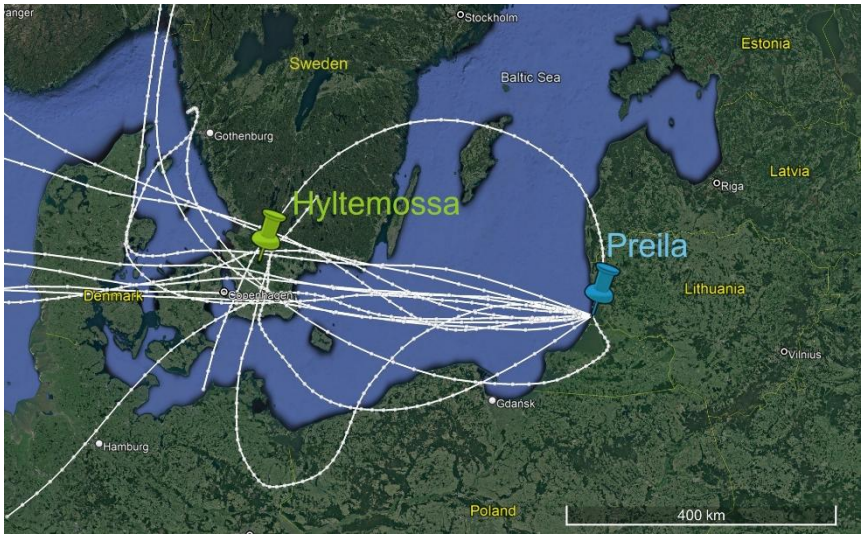

Figure 20. Map of the connected-flow events across Hyltemossa and Preila over the Southern Baltic Sea. Each line represents one event, and the dots mark 1-hour intervals.

3.2.2 Campaign overview

3.2.2.1 Meteorological parameters

To understand how local weather conditions differed at the two sites, meteorological parameters (T, RH, prec., and WD) were investigated. Both sites experienced similar air temperatures, as indicated by the Kruskal-Wallis test, which showed no significant difference between the two medians ($p > 0.05$). During the campaign, the average air temperature was -1.0 °C in Preila and -0.1 °C in Hyltemossa, with median values of 0.1 °C and 0.2 °C, respectively. February was the coldest month at both sites, with average monthly temperatures of -4.7 °C in Preila and -2.5 °C in Hyltemossa, while December was the warmest month, with average monthly temperatures of 3.3 °C in Preila and 2.5 °C in Hyltemossa. The lowest temperature in Preila (-17.4 °C) was recorded on the same day (February 28, 2018) as in Hyltemossa (-13.2 °C). Similarly, the maximum temperature in Hyltemossa (9.4 °C) was recorded on December 23, followed shortly before by the maximum temperature in Preila (8.4 °C) on December 24. The mean RH during the campaign was 84 % in Preila and 92 % in Hyltemossa, with the driest period observed in March (on average 78 % in Preila and 86 % in Hyltemossa). The total amount of precipitation during the campaign was 137.9 mm in Preila and 158.8 mm in Hyltemossa. The prevailing wind directions during the measurement campaign in Preila were southwest (180–210 °) and north-northeast (30–40 °). In Hyltemossa, the prevailing wind directions were southwest (200–230 °) and northeast-east (40–100 °). Thus, the results show good agreement with those of a previous study by Soomere (2003), which showed anisotropy in wind directions in the Baltic proper. In the study, it was found that the angular distribution of the highest wind directions had maxima at the south-west and north winds, while the minimum was for easterly winds. Therefore, prevailing wind directions enable the prediction of the most likely pollution source regions reaching the remote measurement sites. Given all the above, it can be concluded that the Preila and Hyltemossa sites are comparatively similar in their meteorological conditions.

3.2.2.2 PM_1 chemical composition

The time series of PM_1 mass concentration and chemical composition are presented in Figure 21. Throughout the campaign, the absolute PM_1 mass concentrations at the two sites were distinctly different ($p < 0.01$). The mean PM_1 concentration in Hyltemossa was 6.26 µg/m^3, while Preila showed almost twice as high a PM_1 concentration of 11.16 µg/m^3. In Hyltemossa, the concentrations of most aerosol components (OA, NO_3, Chl, NH_4, and eBC) were lower than in Preila, where concentrations were generally higher ($p < 0.01$ for the discussed components). However, sulphate exhibited a higher concentration in Hyltemossa (1.03 µg/m^3) than in Preila (0.51 µg/m^3). The relative contribution of sulphate to the total PM_1 concentration was also higher in Hyltemossa (16 %) than in Preila (5 %).

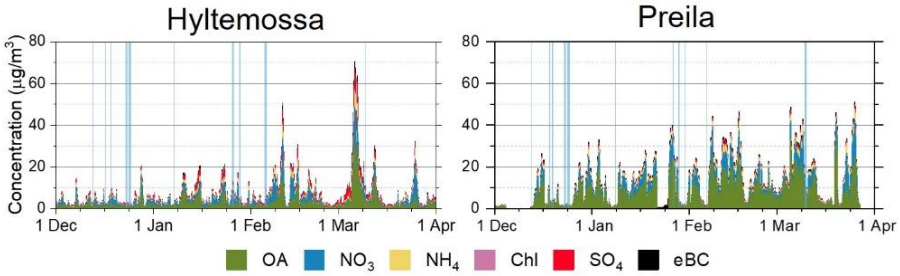

Figure 21. Stacked time series of PM_1 chemical composition at Hyltemossa and Preila during the wintertime measurement campaign of 2017–2018. The blue vertical lines mark the time intervals when an air mass departed from Hyltemossa and arrived at Preila during the connected-flow events.

The relative PM_1 chemical composition was comparable at the two sites, with OA as the dominant aerosol component in both Hyltemossa (39 %) and Preila (28 %) (Figure 22). Nitrate was the second most abundant component, accounting for 24 % in Hyltemossa and 28 % in Preila. At both sites, ammonia, eBC, and Chl contributed only minor fractions of PM_1, accounting for 11 %, 4 %, and 2 % in Hyltemossa and 9 %, 4 %, and 1 % in Preila, respectively.

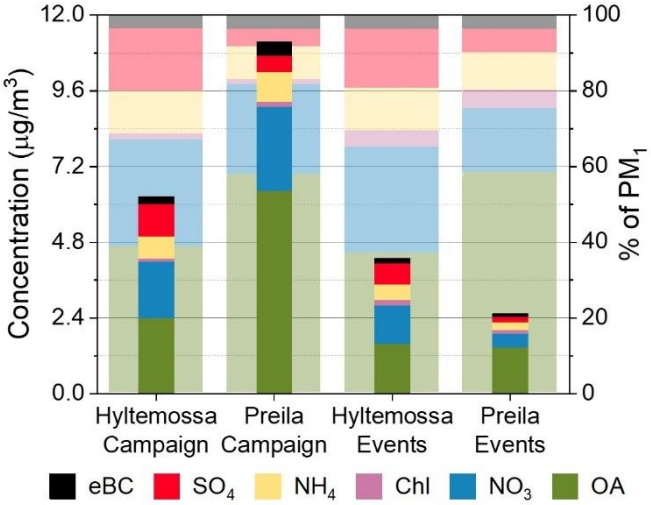

Figure 22. Stacked column graph of PM_1 mass concentration and relative chemical composition averaged for the measurement campaign and for the long-range transport events across Hyltemossa and Preila.

The relatively high levels of nitrate and sulphate in Hyltemossa suggest a strong impact from long-range transported pollutants. Despite the predominantly south-westerly winds at the site, the highest sulphate concentrations are associated with east-southeast winds, while the highest nitrate concentrations are associated with southern winds (Figure 23). Likewise, Ahlberg et al. (2023) reported the impact of anthropogenic emissions from continental Europe, especially eastern Europe, on PM_1 levels in Hyltemossa. Similarly, the elevated contributions of nitrate and sulphate in Preila indicate a substantial influence of long-range transported pollutants on local air quality, as no significant local emission sources are present near the measurement site. The highest sulphate concentrations in Preila were associated with wind directions from the southeast, although a more consistent and stronger sulphate source appeared to the northeast (Figure 23). The sulphate source from the southeast is likely attributable to anthropogenic emissions from regional sources, such as the Kaliningrad region, where domestic heating relies on coal and wood burning (Davulienė et al., 2019). In contrast, the potential northeast source of sulphate could be linked to the Klaipėda shipping harbour, located 36 km to the northeast.

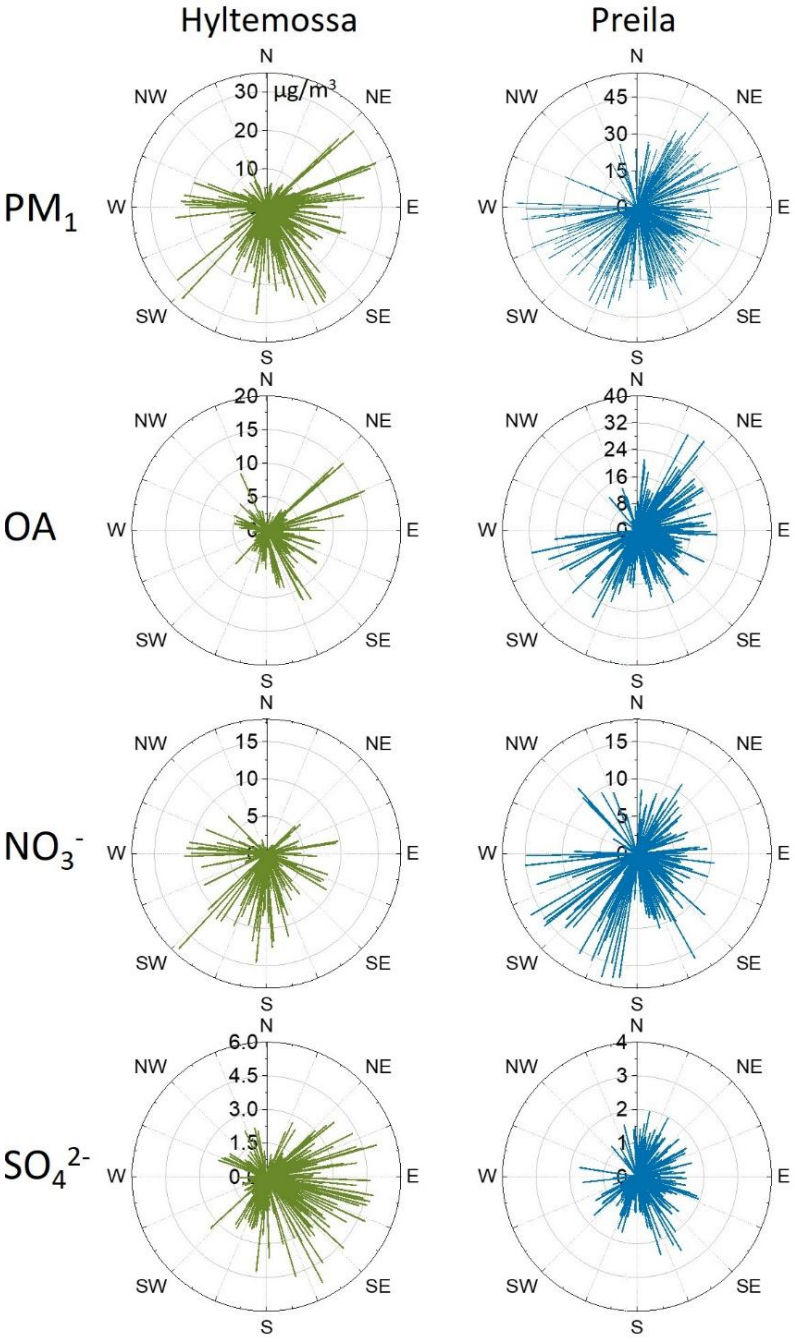

Figure 23. Wind roses illustrating pollutant concentrations associated with the corresponding wind directions at Hyltemossa and Preila. The radial axis shows the absolute pollutant concentration, with increasing radius corresponding to higher concentrations.

During the connected-flow events across Hyltemossa and Preila, the average PM_1 concentration in Hyltemossa was 35 % lower than the campaign average for the site ($p < 0.01$) (Figure 22). However, the chemical composition was relatively similar: organics dominated (37 %), followed by nitrate (28 %), sulphate (16 %), and ammonia (9 %). Chloride was the only investigated component to show an increase during the events, with a 79 % increase in absolute concentration (0.18 μg/m^3) and a 4 % increase in relative contribution compared to the campaign average for Hyltemossa. This increase could be explained by the high proportion (86 %) of trajectories during events arriving at Hyltemossa from the Kattegat, Arkona Basin, and the Danish Straits, where the air masses likely contained sea-salt aerosols emitted by sea spray (Quinn et al., 2017). Similar to Hyltemossa, the PM_1 concentration in Preila was significantly lower (77 %) during the events (2.53 μg/m^3) than during the campaign ($p < 0.01$) (Figure 22). The chemical composition changed due to a decrease in nitrate (17 %) and an increase in chloride (5 %) contributions. Although the absolute chloride concentration in Preila was similar during the events (0.13 μg/m^3) and the campaign (0.15 μg/m^3; $p > 0.05$), its higher relative contribution during the events likely reflects the aerosol uptake along the sea. It is important to note that although the absolute eBC concentration was lower during the events compared to the campaign average, the eBC fraction of PM_1 remained unchanged at both sites (4 %). During the events, the eBC mass concentration measured in Preila was 41 % lower than in Hyltemossa. Overall, the findings reveal substantial changes in PM_1 concentrations between the two sites during both the campaign period and events, which can be attributed to differences in air-mass origin and transport pathways.

3.2.2.3 OA source apportionment

There were three OA factors identified at both sites during the entire measurement campaign: oxygenated OA (OOA) and two types of OA from biomass burning (BBOA1 and BBOA2) (Figure 24).

During the campaign, the predominant OA component was OOA at both sites (63 % in Hyltemossa and 50 % in Preila). Similar to the total PM_1 concentration, OA absolute concentration was also twice as high in Preila (3.15 μg/m^3) as in Hyltemossa (1.52 μg/m^3). The relative contribution of BBOA factors at both sites was comparable in Hyltemossa (17 % of BBOA1 and 21 % of BBOA2) and Preila (28 % of BBOA1 and 21 % of BBOA2). However, the absolute concentrations of BBOAs in Hyltemossa were significantly lower ($p < 0.01$) than in Preila, indicating a strong influence of biomass-burning-related pollutants in the remote marine location. These

results are consistent with previous studies conducted in Preila during the cold season, which reported a strong influence of wood and coal burning (78 % (Kristensson et al., 2020); 58−82 %, (Mašalaitė et al., 2024)). In contrast, the lower BBOA concentrations in Hyltemossa may reflect differences in prevailing domestic heating systems in the surrounding region, where biomass-based residential heating is no longer the primary method or has been replaced by more advanced technologies (Pettersson et al., 2020).

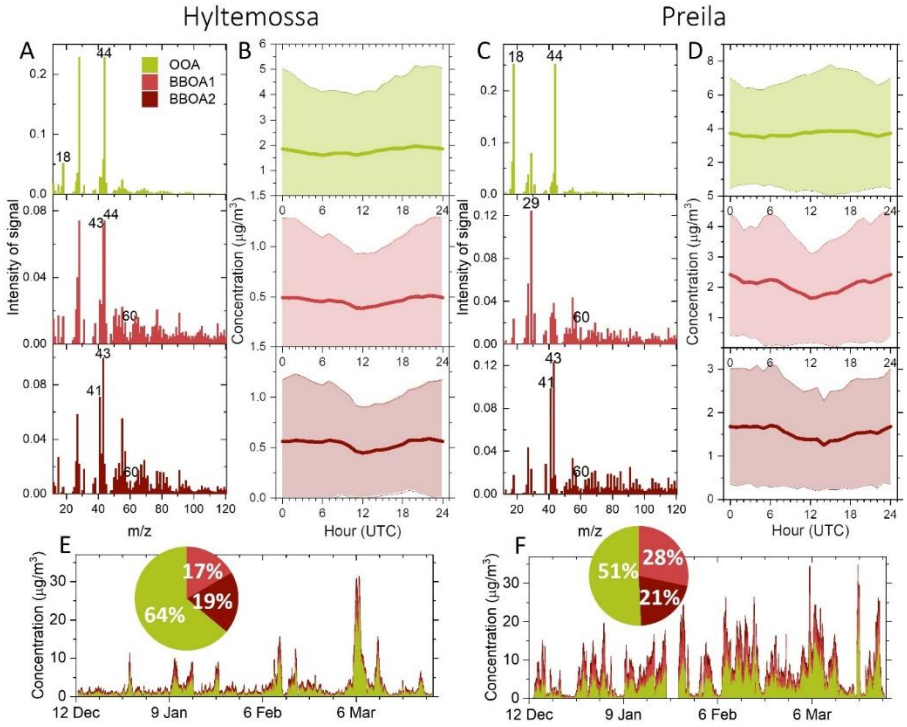

Figure 24. OA source apportionment results: mass spectra (A, C), diurnal trends (B, D), and time series with pie charts showing OOA, BBOA1, and BBOA2 contributions to the total OA (E, F) in Hyltemossa and Preila.

The observed significantly higher ($p < 0.01$ for all OA factors) concentrations of OA in Preila can likely be explained by the proximity of Preila to emission sources in the Kaliningrad region, located about 80 km away from Preila with coal and gas power plants (Davulienė et al., 2019), as well as to the city of Klaipėda, located 40 km to the north. Previous studies have also shown that the annual open-field grass fires (agricultural waste burning) in the Kaliningrad region occurring during March have a strong influence on the OA and eBC concentrations in Preila (Byčenkienė et al.,

2013; Dudoitis et al., 2016; Ulevicius et al., 2016) and even further regions in Northern Europe (Niemi et al., 2009).

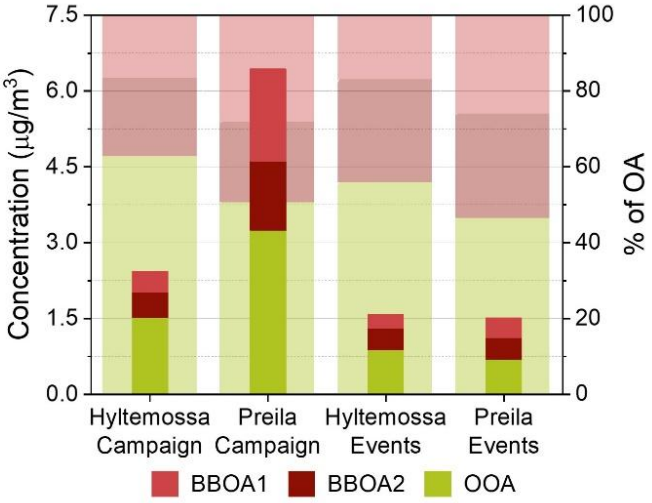

Figure 25. Stacked column graph of source apportioned OA mass concentration and relative composition averaged for the measurement campaign and for the long-range transport events across Hyltemossa and Preila.

However, significant differences were observed in the concentrations of all OA components between the campaign averages and the event averages at both sites. In Hyltemossa, OA concentrations during events were on average 31 % lower than the campaign mean (42 % for OOA, 33 % for BBOA1, 15 % for BBOA2), with statistical significance observed only for OOA ($p < 0.01$), while for the BBOA factors it did not differ significantly ($p > 0.05$) (Figure 25). In contrast, Preila exhibited substantially lower OA concentrations during the events, with reductions of 78 % for OOA, 78 % for BBOA1, and 70 % for BBOA2 compared to the campaign averages ($p < 0.01$ for all OA factors). These results indicate that among all potential wind directions, the westerly air masses characteristic of the HP events are associated with markedly lower OA levels, suggesting that transport over the sea mitigates OA pollution arriving at Preila. Based on these findings, the subsequent sections focus on the investigation of pollutant removal or dispersion during the events.

3.2.3 Assessment of aerosol mass concentration changes

In the next step, both meteorological impacts and spatial factors were considered. The events were classified as described in Section 2.6.5: Class A containing 6 events (HP7–HP12), Class B with 4 events (HP1, HP2, HP5, HP6), and Class C with 4 events (HP3, HP4, HP13, HP14). To derive more general insights into changes in aerosol chemical composition and aerosol mass removal or addition, the PM_1 chemical composition was averaged within each class at both sites (Figure 26). The corresponding source-apportioned OA concentrations and relative contributions for Hyltemossa and Preila, averaged by event class, are also shown in Figure 26. Based on this classification, the observed reductions in PM_1 during the events were expected to reflect the combined effects of the investigated processes: sea transport, wet deposition process, and land-atmosphere interactions.

As discussed earlier, PM_1 concentrations during the events were consistently higher in Hyltemossa (4.23 μg/m^3 in Class A, 3.96 μg/m^3 in Class B, 5.99 μg/m^3 in Class C) than in Preila (2.1 μg/m^3 in Class A, 1.17 μg/m^3 in Class B, 4.37 μg/m^3 in Class C). This pattern was observed across all three event classes. In Class A, which represents events without precipitation, the average 50 % reduction in PM_1 concentration (ranging from 43 % to 59 % for an individual event) suggests a substantial influence of sea transport on aerosol loading. In Class B, the addition of precipitation led to an even larger reduction in PM_1 (70 % on average, with individual events ranging from 28 % to 87 %), indicating an additional effect of wet deposition. Thus, in Class B, both sea transport and precipitation contributed to the observed decreases in PM_1. In Class C, PM_1 concentrations and chemical composition were influenced by the combination of all three investigated factors. Notably, PM_1 reductions during Class C events were considerably lower (27 % on average), with changes ranging from a 65 % reduction to a 28 % increase per event. Class C was the only class in which PM_1 concentrations were occasionally higher in Preila than in Hyltemossa. Although air masses in all event classes passed over the Baltic Sea, Class C is distinguished by an additional air mass transit over land before reaching Preila. The relatively small reductions observed in Class C suggest the influence of anthropogenic emissions encountered over land. This phenomenon is more effectively concealed by dilution, dry deposition, wet deposition, and other processes, which play a role in Classes A and B.

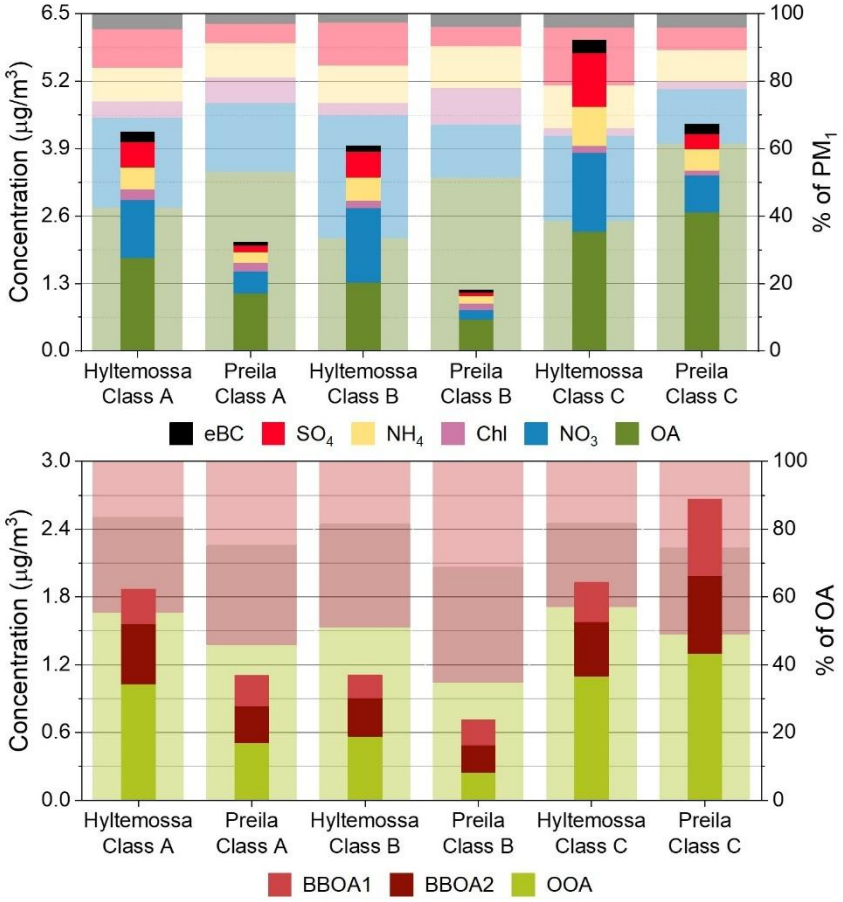

Figure 26. Stacked column graphs of PM_1 (top) and OA (bottom) mass concentration and relative composition averaged for each class of the events in Hyltemossa and Preila.

Before further examining the effects of sea transport, wet deposition, and land-atmosphere interactions, it is important to note that the PM_1 reductions discussed above were calculated for entire events. However, the average event duration varied substantially among the event classes: 17 h for Class A, 14 h for Class B, 34 h for Class C. Consequently, expressing the results solely as absolute relative changes per event does not provide the most informative basis for comparison. Therefore, using the relative change per hour offers a more robust metric, as it accounts for event duration and enables meaningful comparisons across different event classes regardless of trajectory length or duration.

3.2.4 Assessment of hourly aerosol mass concentration changes

For each aerosol component, the relative and absolute hourly mass concentration changes were calculated as presented in Section 2.6.6, equations 14 and 15. Grouped by event class, the changes in aerosol component concentrations per hour are presented in Figure 27 and Table 8 in the supplementary material. However, the relative concentration changes better highlight the variations across all aerosol components, including those with lower ambient concentrations (Chl, NH_4, SO_4, eBC, BBOA1, and BBOA2). The variations are less apparent when focusing solely on the absolute mass concentration changes. Also, presenting the absolute concentrations would be mainly meaningful in locations with similar PM_1 concentrations and chemical compositions. While relative changes allow the qualitative effects of long-range air mass transport on PM_1 to be assessed, even when the baseline concentrations differ across regions. Therefore, the following section focuses on relative concentration changes per hour, although absolute mass concentration changes are provided both numerically and graphically. This ensures clarity in the main discussion while keeping absolute values available to the reader.

In Figure 27, the relative change of chloride concentration is distinguishable from all other aerosol components in Class A. Chloride is the only component to show an increase during the long-range transport over the Baltic Sea (4 %/h on average). This may be due to the high chloride content in marine aerosol (89 %), originating from sea salt released into the atmosphere during wave breaking (A. U. Lewandowska & Falkowska, 2013b). The total PM_1 decrease (-3 %/h) in Class A was mainly driven by sulphate (-5 %/h). In contrast, other aerosol components showed relative hourly decreases ranging from -1 %/h (BBOA1) to -4 %/h (eBC).

In Class B, all PM_1 components decreased more significantly than in Class A. Only chloride exhibited a relative increase (1 %/h), though less pronounced than in Class A. With precipitation included as a factor in Class B, these reductions in aerosol concentrations are attributed to wet deposition processes.

An opposite pattern emerged in Class C, with several components showing increased concentrations. BBOA1 showed the strongest increase in mass concentration (3 %/h), followed by BBOA2 (2 %/h) and chloride (2 %/h). A plausible explanation is that transport across the continental region allowed air masses to acquire additional aerosol particles from more sources than those over marine areas. This potential uptake over land is analysed in the following section.

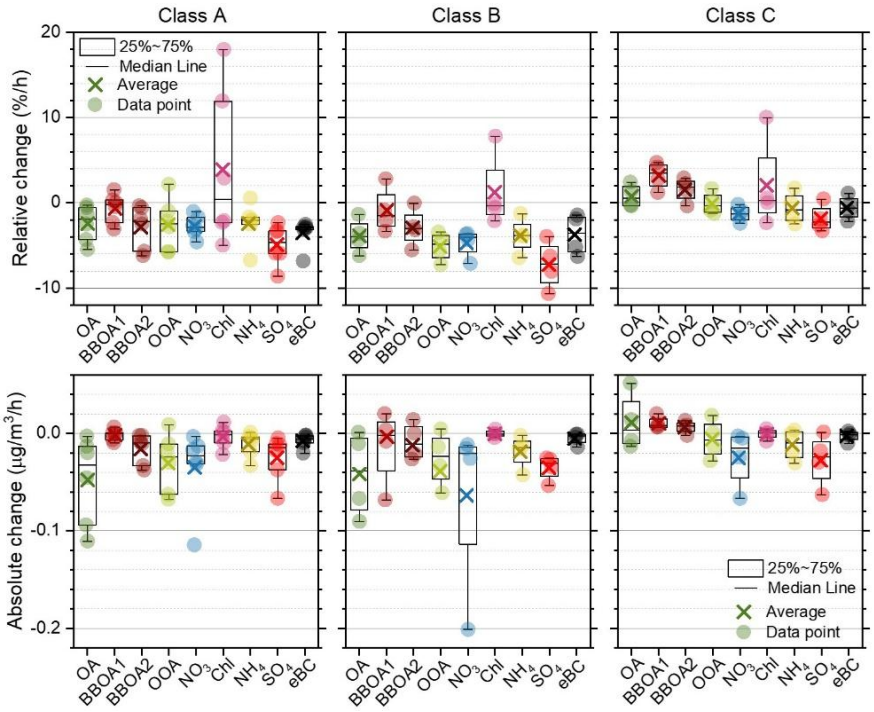

Figure 27. The relative and absolute hourly mass concentration changes for each aerosol component during events in Classes A, B, and C. Source apportioned OA components (BBOA1, BBOA2, OOA) are presented along with OA.

3.2.5 Influence of sea transport, wet deposition processes, and land-atmosphere interaction

To evaluate the combined effect of multiple processes on aerosol chemical composition and concentration – air mass transport over seas, wet deposition processes, and air mass movement over land, the results for all three classes were compared. As previously addressed, the effects of sea transport, wet deposition, and land-atmosphere interactions reflect the net outcomes of dilution, dry deposition, wet deposition, and other processes that occur simultaneously or in sequence during long-range air mass transport. To account for differences in transport time, the relative mass concentration changes were normalised by trajectory duration and averaged per aerosol component within an event class.

The sea transport effect on PM_1 composition is observed in Class A, as there are no other factors playing a role in the class. As shown in Figure 28, the combination of processes during long-range transport over the sea

mitigates PM_1, reducing concentrations of all aerosol components except chloride, which shows an increase. The decrease in aerosol mass during Class A events likely results from several effects, including dry deposition over the sea surface and dilution with cleaner air above. Additional mechanisms may involve chemical transformations and aerosol-cloud interactions, as discussed below.

The strongest sea transport effect was observed for sulphate, with a decrease of -5 %/h. Previous studies of marine aerosol in the southern coastal Baltic Sea have demonstrated substantial sulphate removal when particles grow under high relative humidity and are efficiently scavenged as large, hydrated aerosol particles (A. U. Lewandowska & Falkowska, 2013a). Ammonia plays a key role in neutralising sulphuric and nitric acids in the troposphere, promoting the formation of larger particles and enhancing their susceptibility to precipitation (Jung et al., 2011). Furthermore, Sasakawa et al. (2003) reported that anthropogenic ions, such as sulphate and ammonium, are effectively scavenged as sea fog duration increases. The reduction in inorganic PM_1 components observed in Class A is therefore consistent with previously documented patterns.

The total OA decrease (-2 %/h) was moderate, with the largest reduction observed for BBOA2 (-3 %/h), while BBOA1 showed a smaller reduction (-1 %/h). A decrease of -4 %/h was also observed for eBC. Although eBC is inherently hydrophobic, it can, under certain conditions, acquire a more hydrophilic coating composed of secondary inorganic aerosols (SIA) or secondary organic aerosols (SOA), which promotes particle growth and facilitates its removal (Shan et al., 2021). Ahlberg et al. (2023) similarly reported that eBC particles at the Hyltemossa site exhibited thicker coatings, likely consisting of SIA and SOA.

The increase in chloride concentration indicates uptake of sea-salt aerosol by the air mass during transport over the sea, consistent with sodium chloride being the dominant component of sea-salt aerosol. In the southern Baltic Sea, a study by Lewandowska and Falkowska (2013b) found that marine aerosol generation was more frequent in the cold season. While this study was conducted in the cold season, the findings highlight the potential for future studies that apply this approach to assess sea-transport effects on PM_1 composition during the warm season.

Considering the wet deposition processes, a clear cleaning effect on total PM_1 was observed, with concentrations decreasing by -1 % per event hour. This overall reduction included decreases in OOA, nitrate, chloride, ammonium, and sulphate (Figure 28, Table 8). The inorganic species, being more hygroscopic, readily dissolve in rain or fog droplets, which enhances

their removal via wet deposition (Shan et al., 2021; Shrivastava et al., 2017). The reduction in OOA is consistent with the findings of Witkowska et al. (2016), who reported that OC is efficiently removed by precipitation, particularly rainfall. In contrast, the concentrations of BBOA1, BBOA2, and eBC were less influenced by precipitation (Figure 28, Table 8).

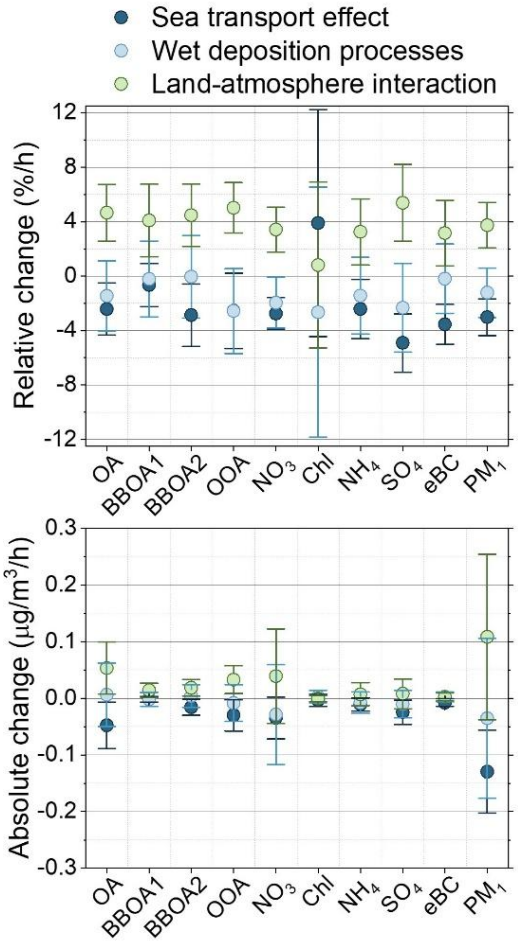

Figure 28. The impact of the sea transport effect, wet deposition processes, and land-atmosphere interaction on individual aerosol components and total PM_1 is presented as relative and absolute concentration changes per hour. Source-apportioned OA components (BBOA1, BBOA2, OOA) are presented along with OA.

Finally, the third factor examined – the land-atmosphere interaction – showed a contrasting behaviour, as it no longer mitigates PM_1 concentrations. Air mass trajectories associated with Class C events (HP3, HP4, HP13, HP14)

passed over continental areas of northern Germany, Poland, western Latvia, and Lithuania before reaching Preila, indicating that the observed increases in aerosol concentrations are attributed to pollution uptake over land. As shown in Figure 28, the land-atmosphere interaction resulted in increases in all PM_1 components, with an average rate of 4 %/h.

Although the southern Baltic coast is less densely populated than inland areas, substantial emissions have been reported from the Gdynia Tri-City region (population of ~1 million), particularly from domestic heating and road transport (A. U. Lewandowska et al., 2018). The Report on Air Quality in Europe by the European Environment Agency (2020) announced increasing $PM_{2.5}$ levels at both urban and rural background sites despite reductions in PM_{10} emissions. Lewandowska et al. (2010) identified the port, domestic heating, and traffic as the main sources of EC and OC in the Tri-City area, which contribute significantly to OC levels and account for 31.6 % of PM_{10} mass. A later study by Witkowska et al. (2016) also highlighted substantial EC and OC pollution originating from shipyards, port facilities, chemical plants, and food-processing industries in this urbanised coastal region.

In the present study, pollution uptake over continental areas had a pronounced effect on OA, with the strongest increase observed for OOA (5 %/h). Increases in biomass-burning-related OA components likely reflect residential heating emissions, as the southern Baltic coast near the Tri-City is surrounded by smaller towns and villages where low-capacity domestic heating units are common (Zgłobicki & Baran-Zgłobicka, 2024). Chloride showed the smallest increase (1 %/h), consistent with its predominantly marine origin. However, a slight enhancement may also arise from the emissions associated with chemical and industrial activities in the region.

Wind roses presented in Figure 23 show that winds arriving at Preila from the southwest consistently carry higher PM_1 concentrations. Overall, this approach enables quantification of the regional contribution to PM_1 concentration and composition in a relatively clean marine environment with no local pollution sources.

3.2.6 Chapter conclusions

The study examined the influence of long-range transport over the sea on PM_1 concentration and chemical composition during the 2017–2018 cold season, based on four months of simultaneous measurements at two remote sites along the southern Baltic Sea. Using HYSPLIT, 72-hour backward air mass trajectories were modelled, originating upwind of Hyltemossa (Sweden), crossing the Baltic Sea, and extending 500 km downwind to Preila (Lithuania). The resulting hourly trajectories were subsequently grouped into 14 long-range transport events. The availability of simultaneous measurements at both sites enabled assessment of the same air mass before and after crossing the Baltic Sea. Throughout the full measurement campaign, PM_1 concentrations in Preila were nearly double those in Hyltemossa (11.2 $\mu g/m^3$ and 6.3 $\mu g/m^3$, respectively). However, during the identified long-range transport events, Preila consistently exhibited lower PM_1 concentrations (2.5 $\mu g/m^3$) than Hyltemossa (4.3 $\mu g/m^3$).

Based on hourly HYSPLIT meteorological parameters, each event was assigned to one of three classes defined by meteorological and spatial factors. Class A events occurred over the Baltic Sea and experienced no precipitation; during the events, an average 50 % decrease in PM_1 concentration was observed after transportation from Hyltemossa to Preila. During events when precipitation occurred along the pathway of the air mass trajectory (Class B), the decrease in PM_1 concentration was larger (70 %), proving the influence of wet deposition processes. In contrast, events in Class C, where air masses passed over land before reaching Preila, showed the smallest net decrease (27 %). The findings suggest that the aerosol removal processes evident in Classes A and B were partially obscured in Class C by additional pollution uptake during transport over land, where such uptake is expected.

The classification proposed in the study enabled examination of the net effects of atmospheric aerosol processes during long-range transport: the sea transport effect, wet deposition processes, and land-atmosphere interaction. Under sea transport conditions, chloride was the only component that increased in concentration during transport over the sea (4 %/h), whereas sulphate showed the strongest removal (-5 %/h). Wet deposition processes had the highest effect on chloride (-3 %/h) and OOA (-3 %/h). In contrast, land-atmosphere interaction led to increases in all aerosol components, ranging from 5 %/h (sulphate) to 1 %/h (chloride).

MAIN CONCLUSIONS

1. Long-range air mass transport has a significant, although secondary, influence on urban eBC mass concentration variability, driving both pollution dilution (50 % on average) and enhancement (64 % on average) events, predominantly affecting fossil-fuel-related emissions. FLEXPART modelling further confirmed that, despite this influence, locally emitted black carbon remains the dominant source, contributing on average 77 % and 87 % in Warsaw and Vilnius during the warm season, respectively, and on average 47 % and 64 % in Warsaw and Vilnius during the cold season, while the transported fraction increases significantly in the cold season (53 % in Warsaw and 46 % in Vilnius). This demonstrates that urban air quality is primarily governed by local emissions, with long-range transport of air masses acting as a dynamic factor.

2. Regardless of the higher concentration of eBC in Warsaw (on average 1.07 μg/m³ and 2.02 μg/m³ during the warm and cold seasons, respectively) than in Vilnius (on average 0.77 μg/m³ and 1.11 μg/m³), the relative source distribution remains similar: eBC_{FF} contribution dominates in both cities (84–86 % in the warm season; 63–71 % in the cold season), while the cold season introduces a significant but secondary contribution from biomass and coal burning (29–37 % of total eBC). Seasonal increases, particularly pronounced in Warsaw, reflect winter amplification of combustion emissions under reduced atmospheric mixing.

3. Domestic heating and transport are the dominant contributors to BC emissions, with domestic heating becoming the leading contributor in the cold season (on average 86 % in Warsaw and 73 % in Vilnius), while transport plays a comparatively larger role in the warm season (on average 27 % in Warsaw and 40 % in Vilnius). These results demonstrate that urban BC variability is primarily controlled by traffic-related emissions, with seasonal modulation driven by heating sources.

4. Seasonal variability in aerosol properties indicates a systematic shift in aerosol composition and particle size distribution, with cold season conditions characterised by larger particle mixtures. This is reflected in increased mean AAE values of 1.53 in Warsaw and 1.42 in Vilnius, together with decreased mean SAE values of 1.20 and 1.48, respectively. Despite these structural changes, SSA remains relatively stable (0.81–0.84), suggesting that enhanced light absorption is primarily driven by increased fossil fuel

combustion emissions rather than changes in total eBC mass concentration. This highlights the intensified radiative impact of wintertime pollution.

5. Long-range air mass transport over the Baltic Sea between Hyltemossa and Preila under non-precipitating conditions resulted in an average 50 % decrease in PM_1 concentration, while the presence of precipitation enhanced removal efficiency to approximately 70 %, underscoring the dominant role of wet deposition processes. In contrast, air masses influenced by continental pathways exhibited a markedly lower net decrease (27 %), reflecting the contribution of additional emission sources. Component-resolved analysis further revealed distinct transformation patterns: chloride increased during marine air mass transport (4 %/h), while sulphate exhibited the most pronounced removal (-5 %/h). Wet deposition most effectively reduced chloride (-3 %/h) and OOA (-3 %/h) concentrations. Land-atmosphere interaction led to increases in all aerosol components, ranging from 1 %/h (chloride) to 5 %/h (sulphate).

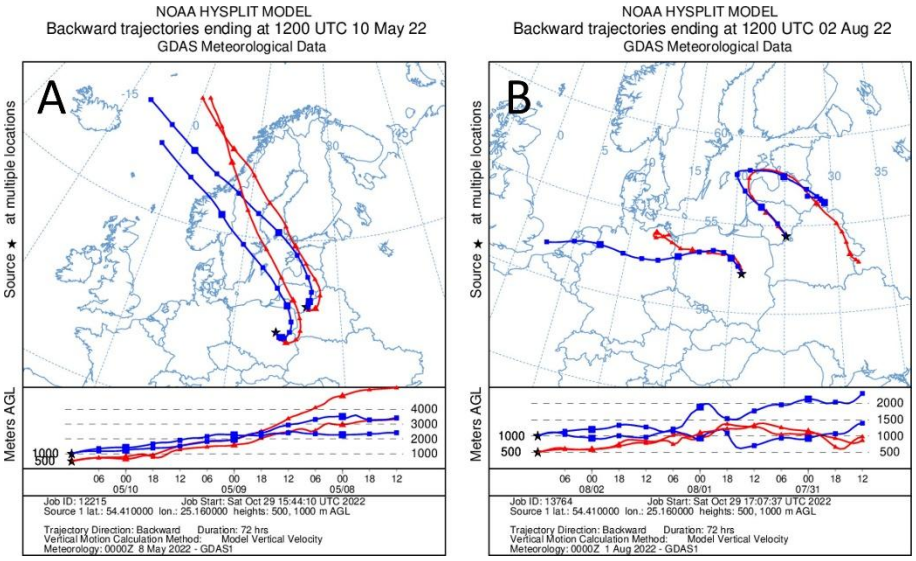

Figure 29. Examples of 72-hour backward air mass trajectories starting at Vilnius and Warsaw at 12:00 UTC, assigned to Categories A and B.

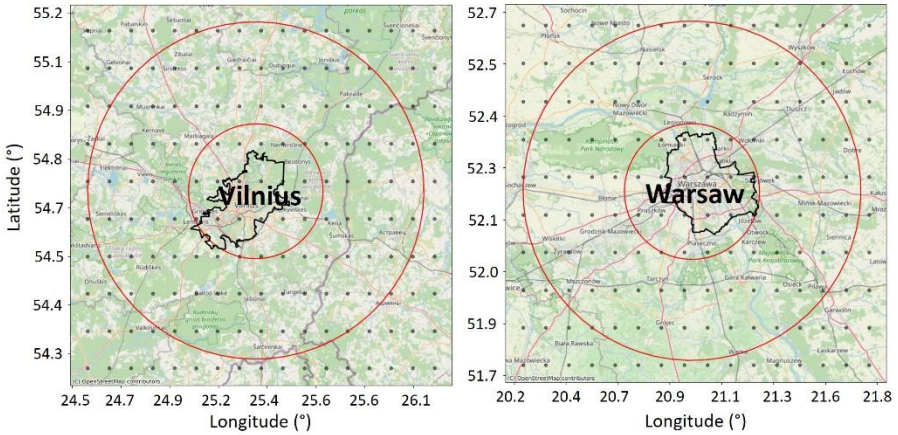

Figure 30. Maps of Vilnius and Warsaw showing the city boundaries and concentric circles with radii of 20 km and 50 km centred on the measurement sites.

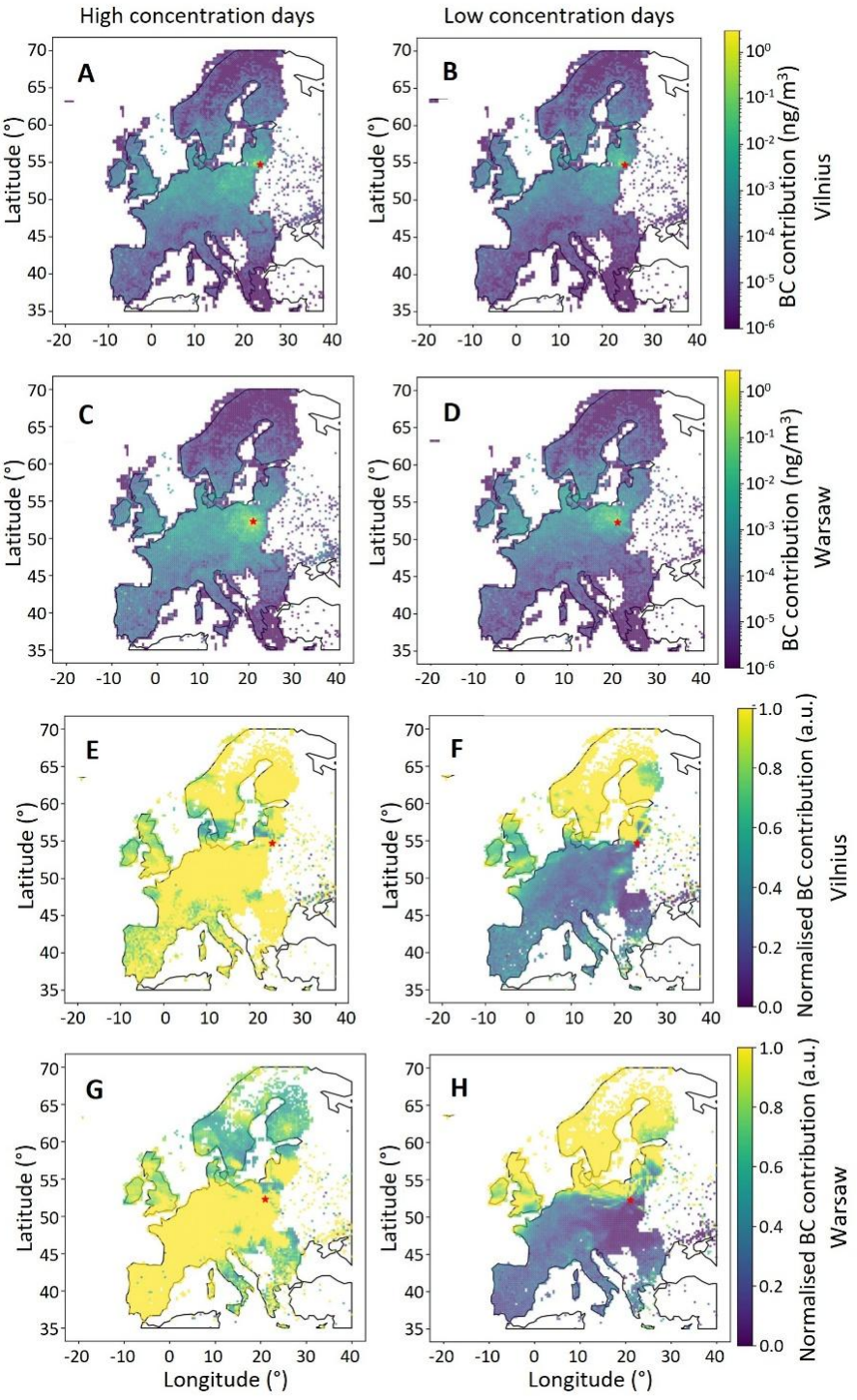

Figure 31. BC contribution maps for high and low concentration episodes: averaged (A, B, C, D) and normalised (D, F, G, H) for the warm season.

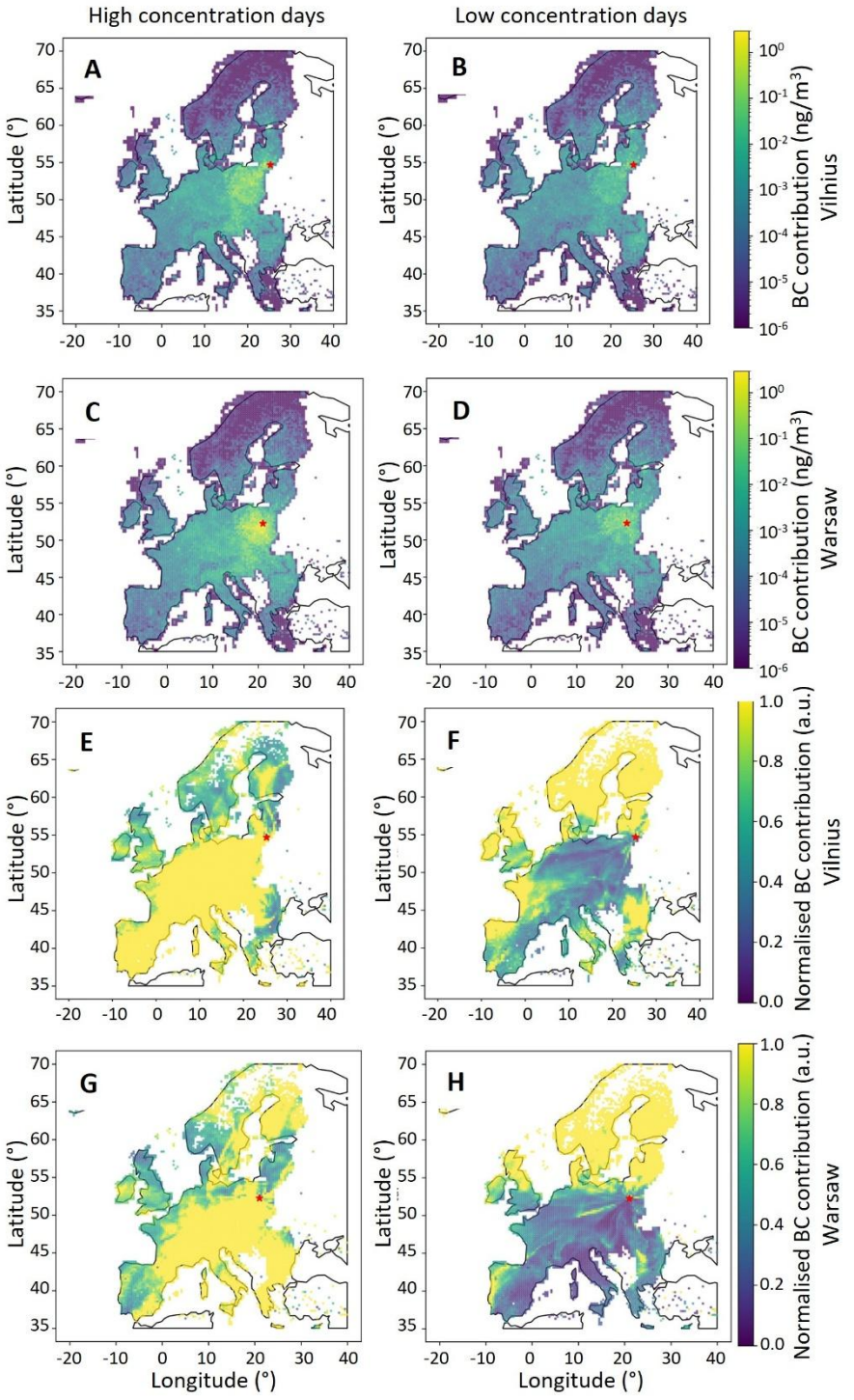

Figure 32. BC contribution maps for high- and low- concentration episodes: averaged (A, B, C, D) and normalised (D, F, G, H) for the cold season.

Table 8. The relative and absolute hourly mass concentration changes for each aerosol component during events. Source-apportioned OA components (BBOA1, BBOA2, OOA) are presented along with OA.

	Class A			**Class B – Class A**	**Class C – Class B**
	Sea transport effect	**Class B**	**Class C**	**Wet deposition processes**	**Land-atmosphere interaction**
Relative mass concentration changes per hour (%/h)					
OA	-2.4	-3.9	0.8	-1.5	4.7
BBOA1	-0.7	-0.9	3.2	-0.2	4.1
BBOA2	-2.9	-2.9	1.5	-0.1	4.5
OOA	-2.5	-5.1	-0.1	-2.6	5.0
NO^-_3	-2.8	-4.7	-1.3	-2.0	3.4
Chl	3.9	1.2	2.1	-2.7	0.8
NH^+_4	-2.4	-3.9	-0.6	-1.4	3.2
SO^{2-}_4	-4.9	-7.2	-1.8	-2.3	5.4
eBC	-3.5	-3.7	-0.6	-0.2	3.2
PM_1	-3.0	-4.2	-0.5	-1.2	3.7
Absolute mass concentration changes per hour ($\mu g/m^3/h$)					
OA	-0.048	-0.042	0.011	0.006	0.053
BBOA1	-0.002	0.002	0.011	0.004	0.008
BBOA2	-0.016	-0.006	0.007	0.010	0.012
OOA	-0.030	-0.039	-0.006	-0.009	0.033
NO^-_3	-0.035	-0.064	-0.025	-0.029	0.039
Chl	-0.003	0.000	-0.001	0.003	0.000
NH^+_4	-0.011	-0.019	-0.012	-0.008	0.007
SO^{2-}_4	-0.025	-0.035	-0.027	-0.010	0.008
eBC	-0.008	-0.005	-0.003	0.002	0.002
PM_1	-0.130	-0.165	-0.056	-0.035	0.108

SANTRAUKA

ĮVADAS

Aktualumas

Į atmosferą patekusios aerozolio dalelės gali būti pernešamos oro masių dideliais atstumais ir daryti reikšmingą poveikį oro kokybei nuo emisijos šaltinių nutolusiose vietovėse. Todėl moksliniai tyrimai tolimąją oro masių pernašą įvardija kaip vieną svarbiausių veiksnių, lemiančių atmosferos taršos pasiskirstymą ir kintamumą žemyniniu mastu (Yang ir kt., 2022). Tolimoji oro masių pernaša yra reikšmingas oro kokybės kintamumą lemiantis veiksnys, darantis įtaką teršalų koncentracijoms, cheminei sudėčiai ir aerozolio savybėms (Atabakhsh ir kt., 2025; Pappin ir kt., 2024; Q. Zhang ir kt., 2017). Į atmosferą patekę oro teršalai į atmosferą, joje gali išlikti nuo kelių dienų iki kelių savaičių ir būti pernešami dideliais atstumais, neretai viršijančiais kelis tūkstančius kilometrų nuo jų šaltinių (Schneider ir kt., 2025). Tokia aerozolio dalelių pernaša yra svarbus visuomenės sveikatos rizikos veiksnys. Vertinama, kad pasaulyje 3,45 milijono priešlaikinių mirčių, siejamos su $KD_{2,5}$ (kietosios (aerozolio) dalelės, kurių aerodinaminis skersmuo mažesnis nei 2,5 μm) poveikiu, gali būti priskiriamos iš nutolusių regionų pernešamiems teršalams (Q. Zhang ir kt., 2017). Šie rezultatai pabrėžia tolimosios oro masių pernašos supratimo svarbą oro kokybės vertinimui vietos ir regioniniu mastu.

Dėl santykinai ilgo išsilaikymo atmosferoje aerozolio dalelės yra tarp tų atmosferos teršalų, kurių koncentracijas ir erdvinį pasiskirstymą labiausiai lemia tolimoji oro masių pernaša. Jų cheminė sudėtis ir dydis lemia sąveiką su Saulės spinduliuote, aerozolio dalelės gali ją sklaidyti arba sugerti, taip tiesiogiai veikdamos atmosferos šiluminę pusiausvyrą. Be to, jos gali veikti kaip debesų kondensacijos branduoliai, keisti debesų fizikines savybes ir atmosferos vandens ciklą. Tarpvyriausybinė klimato kaitos komisija (angl., *Intergovernmental Panel on Climate Change, IPCC*) 2013 m. vertinimo ataskaitoje nurodė, o 2023 m. pakartotinai patvirtino, kad aerozolio dalelės išlieka vienu didžiausiu neapibrėžtumu vertinant jų poveikį Žemės šiluminei pusiausvyrai (IPCC, 2023). Todėl tikslus aerozolio dalelių charakterizavimas ir vietinių bei regioninių šaltinių, įskaitant tolimąją oro masių pernašą, indėlio nustatymas išlieka vienu svarbiausių šiuolaikinių atmosferos ir klimato tyrimų prioritetu.

Dėl sparčios urbanizacijos ir ekonominės plėtros didelė dalis aerozolio dalelių emisijos šaltinių yra sutelkta miestų teritorijose. Miestų atmosferoje aerozolio dalelės sudaro sudėtingą ir dinamišką mišinį, susiformuojantį dėl

įvairių taršos šaltinių ir procesų. Tarp šių dalelių ypatingą reikšmę turi juodoji anglis (angl., *black carbon*, BC) – stipriai šviesą sugerianti aerozolio komponentė, daranti poveikį tiek oro kokybei, tiek klimatui. BC daugiausia aptinkama submikroninio dydžio aerozolio dalelėse (KD_1, (kietosios dalelės, kurių aerodinaminis skersmuo mažesnis nei 1 μm)) ir susidaro nepilno iškastinio kuro ir biomasės degimo metu (Bond ir kt., 2013; Savadkoohi ir kt., 2023). Miesto aplinkoje iškastinio kuro deginimas sudaro didžiausią BC išmetimų į aplinkos orą dalį, nors kietojo biokuro deginimas gyvenamųjų namų šildymui gali sudaryti reikšmingą dalį šaltuoju metų laiku. BC komponentė yra ypač įdomi, nes tai viena efektyviausiai šviesą sugeriančių aerozolio komponenčių, turinti reikšmingą įtaką aerozolio dalelių ir šviesos sąveikoje bei platesniame kontekste, susijusiame su tuo, kaip miestų išmetamieji teršalai dėl tolimosios oro masių pernašos daro įtaką klimatui regioniniu mastu.

Nepaisant didelės aerozolio dalelių tyrimų pažangos, vis dar išlikę neaiškumų dėl BC šaltinių kilmės atskyrimo nustatymo, transformacijos procesų ir pernašos dinamikos, taip pat dėl BC sąveikos su kitomis aerozolio dalelių komponentėmis. Šie iššūkiai ypač išryškėja, kai kartu nagrinėjamos kontrastingos aplinkos, tokios kaip miesto ir regioninės foninės vietos. Norint tiksliai priskirti šaltinį, būtina atskirti lokaliai išmetamas ir oro masių pernešamas aerozolio daleles, tačiau tai vis dar sunku dėl sudėtingos sąveikos tarp emisijos šaltinių ir atmosferos procesų. Todėl, norint pagerinti šį supratimą, reikalingi integruoti kelių stočių stebėjimo ir modeliavimo tyrimai.

Nors naujausiuose tyrimuose buvo nagrinėta tolimoji oro masių pernaša Lietuvoje (Kalinauskaitė ir kt., 2024; Mašalaitė ir kt., 2024), Vidurio ir Šiaurės Europoje vis dar trūksta išsamaus, integruoto jos poveikio skirtingose aplinkose vertinimo (Arora ir kt., 2026). Kiekybinis BC įvertinimas miesto aplinkoje suteikia praktinę priemonę įvertinti, kaip atskiros miestų teritorijos prisideda prie regioninės taršos. Tuo tarpu, KD_1 dinamikos apibūdinimas regioninėje foninėje aplinkoje suteikia matavimais grįstų duomenų, svarbių klimato modeliavimui. Šioje daktaro disertacijoje šie trūkumai sprendžiami taikant integruotus metodus, apjungiančius vietoje atliekamus matavimus, šaltinių kilmės atskyrimą ir atmosferos modeliavimą kontrastingų charakteristikų aplinkose.

Mokslinis naujumas

Šio darbo mokslinis naujumas grindžiamas vietovei būdingo tolimosios oro masių pernašos poveikio juodosios anglies ir submikroninių aerozolio dalelių savybėms vertinimu skirtingose aplinkose – miesto (Vilnius, Varšuva) ir regioninio fono (Preila, Hiltemosa). Derinant eksperimentinių matavimų ir atmosferos modeliavimo duomenis, pritaikytas naujas metodas, leidžiantis miesto aplinkoje išmatuotą juodosios anglies masės koncentraciją atskirti į vietinių emisijos šaltinių ir tolimosios pernašos komponentes.

Pagrindinis tyrimo tikslas

Ištirti tolimosios oro masių pernašos poveikį submikroninėms aerozolio dalelėms, ypatingą dėmesį skiriant juodosios anglies masės koncentracijai ir šaltinių pasiskirstymui, Vidurio ir Šiaurės Europos miestų aplinkoje, taip pat aerozolio dalelių cheminei sudėčiai pietų Baltijos jūros regiono foninėje aplinkoje.

Uždaviniai

1. Kiekybiškai įvertinti juodosios anglies masės koncentraciją miesto aplinkoje ir išsamiai apibūdinti jos laikinį kintamumą įvairiais laiko skerspjūviais (dienos, savaitės, sezono), atsižvelgiant į meteorologinių sąlygų ir taršos šaltinių kilmės įtaką.
2. Atlikti juodosios anglies taršos šaltinių kilmės atskyrimą taikant kelių bangos ilgių optinius matavimus ir apibūdinti aerozolio dalelių optines savybes, siekiant interpretuoti sąsajas su chemine sudėtimi, taršos šaltiniais ir atmosferos procesais miesto aplinkoje.
3. Taikant atmosferinės sklaidos modeliavimą, sumodeliuoti juodosios anglies tolimąją pernašą, kiekybiškai įvertinti skirtingų taršos šaltinių indėlį ir nustatyti vietinės kilmės bei tolimosios pernašos komponenčių indėlį į išmatuotą juodosios anglies masės koncentraciją.
4. Išanalizuoti tolimosios oro masių pernašos poveikį submikroninių aerozolio dalelių cheminei sudėčiai ir masės koncentracijai regioninėje foninėje aplinkoje.

Ginamieji teiginiai

1. Tolimoji oro masių pernaša yra reikšmingas veiksnys, lemiantis juodosios anglies masės koncentraciją miesto aplinkoje. Šaltuoju metų laiku jos indėlis vidutiniškai sudaro 46 % Vilniuje ir 53 % Varšuvoje.
2. Juodosios anglies dominuojančių šaltinių pokytis aiškiai pastebimas skirtingais sezonais Vilniaus ir Varšuvos miestų aplinkoje, nepriklausomai nuo bendro eBC masės koncentracijos lygio: šiltuoju metų laiku vyrauja iškastinio kuro deginimas (vidutiniškai 84–86 %), o šaltuoju metų laiku – biomasės ir anglies deginimas (vidutiniškai 29–37 %).
3. Juodosios anglies masės koncentracijos sezoninį kintamumą miesto aplinkoje lemia vyraujančių ūkio veiklos sektorių santykinio indėlio pokyčiai: šaltuoju metų laiku vyrauja gyvenamųjų pastatų šildymo sektoriaus išmetimai, o šiltuoju metų laiku – transporto sektoriaus išmetimai.
4. Aerozolio dalelių optinės savybės stipriai veikiamos taršos šaltinių pobūdžio, šaltuoju metų laiku aplinkos ore vyrauja stambesnių dalelių mišinys, o šviesą sugeriančios dalelės siejamos su iškastinio kuro deginimo emisijomis.
5. Regioninio fono aplinkoje tolimosios oro masių pernašos poveikis KD_1 masės koncentracijai priklauso nuo oro masių judėjimo trajektorijos: pernaša virš Baltijos jūros lemia didelį aerozolio dalelių masės mažėjimą (-3 %/val.), o pernašos virš žemyninės teritorijos metu aerozolio dalelių masė didėja (4 %/val.) dėl papildomų taršos šaltinių.

Autorės indėlis

Autorė atliko pirminę duomenų analizę, juodosios anglies šaltinių kilmės atskyrimą, aerozolio optinių savybių skaičiavimus, kartu sukūrė slenkstinių verčių pagrindu veikiantį trajektorijų suskirstymą į kategorijas ir oro masių pernašos įvykių klasifikavimą, naudojant atgalines HYPSLIT oro masių trajektorijas. Autorė parengė paveikslus, rašė ir redagavo mokslines publikacijas bei pristatė savo tyrimų rezultatus nacionalinėse ir tarptautinėse konferencijose.

METODAI

Skyriuje pristatomi metodai, naudoti tiriant tolimosios oro masių pernašos įtaką eBC (ekvivalentinė juodoji anglis) masės koncentracijai ir šaltinių pasiskirstymui miesto aplinkoje (tyrimai 1 ir 2) ir įtaką KD_1 cheminei sudėčiai regioninėje foninėje aplinkoje (tyrimas 3).

Aerozolio juodosios anglies miesto aplinkoje tyrimai

Šiems tyrimams buvo naudoti matavimų duomenys iš dviejų vietovių miesto aplinkose – Vilniuje (Lietuva, Šiaurės Europa) ir Varšuvoje (Lenkija, Vidurio Europa) (2 paveikslas). Matavimų laikotarpiai ir kiekvienoje stotyje naudota įranga pateikta 1 lentelėje.

Vilnius yra didžiausias miestas Lietuvoje (~ 600 tūkst. gyventojų). Oro kokybės matavimų stoties vieta (virš 4 aukštų pastato stogo) (54°42′ Š, 25°15’ R) atspindi miesto foninį oro užterštumo lygį, nes yra nutolusi 6–7 km nuo miesto centro, ekranuojama miško zonos nuo intensyvaus transporto srauto gatvės ir mažiau intensyvaus eismo gatvės.

Antroji matavimų vieta Varšuvoje yra ant Varšuvos universiteto Fizikos fakulteto stogo virš 5 aukšto (52°12′ Š, 20°58′ R), apie 3 km į pietvakarius nuo miesto centro. Varšuvoje gyvena 1,9 milijono gyventojų ir tai yra didžiausias miestas Lenkijoje. Aplink matavimų vietą yra gyvenamųjų namų, ligoninė, universiteto miestelis ir dideli parkai, dėl didesnio artumo tiesioginiams taršos šaltiniams (transporto išmetimai ir namų šildymas), vietovė atspindi miesto aplinką.

Tyrimuose 1 ir 2 buvo naudoti nepertraukiami aerozolio dalelių šviesos sugerties ir sklaidos matavimų duomenys, atitinkamai surinkti aetalometru (Vilniuje ir Varšuvoje: Magee Scientific, modelis AE33 (JAV)) ir nefelometru (Vilniuje: TSI Inc. modelis 3563, JAV; Varšuvoje: Aurora 4000, Ecotech Pty, Ltd., Australija). eBC masės koncentracija buvo apskaičiuota naudojant šviesos sugerties koeficientą (ties 880 nm) ir masės sugerties skerspjūvį (MAC) (2.2.1 poskyris, 1 formulė). Terminas eBC vartojamas, kai BC masės koncentracija matuojama netiesiogiai (t. y. išskaičiuojama iš šviesos sugerties koeficiento). Juodosios anglies šaltinių kilmės atskyrimas atliktas naudojant Sandradewi ir kt. (2008) metodiką (2.2.2 poskyris, 3 formulė). Aerozolio dalelių klasifikacijai pagal optines savybes, pritaikytai iš Cappa ir kt. (2016) tyrimo, buvo apskaičiuotos sugerties ir sklaidos Angstremo eksponentės (AAE ir SAE, atitinkamai) (2.2.4 poskyris, 6 ir 8 formulės).

Atgalinės 72 valandų oro masių trajektorijos buvo apskaičiuotos naudojant nacionalinės vandenynų ir atmosferos administracijos (angl. *National Oceanic and Atmospheric Administration, NOAA*) hibridinį modelį HYSPLIT

(angl. *Hybrid Single Particle Lagrangian Integrated Trajectory (HYSPLIT) model*) (Rolph ir kt., 2017; Stein ir kt., 2015). Atgalinės oro masių trajektorijos, prasidedančios receptoriniuose taškuose (Vilniuje ir Varšuvoje) 12:00 UTC, buvo suskirstytos į kategorijas pagal trajektorijos horizontalųjį ir vertikalųjį kelią: kategorija A (trajektorijos turi panašius arba sutampančius oro masių pernašos kelius, todėl tikimasi vienos aerozolio kilmės), kategorija B (trajektorijos į receptorinius taškus vedė skirtingomis kryptimis ir keliais) ir kategorija C (visi atvejai nepriskirti kategorijoms A ir B). Dėl oro masių pernašos eBC taršos padidėjimas arba praskiedimas abiejose miesto aplinkose buvo įvertinti lyginant vidutines eBC masės koncentracijas 6 val. prieš ir po atgalinės oro masių trajektorijos pradžios receptoriniame taške (12 formulė).

FLEXPART (angl. *FLEXible PARTicle dispersion model*) modelis, sukurtas remiantis valandiniais ERA5 pakartotinės analizės meteorologiniais laukais iš Europos vidutinės trukmės orų prognozių centro (ECMWF), buvo naudotas suskaičiuoti į receptorinius taškus (Vilnių ir Varšuvą) oro masių perneštos eBC masės koncentracijos. Šiame darbe naudojami FLEXPART duomenys turi 3 valandų laiko skiriamąją gebą. Išsamesnį modelio struktūros aprašymą galima rasti Pisso ir kt. (2019) darbe. Siekiant kiekybiškai įvertinti vietinės kilmės BC ir tolimosios oro masių perneštos BC masės koncentracijas, išmatuota eBC masės koncentracija buvo padalinta į vietinę ir perneštą komponentes pagal 11 formulę.

Submikroninių aerozolio tyrimai regioninėje foninėje aplinkoje

Šiame tyrime buvo pasirinktos dvi nuošalios vietovės regioninėje foninėje aplinkoje – Preila (Lietuva) ir Hiltemosa (Švedija, Šiaurės Europa) (2 paveikslas). Matavimų laikotarpiai ir kiekvienoje stotyje naudota įranga pateikta 1 lentelėje.

Matavimo vieta Preiloje (55°22′ Š, 21°1′ R) pietrytinėje Baltijos jūros dalyje, Kuršių Nerijoje, nutolusi per 40 ir 80 km atitinkamai nuo artimiausio didesnio miesto Klaipėdos ir pramoninės veiklos Kaliningrade. Matavimų vieta atspindi jūrinę foninę aplinką dėl didelio atstumo nuo bet kokių didelių vietinių taršos šaltinių, o jai daugiausiai įtakos turi tolimoji oro masių pernaša.

Hiltemosos matavimų stotis (56°5′Š, 13°25′ R) yra pietų Švedijos Skonės regione, nutolusi nuo artimiausių miestų per 25 km (Helsingborgas, Švedija), 50 km (Malmė, Švedija) ir 60 km (Kopenhaga, Danija). Vietovė yra apsupta miškų, todėl laikoma kaimo fonine vietove. Netoliese nėra tiesioginių taršos šaltinių; todėl ši vieta labai tinka tolimosiomis oro masėmis pernešamos taršos foniniams stebėjimams, nes šioje vietovėje nestebimi spartūs aerozolio dalelių pokyčiai, būdingi miesto aplinkai, kurioje yra daug aktyvių, tiesioginių šaltinių.

Šiame tyrime naudoti aetalometras (Hiltemosoje: AE33, Magee Scientific, JAV; Preiloje: AE31 Spectrum, Optotek, Slovėnija) bei aerozolio dalelių cheminės sudėties monitorius (angl., *aerosol chemical speciation monitor*) (Aerodyne Research, Inc. (JAV) Hiltemosoje ir Preiloje). Organinio aerozolio dalelių šaltinių suskirstymas buvo atliktas naudojant teigiamos matricos faktorizavimo metodiką.

Šiame tyrime buvo naudotos HYSPLIT modeliu sumodeliuotos atgalinės 72 valandų tolimosios oro masių pernašos trajektorijos, prasidedančios virš Preilos (100 m aukštyje a.s.l.) ir besitęsiančios virš Hiltemosos (50 km spinduliu). Kas valandą prasidedančios valandinės oro masių trajektorijos buvo suskirstytos į pernašos įvykius (angl., *connected-flow events*). Dėl statistinio reikšmingumo, buvo tiriami tik tie įvykiai, kuriuos sudarė trys ar daugiau iš eilės vykstančių valandinių trajektorijų. Įvykiai buvo suskirstyti į tris klases, remiantis sumodeliuotų trajektorijų erdviniais ir meteorologiniais parametrais: klasei A priskirti įvykiai, kurių metu oro masės trajektorija keliavo iš vakarų į rytus, klasei B priskirti įvykiai, kurių metu trajektorijos keliavo iš vakarų į rytus ir modeliuoti meteorologiniai duomenys rodo, kad buvo kritulių, o klasė C apima trajektorijas, besidriekiančias į šiaurę arba į pietus, kertančias žemyninį regioną prieš pasiekiant Preilą, su krituliais trajektorijos kelyje.

Siekiant įvertinti KD_1 masės koncentracijos ir cheminės sudėties pokyčius pernašos tarp Hiltemosos ir Preilos metu, buvo atsižvelgta į trukmę, kurią oro masė keliavo tarp šių taškų. Žinant tikslų perėjimo virš Preilos matavimų stoties laiką (šiuo atveju, atgalinės trajektorijos pradžios laiką), buvo galima nustatyti, kada kiekviena trajektorija keliavo virš Hiltemosos matavimų stoties, apskaičiuojant atgalinę trukmę nuo pradžios laiko. Tokiu būdu aerozolio dalelių sudėties ir cheminių komponenčių koncentracijos duomenų taškai buvo priskirti kiekvienos trajektorijos pradžiai ir pabaigai. Cheminės aerozolio dalelių komponentės masės koncentracijos pokytis buvo apskaičiuotas pagal 14 formulę (2.6.6 poskyris). Skirtingų veiksnių (pernašos virš jūros, drėgnojo nusėdimo ir sausumoje susidarančių antropogeninės kilmės teršalų) ir jų derinių įtaka kiekvienai aerozolio komponentei ir įvykių klasei buvo apskaičiuota pagal 15–18 formules.

REZULTATAI

Tolimosios oro masių pernašos poveikis juodosios anglies masės koncentracijai miesto aplinkoje (1 ir 2 tyrimai)

Juodosios anglies masės koncentracijos miesto aplinkoje (Vilniuje ir Varšuvoje) pasižymėjo ryškiu sezoniniu ir erdviniu kintamumu (4 ir 5 paveikslai). eBC masės koncentracija Varšuvoje nuolat buvo aukštesnė nei Vilniuje, šiltuoju metų laiku vidutiniškai siekdama 1,07 $\mu g/m^3$ (0,77 $\mu g/m^3$, Vilniuje), o šaltuoju metų laiku vidutiniškai padidėjo iki 2,02 $\mu g/m^3$ (1,11 $\mu g/m^3$ Vilniuje). Taigi, lyginant su šiltuoju sezonu, eBC masės koncentracija šaltuoju sezonu Varšuvoje padidėjo 89 %, o Vilniuje 44 %.

eBC masės koncentracijos kintamumą tiek paros, tiek savaitės eigoje daugiausia lėmė eBC susidaranti iškastinio kuro degimo metu (eBC_{FF}) (8 paveikslas). Šiltuoju metų laiku eBC_{FF} sudarė 86 % Varšuvoje ir 84 % Vilniuje visos eBC masės koncentracijos, o šaltuoju sezonu eBC_{FF} indėlis sumažėjo atitinkamai iki 63 % ir 71 % dėl padidėjusios biomasės ir anglies deginimo įtakos. Žiemą su biomasės ir anglies deginimu susijusių eBC ($eBC_{BB,C}$) išmetimų į aplinkos orą indėlis Varšuvoje padidėjo iki 36–40 % (25–75 procentilės), o Vilniuje iki 29–33 %, o tai rodo stipresnį gyvenamųjų namų šildymo išmetimų į aplinkos orą poveikį, ypač Varšuvoje.

Iš aerozolio dalelių optinių savybių matosi reikšmingi sezoniniai pokyčiai. Remiantis aetalometro ir nefelometro matavimais, pagrįsta AAE ir SAE optine aerozolio dalelių klasifikacija (11 paveikslas), šaltuoju sezonu žymiai dažniau pastebėta didesnių dalelių mišinių, kuriuose susimaišiusios BC, rudoji anglis ir mineralinės dulkės – 94 % Varšuvoje ir 42 % Vilniuje. Pavienės sklaidos albedo (SSA) vertės išliko santykinai stabilios tiek skirtingais sezonais, tiek Vilniuje bei Varšuvoje: šaltuoju sezonu šiek tiek padidėjo (0,84 ± 0,05 Varšuvoje ir 0,83 ± 0,07 Vilniuje), lyginant su šiltuoju sezonu (0,81 ± 0,07 Varšuvoje ir 0,81± 0,08 Vilniuje). Sugerties Angstremo eksponentės vertės Varšuvoje padidėjo nuo 1,3 iki 1,53 (vidutiniškai), o Vilniuje nuo 1,26 iki 1,42, o sklaidos Angstremo eksponentės vertės sumažėjo atitinkamai nuo 1,62 iki 1,20 ir nuo 1,75 iki 1,48 Varšuvoje ir Vilniuje, atitinkamai. Nepaisant panašių sezoninių vidurkių verčių, pastebėtas ryškus SSA parinės eigos kintamumas, stipriai koreliuojantis su eBC_{FF} (-0,69 Vilniuje šiltuoju sezonu ir -0,97 Varšuvoje šaltuoju sezonu) (12 paveikslas). Stipri eBC_{FF} įtaka SSA dinamikai pabrėžia šių išmetamųjų teršalų vaidmenį stiprinant aerozolio dalelių šviesos sugertį ir tokiu būdu prisidedant prie atmosferos šiltėjimo.

Tolimosios oro masių pernašos poveikis eBC masės koncentracijai, išreikštas kaip vienu metu vykstantis taršos padidėjimas arba praskiedimas

abiejose miesto aplinkose, buvo įvertintas 1 tyrime, naudojant siūlomą HYSPLIT atgalinių oro masių trajektorijų klasifikaciją. Tolimosios oro masių pernašos sąlygomis, kai oro masės atvykdavo iš tos pačios krypties, abiejose vietovėse sukėlė panašų eBC masės koncentracijos praskiedimą (42 % Varšuvoje ir 50 % Vilniuje), tuo tarpu vienalaikis eBC taršos padidėjimas būdavo ryškesnis Vilniuje (64 %) nei Varšuvoje (30 %) (13 paveikslas). Taršos eBC_{FF} padidėjimas ir praskiedimas buvo ryškesni Vilniuje (50 % padidėjimas, 51 % praskiedimas) nei Varšuvoje (atitinkamai 27 % ir 34 %). Tuo tarpu oro masių pernašos įtaka eBC_{BB} masės koncentracijai buvo santykinai maža ir panaši abiejose miestuose: Vilniuje ji padidėdavo 11 % arba sumažėdavo 5 %, o Varšuvoje padidėdavo 7 % arba sumažėdavo 8 %.

FLEXPART modeliavimo rezultatai 2 tyrime, patvirtino, kad pagrindiniai BC šaltiniai miesto aplinkoje yra gyvenamųjų namų šildymas ir transportas. Su šildymu susijusių išmetimų į aplinkos orą indėlis reikšmingai padidėjo Varšuvoje nuo 63 % šiltuoju sezonu iki 86 % šaltuoju sezonu, o Vilniuje – nuo 42 % iki 73 %, atitinkamai (18 paveikslas). Tuo tarpu transporto sektoriaus indėlis sumažėjo nuo 27 % iki 10 % (Varšuvoje) ir nuo 40 % iki 17 % (Vilniuje), o tai rodo itin aukštą transporto išmetamųjų teršalų indėlį BC masės koncentracijai šiltuoju sezonu Vilniaus mieste. BC atskyrimas į vietinę ir oro masių perneštas komponentes parodė, kad vietinės kilmės BC turėjo didžiausią indėlį išmatuotos eBC masės koncentracijai abiejuose miestuose (19 paveikslas, 6 lentelė). Atsižvelgiant į BC išmetimus susidarančius miesto administracinėse ribose, vietinės kilmės BC Vilniuje ir Varšuvoje sudarė 47 % ir 64 % visos BC šaltuoju sezonu, o šiltuoju – 77 % ir 87 %, atitinkamai. Išplėtus teritoriją, kurioje BC išmetimų taškiniai šaltiniai neįtraukiami į skaičiavimus iki 50 km spindulio nuo matavimų vietovių, vietinės kilmės BC indėlis dar labiau padidėjo. Pagal šį platesnį erdvinį apibrėžimą, mieste susidaranti BC sudarė 85 % ir 91 % išmatuotos BC masės koncentracijos šiltuoju sezonu, o šaltuoju – 61 % ir 67 % Varšuvoje ir Vilniuje, atitinkamai.

Tolimosios oro masių pernašos įtaka submikroninių aerozolio dalelių cheminei sudėčiai žiemos metu tarp Hiltemosos ir Preilos (3 tyrimas)

Tyrime buvo nagrinėjama tolimosios oro masių pernašos per Baltijos jūrą įtaka KD_1 koncentracijai ir cheminei sudėčiai 2017–2018 m. šaltuoju sezonu, remiantis keturių mėnesių trukmės vienalaikiais matavimais pietų Baltijos jūros regiono foninėje aplinkoje – Hiltemosoje ir Preiloje. Naudojant HYSPLIT modelį, sumodeliuotos 102 atgalinės 72 valandų oro masių trajektorijos, prasidedančios Preiloje, kertančios Baltijos jūrą ir besitęsiančios 500 km iki Hiltemosos. Sumodeliuotos oro masių trajektorijos buvo

sugrupuotos į 14 tolimosios pernašos įvykių (20 paveikslas). Vienalaikiai matavimai abiejose Baltijos jūros pusėse (Švedijoje ir Lietuvoje) leido įvertinti KD_1 koncentraciją ir cheminę sudėtį oro masėje prieš ir po pernašos per Baltijos jūrą. Vidutiniškai matavimų kampanijos metu, KD_1 koncentracija Preiloje buvo beveik dvigubai aukštesnė nei Hiltemosoje (atitinkamai 11,2 $\mu g/m^3$ ir 6,3 $\mu g/m^3$) (22 paveikslas). Tačiau nustatytų tolimosios pernašos įvykių metu, Preiloje KD_1 koncentracija buvo žymiai žemesnė (2,5 $\mu g/m^3$) nei Hiltemosoje (4,3 $\mu g/m^3$).

Remiantis meteorologiniais ir erdviniais sumodeliuotų oro masių trajektorijų parametrais, kiekvienas įvykis buvo priskirtas vienai iš trijų įvykių klasių (26 paveikslas). Klasei A priskirtų pernašos įvykių metu tarp Hiltemosos ir Preilos buvo užfiksuotas vidutinis 50 % KD_1 koncentracijos sumažėjimas (nuo 43 % iki 59 % vienam įvykiui). Klasei B priskirtų įvykių metu, kai pernašos įvykio metu buvo kritulių, KD_1 koncentracijos sumažėjimas buvo didesnis (vidutiniškai 70 %, nuo 28 % iki 87 % per įvykį), rodantis drėgnojo nusėdimo procesų įtaką. Klasei C priskirtų pernašos įvykių metu, oro masės praėjo virš sausumos prieš pasiekdamos Preilą, šiuo atveju vidutinis KD_1 koncentracijos sumažėjimas buvo mažiausias tarp klasių (27 %). KD_1 koncentracija klasės C pernašos įvykių metu buvo veikiama visų trijų veiksnių – pernašos virš jūros, drėgnojo nusėdimo procesų ir antropogeninės kilmės teršalų žemyninėje dalyje. Tik klasei C priskirtų pernašos įvykių metu KD_1 koncentracija kartais būdavo žemesnė Hiltemosoje nei Preiloje ir kito nuo 65 % sumažėjimo iki 28 % padidėjimo. Nors visų pernašos įvykių metų oro masės keliavo virš Baltijos jūros, klasei C būdingas oro masės kelias virš žemyninės dalies (Šiaurės Vokietija, Lenkija, Vakarų Latvija) prieš pasiekiant Preilą. Santykinai nedidelis KD_1 koncentracijos sumažėjimas klasės C įvykių metu rodo antropogeninės kilmės išmetimų, susidarančių virš sausumos, įtaką. Šį reiškinį dalinai maskuoja KD_1 koncentracijos skiedimas, sausasis ir drėgnasis nusėdimai bei kiti procesai, veikiantys KD_1 koncentraciją įvykiuose, priskirtuose klasėms A ir B.

Remiantis tyrime pasiūlyta pernašos įvykių klasifikacija, kiekybiškai įvertinti KD_1 koncentracijai įtaką turintys veiksniai: pernašos virš jūros efektas, drėgnojo nusėdimo procesai bei sausumoje susidarantys antropogeninės kilmės teršalai (28 paveikslas). Pernašos virš jūros sąlygomis be kritulių, vienintelė komponentė, kurios masės koncentracija padidėjo buvo chloridai (+4 %/val.), o sulfatai pasižymėjo stipriausiu pašalinimu (-5 %/val.), kitų komponenčių koncentracijos sumažėjo nuo -1 %/val. iki -4 %/val. (8 lentelė). Drėgnojo nusėdimo procesų įtaka labiausiai paveikė chloridų (-3 %/val.) ir oksiduoto organinio aerozolio (-3 %/val.) koncentracijas, o įtaka kitoms komponentėms kito nuo 0 iki -2 %/val. Tuo tarpu sausumoje

susidarančių antropogeninės kilmės teršalų poveikis oro masėms lėmė visų KD_1 komponenčių koncentracijos padidėjimą nuo +1 %/val. (chloridų) iki +5 %/val. (sulfatų).

IŠVADOS

1. Tolimoji oro masių pernaša reikšmingai, nors ir antraeiliškai, veikia eBC masės koncentracijos kaitą miesto aplinkoje, skatindama tiek taršos praskiedimą (vidutiniškai 50 %), tiek padidėjimą (vidutiniškai 64 %), daugiausia paveikdama juodosios anglies, susidarančios iškastinio kuro degimo metu, lygį. FLEXPART modeliavimo rezultatai patvirtina, kad nepaisant tolimosios oro masių pernašos įtakos, miesto aplinkoje vietinės kilmės juodosios anglies masės koncentracija yra dominuojanti ir sudaro vidutiniškai 77 % ir 87 % šiltuoju metų laiku Varšuvoje ir Vilniuje, atitinkamai, o šaltuoju metų laiku atitinkamai sudaro 47 % ir 64 %, kai gerokai padidėja oro masių pernešama dalis (vidutiniškai 53 % Varšuvoje ir 46 % Vilniuje). Tai rodo, kad miesto oro kokybę daugiausia lemia vietiniai išmetamieji teršalai, o tolimoji pernaša veikia kaip dinaminis veiksnys.

2. Nepriklausomai nuo didesnio eBC koncentracijos lygio Varšuvoje (vidutiniškai 1,07 μg/m³ ir 2,02 μg/m³ atitinkamai šiltuoju ir šaltuoju sezonu) nei Vilniuje (0,77 μg/m³ ir 1,11 μg/m³, atitinkamai), šaltinių kilmės pasiskirstymas išlieka panašus, tai yra: su iškastinio kuro deginimu susijusios juodosios anglies indėlis dominuoja (84–86 % vasarą; 63–71 % žiemą), o šaltuoju metų laiku reikšmingą, bet antrinį indėlį sudaro biomasės ir anglies deginimas (29–37 % eBC masės koncentracijos). Sezoninis padidėjimas, ypač ryškus Varšuvoje, atspindi žiemą sustiprėjusį degimo procesų metu išmetamų teršalų kiekį, esant sumažėjusiam atmosferos maišymuisi.

3. Pagrindiniai juodosios anglies šaltiniai yra namų šildymo ir transporto sektoriai; šaltuoju metų laiku daugiausia prisideda namų šildymas (vidutiniškai 86 % Varšuvoje ir 73 % Vilniuje), o šiltuoju metų laiku padidėja transporto sektoriaus indėlis (vidutiniškai 27 % Varšuvoje ir 40 % Vilniuje). Šie rezultatai rodo, kad miesto aplinkoje juodosios anglies kiekio kintamumą daugiausia lemia transporto sektoriaus, o sezoninį kintamumą lemia gyvenamųjų pastatų šildymo sektoriaus emisijos.

4. Sezoninis aerozolio dalelių optinių savybių kintamumas rodo sistemingą dalelių sudėties ir dydžio pasiskirstymo pokytį, kai šaltojo sezono sąlygoms būdingas didesnių dalelių mišinys aplinkos ore. Tai parodo padidėjusios AAE vertės (vidutiniškai 1,53 Varšuvoje ir 1,42 Vilniuje) ir sumažėjusiose SAE vertės (atitinkamai 1,20 ir 1,48). Nepaisant šių pokyčių,

SSA vertės išlieka santykinai stabilios (vidutiniškai 0.81–0.84), o tai rodo, kad padidėjusią šviesos sugertį pirmiausia lemia padidėję iškastinio kuro degimo procesų išmetimai į aplinkos orą, o ne tik bendros eBC masės koncentracijos pokyčiai. Tai pabrėžia sustiprėjusį žiemos taršos šiluminį poveikį.

5. Tolimoji oro masių pernaša virš Baltijos jūros tarp Hiltemosos ir Preilos sąlygomis be kritulių lėmė vidutiniškai 50 % sumažėjusią KD_1 koncentraciją, o sąlygomis su krituliais, KD_1 koncentracija sumažėjo vidutiniškai 70 %, tai pabrėžia dominuojantį drėgnojo nusėdimo procesų vaidmenį. Tuo tarpu, antropogeninės kilmės teršalų virš žemyninės dalies paveiktos oro masės parodė žymiai mažesnį KD_1 koncentracijos sumažėjimą (vidutiniškai 27 %), o tai rodo papildomų taršos šaltinių įtaką. Atlikus komponentų analizę, paaiškėjo skirtingi transformacijos modeliai: chloridų kiekis padidėjo oro masių pernašos virš jūros metu (4 %/val.), o sulfatai pasižymėjo didžiausiu pašalinimo efektyvumu (-5 %/val.). Drėgnojo nusėdimo procesai efektyviausiai sumažino chlorido (-3 %/val.) ir oksiduoto organinio aerozolio (-3 %/val.) koncentracijas. Antropogeninės kilmės teršalai virš žemyninės dalies lėmė visų aerozolio komponenčių padidėjimą oro masėje – nuo 1 %/val. (chloridų) iki 5 %/val. (sulfatų).

AI Statement

The author declares that generative AI was used in the creation of this manuscript. Generative AI tools (Grammarly and ChatGPT, based on GPT-5 model) were used only for language editing, grammar refinement, and text clarity during manuscript preparation. The tool was not used to generate scientific content, perform analyses, or interpret data. The scientific conclusions were developed by the author.

REFERENCES

Aerosol d.o.o. (2018). *Aethalometer ® Model AE33 User Manual* (Issue August). https://gml.noaa.gov/aftp/user/betsy/AE33_UsersManual_Rev154.pdf

Ahlberg, E., Ausmeel, S., Nilsson, L., Spanne, M., Pauraite, J., Klenø Nøjgaard, J., Bertò, M., Skov, H., Roldin, P., Kristensson, A., Swietlicki, E., & Eriksson, A. (2023). Measurement report: Black carbon properties and concentrations in southern Sweden urban and rural air – the importance of long-range transport. *Atmospheric Chemistry and Physics*, *23*(5), 3051–3064. https://doi.org/10.5194/acp-23-3051-2023

Alshetty, D., & Nagendra, S. M. S. (2022). Impact of vehicular movement on road dust resuspension and spatiotemporal distribution of particulate matter during construction activities. *Atmospheric Pollution Research*, *13*(1), 101256. https://doi.org/10.1016/j.apr.2021.101256

Anderson, T. L., & Ogren, J. A. (1998). Determining Aerosol Radiative Properties Using the TSI 3563 Integrating Nephelometer. *Aerosol Science and Technology*, *29*(1), 57–69. https://doi.org/10.1080/02786829808965551

Arora, S., Poulain, L., Lhotka, R., Schwarz, J., Vodi, P., Pokorn, P., & Herrmann, H. (2026). *Tracing local and long-range aerosol emission areas using multi-method and multi-site analyses in central Europe zda Zikov a*. *367*(December 2025). https://doi.org/10.1016/j.atmosenv.2025.121733

Atabakhsh, S., Poulain, L., Pöhlker, M., Fomba, K. W., & Herrmann, H. (2025). Effect of Long-Range Transported Aerosol on Urban Air Quality in Eastern Germany. *ACS ES&T Air*, *2*(8), 1725–1737. https://doi.org/10.1021/acsestair.5c00126

Ausmeel, S., Eriksson, A., Ahlberg, E., & Kristensson, A. (2019). Methods for identifying aged ship plumes and estimating contribution to aerosol exposure downwind of shipping lanes. *Atmospheric Measurement Techniques*, *12*(8), 4479–4493. https://doi.org/10.5194/amt-12-4479-2019

Ausmeel, S., Eriksson, A., Ahlberg, E., Sporre, M. K., Spanne, M., & Kristensson, A. (2020). Ship plumes in the Baltic Sea Sulfur Emission Control Area: chemical characterization and contribution to coastal aerosol concentrations. *Atmospheric Chemistry and Physics*, *20*(15), 9135–9151. https://doi.org/10.5194/acp-20-9135-2020

Bakels, L., Tatsii, D., Tipka, A., Thompson, R., Dütsch, M., Blaschek, M., Seibert, P., Baier, K., Bucci, S., Cassiani, M., Eckhardt, S., Groot Zwaaftink, C., Henne, S., Kaufmann, P., Lechner, V., Maurer, C., Mulder,

M. D., Pisso, I., Plach, A., … Stohl, A. (2024). FLEXPART version 11: Improved accuracy, efficiency, and flexibility. *Geoscientific Model Development*, *17*(21), 7595–7627. https://doi.org/10.5194/gmd-17-7595-2024

Bian, H., Chin, M., Hauglustaine, D. A., Schulz, M., Myhre, G., Bauer, S. E., Lund, M. T., Karydis, V. A., Kucsera, T. L., Pan, X., Pozzer, A., Skeie, R. B., Steenrod, S. D., Sudo, K., Tsigaridis, K., Tsimpidi, A. P., & Tsyro, S. G. (2017). Investigation of global particulate nitrate from the AeroCom phase III experiment. *Atmospheric Chemistry and Physics*, *17*(21), 12911–12940. https://doi.org/10.5194/acp-17-12911-2017

Birmili, W., Heinke, K., Pitz, M., Matschullat, J., Wiedensohler, A., Cyrys, J., Wichmann, H.-E., & Peters, A. (2010). Particle number size distributions in urban air before and after volatilisation. *Atmospheric Chemistry and Physics*, *10*(10), 4643–4660. https://doi.org/10.5194/acp-10-4643-2010

Bond, T. C., Doherty, S. J., Fahey, D. W., Forster, P. M., Berntsen, T., DeAngelo, B. J., Flanner, M. G., Ghan, S., Kärcher, B., Koch, D., Kinne, S., Kondo, Y., Quinn, P. K., Sarofim, M. C., Schultz, M. G., Schulz, M., Venkataraman, C., Zhang, H., Zhang, S., … Zender, C. S. (2013). Bounding the role of black carbon in the climate system: A scientific assessment. *Journal of Geophysical Research: Atmospheres*, *118*(11), 5380–5552. https://doi.org/10.1002/jgrd.50171

Byčenkienė, S., Plauškaitė, K., Dudoitis, V., & Ulevičius, V. (2014). Urban background levels of particle number concentration and sources in Vilnius, Lithuania. *Atmospheric Research*, *143*, 279–292. https://doi.org/10.1016/j.atmosres.2014.02.019

Byčenkienė, S., Ulevičius, V., Dudoitis, V., & Pauraite, J. (2013). Identification and characterization of black carbon aerosol sources in the East Baltic Region. *Advances in Meteorology*, *2013*. https://doi.org/10.1155/2013/380614

Cao, S., Zhang, S., Gao, C., Yan, Y., Bao, J., Su, L., Liu, M., Peng, N., & Liu, M. (2021). A long-term analysis of atmospheric black carbon MERRA-2 concentration over China during 1980–2019. *Atmospheric Environment*, *264*(April), 118662. https://doi.org/10.1016/j.atmosenv.2021.118662

Cappa, C. D., Kolesar, K. R., Zhang, X., Atkinson, D. B., Pekour, M. S., Zaveri, R. A., Zelenyuk, A., & Zhang, Q. (2016). Understanding the optical properties of ambient sub- and supermicron particulate matter: results from the CARES 2010 field study in northern California. *Atmospheric Chemistry and Physics*, *16*(10), 6511–6535. https://doi.org/10.5194/acp-16-6511-2016

Carneiro, R. G., Karasewicz, M., Borges, C. K., Janicka, L., Wang, D., Fisch, G., & Stachlewska, I. S. (2024). Seasonal Analysis of Planetary Boundary Layer and Turbulence in Warsaw, Poland Through Lidar and LES Simulations. *Remote Sensing*, *16*(24). https://doi.org/10.3390/rs16244728

Carslaw, D. C., Beevers, S. D., Ropkins, K., & Bell, M. C. (2006). Detecting and quantifying aircraft and other on-airport contributions to ambient nitrogen oxides in the vicinity of a large international airport. *Atmospheric Environment*, *40*(28), 5424–5434. https://doi.org/10.1016/j.atmosenv.2006.04.062

Cavalli, F., Alastuey, A., Areskoug, H., Ceburnis, D., Čech, J., Genberg, J.,

Harrison, R. M., Jaffrezo, J. L., Kiss, G., Laj, P., Mihalopoulos, N., Perez, N., Quincey, P., Schwarz, J., Sellegri, K., Spindler, G., Swietlicki, E., Theodosi, C., Yttri, K. E., … Putaud, J. P. (2016). A European aerosol phenomenology -4: Harmonized concentrations of carbonaceous aerosol at 10 regional background sites across Europe. *Atmospheric Environment*, *144*, 133–145. https://doi.org/10.1016/j.atmosenv.2016.07.050

Cazorla, A., Bahadur, R., Suski, K. J., Cahill, J. F., Chand, D., Schmid, B., Ramanathan, V., & Prather, K. A. (2013). Relating aerosol absorption due to soot, organic carbon, and dust to emission sources determined from in-situ chemical measurements. *Atmospheric Chemistry and Physics*, *13*(18), 9337–9350. https://doi.org/10.5194/acp-13-9337-2013

Chowdhury, S., Pozzer, A., Haines, A., Klingmüller, K., Münzel, T., Paasonen, P., Sharma, A., Venkataraman, C., & Lelieveld, J. (2022). Global health burden of ambient PM2.5 and the contribution of anthropogenic black carbon and organic aerosols. *Environment International*, *159*, 107020. https://doi.org/10.1016/j.envint.2021.107020

Contini, D., Vecchi, R., & Viana, M. (2018). Carbonaceous aerosols in the atmosphere. *Atmosphere*, *9*(5), 1–8. https://doi.org/10.3390/atmos9050181

Dasari, S., Andersson, A., Stohl, A., Evangeliou, N., Holmstrand, H., Budhavant, K., Salam, A., & Gustafsson, Ö. (2020). Source Quantification of South Asian Black Carbon Aerosols with Isotopes and Modeling. *Environmental Science and Technology*, *54*(19), 11771–11779. https://doi.org/10.1021/acs.est.0c02193

Davuliene, L., Sakalys, J., Dudoitis, V., Reklaite, A., & Ulevicius, V. (2019). Long-term black carbon variation in the South-Eastern Baltic Region in 2008–2015. *Atmospheric Pollution Research*, *10*(1), 123–133. https://doi.org/10.1016/j.apr.2018.06.013

Diapouli, E., Kalogridis, A.-C., Markantonaki, C., Vratolis, S., Fetfatzis, P., Colombi, C., & Eleftheriadis, K. (2017). Annual Variability of Black Carbon Concentrations Originating from Biomass and Fossil Fuel Combustion for the Suburban Aerosol in Athens, Greece. *Atmosphere*, *8*(12), 234. https://doi.org/10.3390/atmos8120234

Draxler, R. R., & Hess, G. D. (1998). An overview of the HYSPLIT_4 modelling system for trajectories, dispersion and deposition. *Australian Meteorological Magazine*, *47*(4), 295–308. https://doi.org/10.1071/ES98032

Draxler, R. R., & Rolph, G. D. (2003). *HYSPLIT (HYbrid Single-Particle Lagrangian Integrated Trajectory); NOAA Air Resources Laboratory: Silver Spring*. https://www.arl.noaa.gov/

Drinovec, L., Močnik, G., Zotter, P., Prévôt, A. S. H., Ruckstuhl, C., Coz, E., Rupakheti, M., Sciare, J., Müller, T., Wiedensohler, A., & Hansen, A. D. A. (2015). The "dual-spot" Aethalometer: an improved measurement of aerosol black carbon with real-time loading compensation. *Atmospheric Measurement Techniques*, *8*(5), 1965–1979. https://doi.org/10.5194/amt-8-1965-2015

Dudoitis, V., Byčenkienė, S., Plauškaitė, K., Bozzetti, C., Fröhlich, R., Mordas, G., & Ulevičius, V. (2016). Spatial distribution of carbonaceous aerosol in the southeastern Baltic Sea region (event of grass fires). *Acta Geophysica*,

64(3), 711–731. https://doi.org/10.1515/acgeo-2016-0018

Ealo, M., Alastuey, A., Ripoll, A., Pérez, N., Minguillón, M. C., Querol, X., & Pandolfi, M. (2016). Detection of Saharan dust and biomass burning events using near-real-time intensive aerosol optical properties in the north-western Mediterranean. *Atmospheric Chemistry and Physics*, *16*(19), 12567–12586. https://doi.org/10.5194/acp-16-12567-2016

Eckhardt, S., Quennehen, B., Olivié, D. J. L., Berntsen, T. K., Cherian, R., Christensen, J. H., Collins, W., Crepinsek, S., Daskalakis, N., Flanner, M., Herber, A., Heyes, C., Hodnebrog, Huang, L., Kanakidou, M., Klimont, Z., Langner, J., Law, K. S., Lund, M. T., … Stohl, A. (2015). Current model capabilities for simulating black carbon and sulfate concentrations in the Arctic atmosphere: A multi-model evaluation using a comprehensive measurement data set. *Atmospheric Chemistry and Physics*, *15*(16), 9413–9433. https://doi.org/10.5194/acp-15-9413-2015

Escudero, M., Stein, A. F., Draxler, R. R., Querol, X., Alastuey, A., Castillo, S., & Avila, A. (2011). Source apportionment for African dust outbreaks over the Western Mediterranean using the HYSPLIT model. *Atmospheric Research*, *99*(3–4), 518–527. https://doi.org/10.1016/j.atmosres.2010.12.002

European Commision. (2022). *Directive of the European Parliament and of the Council on ambient air quality and cleaner air of Europe*. https://eur-lex.europa.eu/legal-content/EN/TXT/HTML/?uri=CELEX:52022PC0542&from=EN

European Environment Agency. (2020). *Air quality in Europe — 2020 report* (Issue 09). https://doi.org/10.2800/786656

Evangeliou, N., Kylling, A., Eckhardt, S., Myroniuk, V., Stebel, K., Paugam, R., Zibtsev, S., & Stohl, A. (2019). Open fires in Greenland in summer 2017: Transport, deposition and radiative effects of BC, OC and BrC emissions. *Atmospheric Chemistry and Physics*, *19*(2), 1393–1411. https://doi.org/10.5194/acp-19-1393-2019

Evangeliou, N., Platt, S. M., Eckhardt, S., Lund Myhre, C., Laj, P., Alados-Arboledas, L., Backman, J., Brem, B. T., Fiebig, M., Flentje, H., Marinoni, A., Pandolfi, M., Yus-Dìez, J., Prats, N., Putaud, J. P., Sellegri, K., Sorribas, M., Eleftheriadis, K., Vratolis, S., … Stohl, A. (2021). Changes in black carbon emissions over Europe due to COVID-19 lockdowns. *Atmospheric Chemistry and Physics*, *21*(4), 2675–2692. https://doi.org/10.5194/acp-21-2675-2021

Evangeliou, N., Thompson, R. L., Eckhardt, S., & Stohl, A. (2018). Top-down estimates of black carbon emissions at high latitudes using an atmospheric transport model and a Bayesian inversion framework. *Atmospheric Chemistry and Physics*, *18*(20), 15307–15327. https://doi.org/10.5194/acp-18-15307-2018

Feng, Y., Ramanathan, V., & Kotamarthi, V. R. (2013). Brown carbon: A significant atmospheric absorber of solar radiation. *Atmospheric Chemistry and Physics*, *13*(17), 8607–8621. https://doi.org/10.5194/acp-13-8607-2013

Forster, C., Stohl, A., & Seibert, P. (2007). Parameterization of convective transport in a Lagrangian particle dispersion model and its evaluation. *Journal of Applied Meteorology and Climatology*, *46*(4), 403–422.

https://doi.org/10.1175/JAM2470.1
Fourtziou, L., Liakakou, E., Stavroulas, I., Theodosi, C., Zarmpas, P., Psiloglou, B., Sciare, J., Maggos, T., Bairachtari, K., Bougiatioti, A., Gerasopoulos, E., Sarda-Estève, R., Bonnaire, N., & Mihalopoulos, N. (2017). Multi-tracer approach to characterize domestic wood burning in Athens (Greece) during wintertime. *Atmospheric Environment*, *148*, 89–101. https://doi.org/10.1016/j.atmosenv.2016.10.011
Fu, B., Gasser, T., Li, B., Tao, S., Ciais, P., Piao, S., Balkanski, Y., Li, W., Yin, T., Han, L., Li, X., Han, Y., An, J., Peng, S., & Xu, J. (2020). Short-lived climate forcers have long-term climate impacts via the carbon–climate feedback. *Nature Climate Change*, *10*(9), 851–855. https://doi.org/10.1038/s41558-020-0841-x
Garbarienė, I., Pauraitė, J., Pashneva, D., Minderytė, A., Sarka, K., Dudoitis, V., Davulienė, L., Gaspariūnas, M., Kovalevskij, V., Lingis, D., Bučinskas, L., Šapolaitė, J., Ežerinskis, Ž., Mainelis, G., Ovadnevaitė, J., Kecorius, S., Plauškaitė-Šukienė, K., & Byčenkienė, S. (2022). Indoor-outdoor relationship of submicron particulate matter in mechanically ventilated building: Chemical composition, sources and infiltration factor. *Building and Environment*, *222*(May), 109429. https://doi.org/10.1016/j.buildenv.2022.109429
Garg, S., Chandra, B. P., Sinha, V., Sarda-Esteve, R., Gros, V., & Sinha, B. (2016). Limitation of the Use of the Absorption Angstrom Exponent for Source Apportionment of Equivalent Black Carbon: a Case Study from the North West Indo-Gangetic Plain. *Environmental Science & Technology*, *50*(2), 814–824. https://doi.org/10.1021/acs.est.5b03868
Grange, S. K., Lötscher, H., Fischer, A., Emmenegger, L., & Hueglin, C. (2020). Evaluation of equivalent black carbon source apportionment using observations from Switzerland between 2008 and 2018. *Atmospheric Measurement Techniques*, *13*(4), 1867–1885. https://doi.org/10.5194/amt-13-1867-2020
Hall, J. V., Zibtsev, S. V., Giglio, L., Skakun, S., Myroniuk, V., Zhuravel, O., Goldammer, J. G., & Kussul, N. (2021). Environmental and political implications of underestimated cropland burning in Ukraine. *Environmental Research Letters*, *16*(6). https://doi.org/10.1088/1748-9326/abfc04
Heliasz, M., & Biermann, T. (2024). *ICOS ATC Meteo Release, Hyltemossa (30.0 m), 2017-09-26–2024-03-31*. https://hdl.handle.net/11676/OVieLf7Fv5GGYdx1UxkciTFE
Helin, A., Niemi, J. V., Virkkula, A., Pirjola, L., Teinilä, K., Backman, J., Aurela, M., Saarikoski, S., Rönkkö, T., Asmi, E., & Timonen, H. (2018). Characteristics and source apportionment of black carbon in the Helsinki metropolitan area, Finland. *Atmospheric Environment*, *190*(January), 87–98. https://doi.org/10.1016/j.atmosenv.2018.07.022
Herndon, S. C., Jayne, J. T., Lobo, P., Onasch, T. B., Fleming, G., Hagen, D. E., Whitefield, P. D., & Miake-Lye, R. C. (2008). Commercial aircraft engine emissions characterization of in-use aircraft at Hartsfield-Jackson Atlanta International Airport. *Environmental Science and Technology*, *42*(6), 1877–1883. https://doi.org/10.1021/es072029+
Hersbach, H., Bell, B., Berrisford, P., Hirahara, S., Horányi, A., Muñoz-Sabater,

J., Nicolas, J., Peubey, C., Radu, R., Schepers, D., Simmons, A., Soci, C., Abdalla, S., Abellan, X., Balsamo, G., Bechtold, P., Biavati, G., Bidlot, J., Bonavita, M., … Thépaut, J. N. (2020). The ERA5 global reanalysis. *Quarterly Journal of the Royal Meteorological Society*, *146*(730), 1999–2049. https://doi.org/10.1002/qj.3803

Hu, D., Chen, Y., Wang, Y., Daële, V., Idir, M., Yu, C., Wang, J., & Mellouki, A. (2019). Photochemical reaction playing a key role in particulate matter pollution over Central France: Insight from the aerosol optical properties. *Science of The Total Environment*, *657*, 1074–1084. https://doi.org/10.1016/j.scitotenv.2018.12.084

Hyde, J. C., Yedinak, K. M., Talhelm, A. F., Smith, A. M. S., Bowman, D. M. J. S., Johnston, F. H., Lahm, P., Fitch, M., & Tinkham, W. T. (2017). Air quality policy and fire management responses addressing smoke from wildland fires in the United States and Australia. *International Journal of Wildland Fire*, *26*(5), 347–363. https://doi.org/10.1071/WF16154

IPCC. (2023). Short-lived Climate Forcers. In *Climate Change 2021 – The Physical Science Basis* (pp. 817–922). Cambridge University Press. https://doi.org/10.1017/9781009157896.008

Jacobson, M. Z. (1998). Studying the effects of aerosols on vertical photolysis rate coefficient and temperature profiles over an urban airshed. *Journal of Geophysical Research: Atmospheres*, *103*(3339), 10593–10604. https://doi.org/10.1029/98jd00287

Jacobson, M. Z. (2005). Particle components, size distributions, and size structures. In *Fundamentals of Atmospheric Modeling* (pp. 446–469). Cambridge University Press. https://doi.org/10.1017/CBO9781139165389.014

Jafar, H. A., & Harrison, R. M. (2021). Spatial and temporal trends in carbonaceous aerosols in the United Kingdom. *Atmospheric Pollution Research*, *12*(1), 295–305. https://doi.org/10.1016/j.apr.2020.09.009

Janicka, L., Stachlewska, I. S., Veselovskii, I., & Baars, H. (2017). Temporal variations in optical and microphysical properties of mineral dust and biomass burning aerosol derived from daytime Raman lidar observations over Warsaw, Poland. *Atmospheric Environment*, *169*(July 2013), 162–174. https://doi.org/10.1016/j.atmosenv.2017.09.022

Janssen, N. A. H., Gerlofs-Nijland, M. E., Lanki, T., Salonen, R. O., Cassee, F., Hoek, G., Fischer, P., Brunekreef, B., & Krzyzanowski, M. (2012). *Health effects of Black Carbon*.

Jia, H., Pan, J., Huo, J., Fu, Q., Duan, Y., Lin, Y., Hu, X., & Cheng, J. (2021). Atmospheric black carbon in urban and traffic areas in Shanghai: Temporal variations, source characteristics, and population exposure. *Environmental Pollution*, *289*(July), 117868. https://doi.org/10.1016/j.envpol.2021.117868

Jia, M., Evangeliou, N., Eckhardt, S., Huang, X., Gao, J., Ding, A., & Stohl, A. (2021). Black Carbon Emission Reduction Due to COVID-19 Lockdown in China. *Geophysical Research Letters*, *48*(8), 1–10. https://doi.org/10.1029/2021GL093243

Jia, M., Jiang, F., Evangeliou, N., Eckhardt, S., Huang, X., Ding, A., & Stohl, A. (2023). Rapid decline of carbon monoxide emissions in the Fenwei Plain in China during the three-year Action Plan on defending the blue sky. *Journal*

of Environmental Management, *337*(February), 117735. https://doi.org/10.1016/j.jenvman.2023.117735

Jonson, J. E., Gauss, M., Jalkanen, J.-P., & Johansson, L. (2019). Effects of strengthening the Baltic Sea ECA regulations. *Atmospheric Chemistry and Physics*, *19*(21), 13469–13487. https://doi.org/10.5194/acp-19-13469-2019

Jonson, J. E., Gauss, M., Schulz, M., Jalkanen, J.-P., & Fagerli, H. (2020). Effects of global ship emissions on European air pollution levels. *Atmospheric Chemistry and Physics*, *20*(19), 11399–11422. https://doi.org/10.5194/acp-20-11399-2020

Juda-Rezler, K., Reizer, M., Maciejewska, K., Błaszczak, B., & Klejnowski, K. (2020). Characterization of atmospheric $PM_{2.5}$ sources at a Central European urban background site. *Science of The Total Environment*, *713*, 136729. https://doi.org/10.1016/j.scitotenv.2020.136729

Jung, J., Furutani, H., & Uematsu, M. (2011). Atmospheric inorganic nitrogen in marine aerosol and precipitation and its deposition to the North and South Pacific Oceans. *Journal of Atmospheric Chemistry*, *68*(2), 157–181. https://doi.org/10.1007/s10874-012-9218-5

Kaiser, J. W., Heil, A., Andreae, M. O., Benedetti, A., Chubarova, N., Jones, L., Morcrette, J. J., Razinger, M., Schultz, M. G., Suttie, M., & Van Der Werf, G. R. (2012). Biomass burning emissions estimated with a global fire assimilation system based on observed fire radiative power. *Biogeosciences*, *9*(1), 527–554. https://doi.org/10.5194/bg-9-527-2012

Kalinauskaitė, A., Davulienė, L., Pauraite, J., Minderytė, A., & Byčenkienė, S. (2024). New Year Fireworks Influence on Air Quality in Case of Stagnant Foggy Conditions. *Urban Science*, *8*(2), 54. https://doi.org/10.3390/urbansci8020054

Karl, M., Jonson, J. E., Uppstu, A., Aulinger, A., Prank, M., Sofiev, M., Jalkanen, J.-P., Johansson, L., Quante, M., & Matthias, V. (2019). Effects of ship emissions on air quality in the Baltic Sea region simulated with three different chemistry transport models. *Atmospheric Chemistry and Physics*, *19*(10), 7019–7053. https://doi.org/10.5194/acp-19-7019-2019

Kaskaoutis, D. G., Grivas, G., Stavroulas, I., Bougiatioti, A., Liakakou, E., Dumka, U. C., Gerasopoulos, E., & Mihalopoulos, N. (2021c). Apportionment of black and brown carbon spectral absorption sources in the urban environment of Athens, Greece, during winter. *Science of the Total Environment*, *801*, 149739. https://doi.org/10.1016/j.scitotenv.2021.149739

Kaskaoutis, D. G., Grivas, G., Stavroulas, I., Liakakou, E., Dumka, U. C., Dimitriou, K., Gerasopoulos, E., & Mihalopoulos, N. (2021a). In situ identification of aerosol types in Athens, Greece, based on long-term optical and on online chemical characterization. *Atmospheric Environment*, *246*(July 2020), 118070. https://doi.org/10.1016/j.atmosenv.2020.118070

Kaskaoutis, D. G., Grivas, G., Stavroulas, I., Liakakou, E., Dumka, U. C., Gerasopoulos, E., & Mihalopoulos, N. (2021b). Effect of aerosol types from various sources at an urban location on spectral curvature of scattering and absorption coefficients. *Atmospheric Research*, *264*(September), 105865. https://doi.org/10.1016/j.atmosres.2021.105865

Kaskaoutis, D. G., Pikridas, M., Barmpounis, K., Kassell, G., Logan, D., Rigler,

M., Ivančič, M., Mohammadpour, K., Mihalopoulos, N., Lelieveld, J., & Sciare, J. (2023). Aerosol characteristics and types in the marine environments surrounding the East Mediterranean - Middle East (EMME) region during the AQABA campaign. *Atmospheric Environment*, *298*(November 2022), 119633. https://doi.org/10.1016/j.atmosenv.2023.119633

Kecorius, S., Kivekäs, N., Kristensson, A., Tuch, T., Covert, D. S., Birmili, W., Lihavainen, H., Hyvärinen, A.-P., Martinsson, J., Sporre, M. K., Swietlicki, E., Wiedensohler, A., & Ulevicius, V. (2016). Significant increase of aerosol number concentrations in air masses crossing a densely trafficked sea area. *Oceanologia*, *58*(1), 1–12. https://doi.org/10.1016/j.oceano.2015.08.001

Kecorius, S., Madueño, L., Birmili, W., Löndahl, J., Plauškaitė, K., Byčenkienė, S., Lovrić, M., Petrić, V., Carranza-García, M., Jiménez-Navarro, M. J., Martínez-Ballesteros, M., Weiss, M., Schmid, O., Cyrys, J., Peters, A., & Kecorius, G. (2025). Urban pollution impact assessment in six lithuanian cities with a focus on road traffic emissions - integrated framework for environmental health studies. *Journal of Hazardous Materials*, *497*(May). https://doi.org/10.1016/j.jhazmat.2025.139725

Khadir, T., Riipinen, I., Talvinen, S., Heslin-Rees, D., Pöhlker, C., Rizzo, L., Machado, L. A. T., Franco, M. A., Kremper, L. A., Artaxo, P., Petäjä, T., Kulmala, M., Tunved, P., Ekman, A. M. L., Krejci, R., & Virtanen, A. (2023). Sink, Source or Something In-Between? Net Effects of Precipitation on Aerosol Particle Populations. *Geophysical Research Letters*, *50*(19), 1–11. https://doi.org/10.1029/2023GL104325

Kirchstetter, T. W., Novakov, T., & Hobbs, P. V. (2004). Evidence that the spectral dependence of light absorption by aerosols is affected by organic carbon. *Journal of Geophysical Research: Atmospheres*, *109*(D21), 1–12. https://doi.org/10.1029/2004JD004999

Kivekäs, N., Massling, A., Grythe, H., Lange, R., Rusnak, V., Carreno, S., Skov, H., Swietlicki, E., Nguyen, Q. T., Glasius, M., & Kristensson, A. (2014). Contribution of ship traffic to aerosol particle concentrations downwind of a major shipping lane. *Atmospheric Chemistry and Physics*, *14*(16), 8255–8267. https://doi.org/10.5194/acp-14-8255-2014

Klimont, Z., Kupiainen, K., Heyes, C., Purohit, P., Cofala, J., Rafaj, P., Borken-Kleefeld, J., & Schöpp, W. (2017). Global anthropogenic emissions of particulate matter including black carbon. *Atmospheric Chemistry and Physics*, *17*(14), 8681–8723. https://doi.org/10.5194/acp-17-8681-2017

Kostenidou, E., Lee, B.-H. H., Engelhart, G. J., Pierce, J. R., & Pandis, S. N. (2009). Mass spectra deconvolution of low, medium, and high volatility biogenic secondary organic aerosol. *Environmental Science and Technology*, *43*(13), 4884–4889. https://doi.org/10.1021/es803676g

Kristensson, A., Ausmeel, S., Pauraite, J., Eriksson, A., Ahlberg, E., Byčenkienė, S., & Degórska, A. (2020). Source Contributions to Rural Carbonaceous Winter Aerosol in North-Eastern Poland. *Atmosphere*, *11*(3), 263. https://doi.org/10.3390/atmos11030263

Kumar, P., Sharma, K., Malu, A., Rajak, R., Gupta, A., Baruah, B., Yadav, S. K., Angchuck, T., Sharma, J., Ranjan, R. K., Misra, A. K., & Wanjari, N.

(2023). *Measurement report: Intra-annual Variability of Black/Brown Carbon and Its Interrelation with Meteorological Conditions over Gangtok, Sikkim* (Issue October, pp. 31–41). https://doi.org/10.5194/egusphere-2023-702

Kutzner, R. D., von Schneidemesser, E., Kuik, F., Quedenau, J., Weatherhead, E. C., & Schmale, J. (2018). Long-term monitoring of black carbon across Germany. *Atmospheric Environment*, *185*(April), 41–52. https://doi.org/10.1016/j.atmosenv.2018.04.039

Kuwata, M., Kondo, Y., & Takegawa, N. (2009). Critical condensed mass for activation of black carbon as cloud condensation nuclei in Tokyo. *Journal of Geophysical Research Atmospheres*, *114*(20), 1–9. https://doi.org/10.1029/2009JD012086

Lewandowska, A., Falkowska, L., Murawiec, D., Pryputniewicz, D., Burska, D., & Bełdowska, M. (2010). Elemental and organic carbon in aerosols over urbanized coastal region (southern Baltic Sea, Gdynia). *Science of The Total Environment*, *408*(20), 4761–4769. https://doi.org/10.1016/j.scitotenv.2010.06.017

Lewandowska, A. U., & Falkowska, L. M. (2013a). Sea salt in aerosols over the southern Baltic. Part 1. The generation and transportation of marine particles**Parts of this paper were originally published in Polish: Lewandowska A., 2011, Chemizm aerozoli w rejonie Zatoki Gdańskiej, Wyd. UG, Gdańsk, 184p. *Oceanologia*, *55*(2), 279–298. https://doi.org/10.5697/oc.55-2.279

Lewandowska, A. U., & Falkowska, L. M. (2013b). Sea salt in aerosols over the southern Baltic. Part 2. The neutralizing properties of sea salt and ammonia**Parts of this paper were originally published in Polish: Lewandowska A., 2011, Chemizm aerozoli w rejonie Zatoki Gdańskiej, Wyd. UG, Gdańsk, 184pp. *Oceanologia*, *55*(2), 299–318. https://doi.org/10.5697/oc.55-2.299

Lewandowska, A. U., Staniszewska, M., Witkowska, A., Machuta, M., & Falkowska, L. (2018). Benzo(a)pyrene parallel measurements in PM1 and PM2.5 in the coastal zone of the Gulf of Gdansk (Baltic Sea) in the heating and non-heating seasons. *Environmental Science and Pollution Research*, *25*(20), 19458–19469. https://doi.org/10.1007/s11356-018-2089-9

Li, J., Carlson, B. E., Yung, Y. L., Lv, D., Hansen, J., Penner, J. E., Liao, H., Ramaswamy, V., Kahn, R. A., Zhang, P., Dubovik, O., Ding, A., Lacis, A. A., Zhang, L., & Dong, Y. (2022). Scattering and absorbing aerosols in the climate system. *Nature Reviews Earth and Environment*, *3*(6), 363–379. https://doi.org/10.1038/s43017-022-00296-7

Liakakou, E., Stavroulas, I., Kaskaoutis, D. G., Grivas, G., Paraskevopoulou, D., Dumka, U. C., Tsagkaraki, M., Bougiatioti, A., Oikonomou, K., Sciare, J., Gerasopoulos, E., & Mihalopoulos, N. (2020). Long-term variability, source apportionment and spectral properties of black carbon at an urban background site in Athens, Greece. *Atmospheric Environment*, *222*(November 2019), 117137. https://doi.org/10.1016/j.atmosenv.2019.117137

Lithuanian State Enterprise Centre of Registers. (n.d.). Retrieved June 4, 2025, from https://osp.stat.gov.lt/gyventojai1

Liu, C., Chung, C. E., Yin, Y., & Schnaiter, M. (2018). The absorption Ångström exponent of black carbon: from numerical aspects. *Atmospheric Chemistry and Physics*, *18*(9), 6259–6273. https://doi.org/10.5194/acp-18-6259-2018

Long, C. M., Nascarella, M. A., & Valberg, P. A. (2013). Carbon black vs. black carbon and other airborne materials containing elemental carbon: Physical and chemical distinctions. *Environmental Pollution*, *181*, 271–286. https://doi.org/10.1016/j.envpol.2013.06.009

Macuk, R. (2019). Heating in Poland. *Forum Energii*.

Makuch, P., Sitarek, S., Markuszewski, P., Petelski, T., & Stacewicz, T. (2021). Lidar observation of aerosol transformation in the atmospheric boundary layer above the Baltic Sea. *Oceanologia*, 238–246. https://doi.org/10.1016/j.oceano.2021.01.002

Manousakas, M., Papaefthymiou, H., Diapouli, E., Migliori, A., Karydas, A. G., Bogdanovic-Radovic, I., & Eleftheriadis, K. (2017). Assessment of PM2.5 sources and their corresponding level of uncertainty in a coastal urban area using EPA PMF 5.0 enhanced diagnostics. *Science of the Total Environment*. https://doi.org/10.1016/j.scitotenv.2016.09.047

Mašalaitė, A., Garbarienė, I., Garbaras, A., Šapolaitė, J., Ežerinskis, Bučinskas, L., Dudoitis, V., Kalinauskaitė, A., Pashneva, D., Minderytė, A., Remeikis, V., & Byčenkienė, S. (2024). Dual-isotope ratios of carbonaceous aerosols for seasonal observation and their assessment as source indicators. *Science of the Total Environment*, *949*(May). https://doi.org/10.1016/j.scitotenv.2024.175094

Matei, E., Râpă, M., Mateș, I. M., Popescu, A. F., Bădiceanu, A., Balint, A. I., & Covaliu-Mierlă, C. I. (2025). Heavy Metals in Particulate Matter—Trends and Impacts on Environment. *Molecules*, *30*(7), 1–29. https://doi.org/10.3390/molecules30071455

Meteo.lt API. (n.d.). Retrieved April 9, 2026, from https://api.meteo.lt/

Middlebrook, A. M., Bahreini, R., Jimenez, J. L., & Canagaratna, M. R. (2012). Evaluation of composition-dependent collection efficiencies for the Aerodyne aerosol mass spectrometer using field data. *Aerosol Science and Technology*, *46*(3), 258–271. https://doi.org/10.1080/02786826.2011.620041

Minderytė, A., Pauraite, J., Dudoitis, V., Plauškaitė, K., Kilikevičius, A., Matijošius, J., Rimkus, A., Kilikevičienė, K., Vainorius, D., & Byčenkienė, S. (2022). Carbonaceous aerosol source apportionment and assessment of transport-related pollution. *Atmospheric Environment*, *279*(February), 119043. https://doi.org/10.1016/j.atmosenv.2022.119043

Müller, T., Laborde, M., Kassell, G., & Wiedensohler, A. (2011). Design and performance of a three-wavelength LED-based total scatter and backscatter integrating nephelometer. *Atmospheric Measurement Techniques*, *4*(6), 1291–1303. https://doi.org/10.5194/amt-4-1291-2011

Ng, N. L., Herndon, S. C., Trimborn, A., Canagaratna, M. R., Croteau, P. L., Onasch, T. B., Sueper, D., Worsnop, D. R., Zhang, Q., Sun, Y. L., & Jayne, J. T. (2011). An Aerosol Chemical Speciation Monitor (ACSM) for Routine Monitoring of the Composition and Mass Concentrations of Ambient Aerosol. *Aerosol Science and Technology*, *45*(7), 780–794. https://doi.org/10.1080/02786826.2011.560211

Niemi, J. V., Saarikoski, S., Aurela, M., Tervahattu, H., Hillamo, R., Westphal, D. L., Aarnio, P., Koskentalo, T., Makkonen, U., Vehkamäki, H., & Kulmala, M. (2009). Long-range transport episodes of fine particles in southern Finland during 1999–2007. *Atmospheric Environment*, *43*(6), 1255–1264. https://doi.org/10.1016/j.atmosenv.2008.11.022

O'Dowd, C. D., & De Leeuw, G. (2007). Marine aerosol production: A review of the current knowledge. *Philosophical Transactions of the Royal Society A: Mathematical, Physical and Engineering Sciences*, *365*(1856), 1753–1774. https://doi.org/10.1098/rsta.2007.2043

Ovadnevaite, J., Ceburnis, D., Leinert, S., Dall'Osto, M., Canagaratna, M., O'Doherty, S., Berresheim, H., & O'Dowd, C. (2014). Submicron NE Atlantic marine aerosol chemical composition and abundance: Seasonal trends and air mass categorization. *Journal of Geophysical Research: Atmospheres*, *119*(20), 11,850-11,863. https://doi.org/10.1002/2013JD021330

Paatero, P. (1997). A weighted non-negative least squares algorithm for three-way 'PARAFAC' factor analysis. *Chemometrics and Intelligent Laboratory Systems*, *38*(2), 223–242. https://doi.org/10.1016/S0169-7439(97)00031-2

Paglione, M., Gilardoni, S., Rinaldi, M., Decesari, S., Zanca, N., Sandrini, S., Giulianelli, L., Bacco, D., Ferrari, S., Poluzzi, V., Scotto, F., Trentini, A., Poulain, L., Herrmann, H., Wiedensohler, A., Canonaco, F., Prévôt, A. S. H., Massoli, P., Carbone, C., … Fuzzi, S. (2020). The impact of biomass burning and aqueous-phase processing on air quality: a multi-year source apportionment study in the Po Valley, Italy. *Atmospheric Chemistry and Physics*, *20*(3), 1233–1254. https://doi.org/10.5194/acp-20-1233-2020

Pandolfi, M., Alados-Arboledas, L., Alastuey, A., Andrade, M., Angelov, C., Artiñano, B., Backman, J., Baltensperger, U., Bonasoni, P., Bukowiecki, N., Collaud Coen, M., Conil, S., Coz, E., Crenn, V., Dudoitis, V., Ealo, M., Eleftheriadis, K., Favez, O., Fetfatzis, P., … Laj, P. (2018). A European aerosol phenomenology – 6: scattering properties of atmospheric aerosol particles from 28 ACTRIS sites. *Atmospheric Chemistry and Physics*, *18*(11), 7877–7911. https://doi.org/10.5194/acp-18-7877-2018

Pappin, A. J., Charman, N., Egyed, M., Blagden, P., Duhamel, A., Miville, J., Popadic, I., Manseau, P. M., Marcotte, G., Mashayekhi, R., Racine, J., Rittmaster, R., Edwards, B., Kipusi, W., & Smith-Doiron, M. (2024). Attribution of fine particulate matter and ozone health impacts in Canada to domestic and US emission sources. *Science of the Total Environment*, *909*, 168529. https://doi.org/10.1016/j.scitotenv.2023.168529

Pauraite, J., Dudoitis, V., & Byčenkienė, S. (2023). Assessment of Carbonaceous Aerosol Properties across an Urban Environment during the Cold Season. *Atmosphere*, *14*(7), 1054. https://doi.org/10.3390/atmos14071054

Pauraite, J., Mainelis, G., Kecorius, S., Minderytė, A., Dudoitis, V., Garbarienė, I., Plauškaitė, K., Ovadnevaite, J., & Byčenkienė, S. (2021). Office Indoor PM and BC Level in Lithuania: The Role of a Long-Range Smoke Transport Event. *Atmosphere*, *12*(8), 1047. https://doi.org/10.3390/atmos12081047

Pauraite, J., Minderytė, A., Dudoitis, V., Plauškaitė, K., & Byčenkienė, S. (2022). Effect of urban submicron particles on single scattering albedo: the case study of high pollution event. *Journal of Quantitative Spectroscopy and*

Radiative Transfer, *280*, 108075. https://doi.org/10.1016/j.jqsrt.2022.108075

Pauraite, J., Plauškaitė, K., Dudoitis, V., & Ulevicius, V. (2018). Relationship between the Optical Properties and Chemical Composition of Urban Aerosol Particles in Lithuania. *Advances in Meteorology*, *2018*, 1–10. https://doi.org/10.1155/2018/8674173

Pettersson, K., Axelsson, E., Eriksson, L., Svensson, E., Berntsson, T., & Harvey, S. (2020). Holistic methodological framework for assessing the benefits of delivering industrial excess heat to a district heating network. *International Journal of Energy Research*, *44*(4), 2634–2651. https://doi.org/10.1002/er.5005

Pirjola, L., Niemi, J. V., Saarikoski, S., Aurela, M., Enroth, J., Carbone, S., Saarnio, K., Kuuluvainen, H., Kousa, A., Rönkkö, T., & Hillamo, R. (2017). Physical and chemical characterization of urban winter-time aerosols by mobile measurements in Helsinki, Finland. *Atmospheric Environment*, *158*(1), 60–75. https://doi.org/10.1016/j.atmosenv.2017.03.028

Pisso, I., Sollum, E., Grythe, H., Kristiansen, N. I., Cassiani, M., Eckhardt, S., Arnold, D., Morton, D., Thompson, R. L., Groot Zwaaftink, C. D., Evangeliou, N., Sodemann, H., Haimberger, L., Henne, S., Brunner, D., Burkhart, J. F., Fouilloux, A., Brioude, J., Philipp, A., … Stohl, A. (2019). The Lagrangian particle dispersion model FLEXPART version 10.4. *Geoscientific Model Development*, *12*(12), 4955–4997. https://doi.org/10.5194/gmd-12-4955-2019

Plauškaitė, K., Špirkauskaitė, N., Byčenkienė, S., Kecorius, S., Jasinevičienė, D., Petelski, T., Zielinski, T., Andriejauskienė, J., Barisevičiūtė, R., Garbaras, A., Makuch, P., Dudoitis, V., & Ulevicius, V. (2017). Characterization of aerosol particles over the southern and South-Eastern Baltic Sea. *Marine Chemistry*, *190*, 13–27. https://doi.org/10.1016/j.marchem.2017.01.003

Pokhrel, R. P., Wagner, N. L., Langridge, J. M., Lack, D. A., Jayarathne, T., Stone, E. A., Stockwell, C. E., Yokelson, R. J., & Murphy, S. M. (2016). Parameterization of single-scattering albedo (SSA) and absorption Ångström exponent (AAE) with EC / OC for aerosol emissions from biomass burning. *Atmospheric Chemistry and Physics*, *16*(15), 9549–9561. https://doi.org/10.5194/acp-16-9549-2016

Popovicheva, O. B., Evangeliou, N., Eleftheriadis, K., Kalogridis, A. C., Sitnikov, N., Eckhardt, S., & Stohl, A. (2017). Black Carbon Sources Constrained by Observations in the Russian High Arctic. *Environmental Science and Technology*, *51*(7), 3871–3879. https://doi.org/10.1021/acs.est.6b05832

Popovicheva, O., Chichaeva, M., Kovach, R., Tsai, Y. I., Diapouli, E., & Kasimov, N. (2025). Seasonal and wildfire biomass burning impact on gas-fuel heated northern European megacity: brown carbon apportionment. *Atmospheric Environment*, *357*(May), 121325. https://doi.org/10.1016/j.atmosenv.2025.121325

Putaud, J. P., Cavalli, F., & Crippa, M. (2018). Long-term trends in black carbon from biomass and fossil fuel combustion detected at the JRC atmospheric observatory in Ispra. *European Commission*. https://publications.jrc.ec.europa.eu/repository/bitstream/JRC110502/kjna29147enn.pdf

Putaud, J. P., Raes, F., Van Dingenen, R., Brüggemann, E., Facchini, M. C., Decesari, S., Fuzzi, S., Gehrig, R., Hüglin, C., Laj, P., Lorbeer, G., Maenhaut, W., Mihalopoulos, N., Müller, K., Querol, X., Rodriguez, S., Schneider, J., Spindler, G., Ten Brink, H., … Wiedensohler, A. (2004). A European aerosol phenomenology - 2: Chemical characteristics of particulate matter at kerbside, urban, rural and background sites in Europe. *Atmospheric Environment*, *38*(16), 2579–2595. https://doi.org/10.1016/j.atmosenv.2004.01.041

Putaud, J. P., Van Dingenen, R., Alastuey, A., Bauer, H., Birmili, W., Cyrys, J., Flentje, H., Fuzzi, S., Gehrig, R., Hansson, H. C., Harrison, R. M., Herrmann, H., Hitzenberger, R., Hüglin, C., Jones, A. M., Kasper-Giebl, A., Kiss, G., Kousa, A., Kuhlbusch, T. A. J., … Raes, F. (2010). A European aerosol phenomenology - 3: Physical and chemical characteristics of particulate matter from 60 rural, urban, and kerbside sites across Europe. *Atmospheric Environment*, *44*(10), 1308–1320. https://doi.org/10.1016/j.atmosenv.2009.12.011

Quinn, P. K., Coffman, D. J., Johnson, J. E., Upchurch, L. M., & Bates, T. S. (2017). Small fraction of marine cloud condensation nuclei made up of sea spray aerosol. *Nature Geoscience*, *10*(9), 674–679. https://doi.org/10.1038/ngeo3003

Rafaqat, W., Sanchez, P., Botnen, D., & Fernandez-Anez, N. (2025). Analysing historical events and current management strategies of wildfires in Norway. *Scientific Reports*, *15*(1), 1–17. https://doi.org/10.1038/s41598-025-08760-2

Rajesh, T. A., & Ramachandran, S. (2018). Black carbon aerosol mass concentration, absorption and single scattering albedo from single and dual spot aethalometers: Radiative implications. *Journal of Aerosol Science*, *119*(January), 77–90. https://doi.org/10.1016/j.jaerosci.2018.02.001

Reddington, C. L., McMeeking, G., Mann, G. W., Coe, H., Frontoso, M. G., Liu, D., Flynn, M., Spracklen, D. V., & Carslaw, K. S. (2013). The mass and number size distributions of black carbon aerosol over Europe. *Atmospheric Chemistry and Physics*, *13*(9), 4917–4939. https://doi.org/10.5194/acp-13-4917-2013

Rolph, G., Stein, A., & Stunder, B. (2017). Real-time Environmental Applications and Display sYstem: READY. *Environmental Modelling & Software*, *95*, 210–228. https://doi.org/10.1016/j.envsoft.2017.06.025

Romano, S., Perrone, M. R., Pavese, G., Esposito, F., & Calvello, M. (2019). Optical properties of PM2.5 particles: Results from a monitoring campaign in southeastern Italy. *Atmospheric Environment*, *203*(June 2018), 35–47. https://doi.org/10.1016/j.atmosenv.2019.01.037

Rönkkö, T., Saarikoski, S., Kuittinen, N., Karjalainen, P., Keskinen, H., Järvinen, A., Mylläri, F., Aakko-Saksa, P., & Timonen, H. (2023). Review of black carbon emission factors from different anthropogenic sources. *Environmental Research Letters*, *18*(3), 033004. https://doi.org/10.1088/1748-9326/acbb1b

Rovira, J., Savadkoohi, M., Chen, G. I., Močnik, G., Aas, W., Alados-Arboledas, L., Artiñano, B., Aurela, M., Backman, J., Banerji, S., Beddows, D., Brem, B., Chazeau, B., Coen, M. C., Colombi, C., Conil, S., Costabile, F., Coz, E.,

de Brito, J. F., … Pandolfi, M. (2025). A European aerosol phenomenology – 9: Light absorption properties of carbonaceous aerosol particles across surface Europe. *Environment International*, *195*(November 2024), 109185. https://doi.org/10.1016/j.envint.2024.109185

Saarikoski, S., Niemi, J. V., Aurela, M., Pirjola, L., Kousa, A., Rönkkö, T., & Timonen, H. (2021). Sources of black carbon at residential and traffic environments obtained by two source apportionment methods. *Atmospheric Chemistry and Physics*, *21*(19), 14851–14869. https://doi.org/10.5194/acp-21-14851-2021

Sandradewi, J., Prévôt, A. S. H., Weingartner, E., Schmidhauser, R., Gysel, M., & Baltensperger, U. (2008). A study of wood burning and traffic aerosols in an Alpine valley using a multi-wavelength Aethalometer. *Atmospheric Environment*, *42*(1), 101–112. https://doi.org/10.1016/j.atmosenv.2007.09.034

Sandrini, S., Van Pinxteren, D., Giulianelli, L., Herrmann, H., Poulain, L., Cristina Facchini, M., Gilardoni, S., Rinaldi, M., Paglione, M., Turpin, B. J., Pollini, F., Bucci, S., Zanca, N., & Decesari, S. (2016). Size-resolved aerosol composition at an urban and a rural site in the Po Valley in summertime: Implications for secondary aerosol formation. *Atmospheric Chemistry and Physics*, *16*(17), 10879–10897. https://doi.org/10.5194/acp-16-10879-2016

Sasakawa, M., Ooki, A., & Uematsu, M. (2003). Aerosol size distribution during sea fog and its scavenge process of chemical substances over the northwestern North Pacific. *Journal of Geophysical Research: Atmospheres*, *108*(D3), 1–9. https://doi.org/10.1029/2002JD002329

Sauvage, B., Fontaine, A., Eckhardt, S., Auby, A., Boulanger, D., Petetin, H., Paugam, R., Athier, G., Cousin, J. M., Darras, S., Nédélec, P., Stohl, A., Turquety, S., Cammas, J. P., & Thouret, V. (2017). Source attribution using FLEXPART and carbon monoxide emission inventories: SOFT-IO version 1.0. *Atmospheric Chemistry and Physics*, *17*(24), 15271–15292. https://doi.org/10.5194/acp-17-15271-2017

Savadkoohi, M., Pandolfi, M., Favez, O., Putaud, J.-P., Eleftheriadis, K., Fiebig, M., Hopke, P. K., Laj, P., Wiedensohler, A., Alados-Arboledas, L., Bastian, S., Chazeau, B., María, Á. C., Colombi, C., Costabile, F., Green, D. C., Hueglin, C., Liakakou, E., Luoma, K., … Querol, X. (2024). Recommendations for reporting equivalent black carbon (eBC) mass concentrations based on long-term pan-European in-situ observations. *Environment International*, *185*(December 2023), 108553. https://doi.org/10.1016/j.envint.2024.108553

Savadkoohi, M., Pandolfi, M., Reche, C., Niemi, J. V., Mooibroek, D., Titos, G., Green, D. C., Tremper, A. H., Hueglin, C., Liakakou, E., Mihalopoulos, N., Stavroulas, I., Artiñano, B., Coz, E., Alados-Arboledas, L., Beddows, D., Riffault, V., De Brito, J. F., Bastian, S., … Querol, X. (2023). The variability of mass concentrations and source apportionment analysis of equivalent black carbon across urban Europe. *Environment International*, *178*(July), 108081. https://doi.org/10.1016/j.envint.2023.108081

Schmeisser, L., Andrews, E., Ogren, J. A., Sheridan, P., Jefferson, A., Sharma, S., Kim, J. E., Sherman, J. P., Sorribas, M., Kalapov, I., Arsov, T., Angelov,

C., Mayol-Bracero, O. L., Labuschagne, C., Kim, S. W., Hoffer, A., Lin, N. H., Chia, H. P., Bergin, M., … Wu, H. (2017). Classifying aerosol type using in situ surface spectral aerosol optical properties. *Atmospheric Chemistry and Physics*, *17*(19), 12097–12120. https://doi.org/10.5194/acp-17-12097-2017

Schneider, M. Y., Jiang, J., Chen, Y., Aas, W., Atabakhsh, S., Aurela, M., Belis, C., Bougiatioti, A., Bressi, M., Canonaco, F., Chazeau, B., Chebaicheb, H., Ehn, M., Eleftheriadis, K., Favez, O., Flentje, H., Font, A., Freney, E., Gilardoni, S., … Prévôt, A. S. H. (2025). Analysis of source regions and transport pathways of sub-micron aerosol components in Europe. *Environmental Pollution*, *385*(September). https://doi.org/10.1016/j.envpol.2025.127110

Scotto, F., Bacco, D., Lasagni, S., Trentini, A., Poluzzi, V., & Vecchi, R. (2021). A multi-year source apportionment of PM2.5 at multiple sites in the southern Po Valley (Italy). *Atmospheric Pollution Research*, *12*(11), 101192. https://doi.org/10.1016/j.apr.2021.101192

Sedlacek, A. J. (2016). Aethalometer™ Instrument Handbook. *U.S. Department of Energy*, *DOE/SC-ARM*(April), 1–28. https://www.arm.gov/publications/tech_reports/handbooks/aeth_handbook.pdf

Seinfeld, J. H., & Pandis, S. N. (2006). ATMOSPHERIC CHEMISTRY AND PHYSICS. In *The Earth as transformed by human action* (2nd ed.). https://doi.org/10.1063/1.882420

Seppälä, S. D., Kuula, J., Hyvärinen, A.-P., Saarikoski, S., Rönkkö, T., Keskinen, J., Jalkanen, J.-P., & Timonen, H. (2021). Effects of marine fuel sulfur restrictions on particle number concentrations and size distributions in ship plumes in the Baltic Sea. *Atmospheric Chemistry and Physics*, *21*(4), 3215–3234. https://doi.org/10.5194/acp-21-3215-2021

Shan, Y., Liu, X., Lin, L., Ke, Z., & Lu, Z. (2021). An Improved Representation of Aerosol Wet Removal by Deep Convection and Impacts on Simulated Aerosol Vertical Profiles. *Journal of Geophysical Research: Atmospheres*, *126*(13), 1–23. https://doi.org/10.1029/2020JD034173

Shrivastava, M., Cappa, C. D., Fan, J., Goldstein, A. H., Guenther, A. B., Jimenez, J. L., Kuang, C., Laskin, A., Martin, S. T., Ng, N. L., Petaja, T., Pierce, J. R., Rasch, P. J., Roldin, P., Seinfeld, J. H., Shilling, J., Smith, J. N., Thornton, J. A., Volkamer, R., … Zhang, Q. (2017). Recent advances in understanding secondary organic aerosol: Implications for global climate forcing. *Reviews of Geophysics*, *55*(2), 509–559. https://doi.org/10.1002/2016RG000540

Soomere, T. (2003). Anisotropy of wind and wave regimes in the Baltic proper. *Journal of Sea Research*, *49*(4), 305–316. https://doi.org/10.1016/S1385-1101(03)00034-0

Spracklen, D. V., Carslaw, K. S., Pöschl, U., Rap, A., & Forster, P. M. (2011). Global cloud condensation nuclei influenced by carbonaceous combustion aerosol. *Atmospheric Chemistry and Physics*, *11*(17), 9067–9087. https://doi.org/10.5194/acp-11-9067-2011

Stachlewska, I., Samson, M., Zawadzka, O., Harenda, K., Janicka, L., Poczta, P., Szczepanik, D., Heese, B., Wang, D., Borek, K., Tetoni, E., Proestakis, E.,

Siomos, N., Nemuc, A., Chojnicki, B., Markowicz, K., Pietruczuk, A., Szkop, A., Althausen, D., … Zehner, C. (2018). Modification of Local Urban Aerosol Properties by Long-Range Transport of Biomass Burning Aerosol. *Remote Sensing*, *10*(3), 412. https://doi.org/10.3390/rs10030412

Stachlewska, I., Zawadzka, O., & Engelmann, R. (2017). Effect of Heat Wave Conditions on Aerosol Optical Properties Derived from Satellite and Ground-Based Remote Sensing over Poland. *Remote Sensing*, *9*(11), 1199. https://doi.org/10.3390/rs9111199

Statistics Poland. (n.d.). Retrieved June 4, 2025, from https://stat.gov.pl/podstawowe-dane/

Stein, A. F., Draxler, R. R., Rolph, G. D., Stunder, B. J. B. B., Cohen, M. D., & Ngan, F. (2015). Noaa's hysplit atmospheric transport and dispersion modeling system. *Bulletin of the American Meteorological Society*, *96*(12), 2059–2077. https://doi.org/10.1175/BAMS-D-14-00110.1

Stohl, A., Forster, C., Frank, A., Seibert, P., & Wotawa, G. (2005). Technical note: The Lagrangian particle dispersion model FLEXPART version 6.2. *Atmospheric Chemistry and Physics*, *5*(9), 2461–2474. https://doi.org/10.5194/acp-5-2461-2005

Tang, P., Shao, S., Zhan, J., Zhou, L., Hu, Z., Mu, Y., & Ye, L. (2026). Contrasting pathways of spring black carbon pollution in Northeastern Sichuan basin: Biomass burning transport versus local fossil fuel accumulation. *Atmospheric Environment*, *368*(December 2025), 121765. https://doi.org/10.1016/j.atmosenv.2025.121765

Tichý, O., Eckhardt, S., Balkanski, Y., Hauglustaine, D., & Evangeliou, N. (2023). Decreasing trends of ammonia emissions over Europe seen from remote sensing and inverse modelling. *Atmospheric Chemistry and Physics*, *23*(24), 15235–15252. https://doi.org/10.5194/acp-23-15235-2023

Timko, M. T., Albo, S. E., Onasch, T. B., Fortner, E. C., Yu, Z., Miake-Lye, R. C., Canagaratna, M. R., Ng, N. L., & Worsnop, D. R. (2014). Composition and sources of the organic particle emissions from aircraft engines. *Aerosol Science and Technology*, *48*(1), 61–73. https://doi.org/10.1080/02786826.2013.857758

Tu, Y., Liu, Y., Zhang, M., Cao, Q., & Wang, L. (2026). The effect of open biomass burning on air quality and radiation before spring plowing in Northeast China. *Atmospheric Environment*, *367*(August 2025), 121685. https://doi.org/10.1016/j.atmosenv.2025.121685

Ulevicius, V., Byčenkienė, S., Bozzetti, C., Vlachou, A., Plauškaitė, K., Mordas, G., Dudoitis, V., Abbaszade, G., Remeikis, V., Garbaras, A., Masalaite, A., Blees, J., Fröhlich, R., Dällenbach, K. R., Canonaco, F., Slowik, J. G., Dommen, J., Zimmermann, R., Schnelle-Kreis, J., … Prévôt, A. S. H. (2016). Fossil and non-fossil source contributions to atmospheric carbonaceous aerosols during extreme spring grassland fires in Eastern Europe. *Atmospheric Chemistry and Physics*, *16*(9), 5513–5529. https://doi.org/10.5194/acp-16-5513-2016

Van Dingenen, R., Raes, F., Putaud, J. P., Baltensperger, U., Charron, A., Facchini, M. C., Decesari, S., Fuzzi, S., Gehrig, R., Hansson, H. C., Harrison, R. M., Hüglin, C., Jones, A. M., Laj, P., Lorbeer, G., Maenhaut, W., Palmgren, F., Querol, X., Rodriguez, S., … Wåhlin, P. (2004). A

European aerosol phenomenology - 1: Physical characteristics of particulate matter at kerbside, urban, rural and background sites in Europe. *Atmospheric Environment*, *38*(16), 2561–2577. https://doi.org/10.1016/j.atmosenv.2004.01.040

Wang, D., Szczepanik, D., & Stachlewska, I. S. (2019). Interrelations between surface, boundary layer, and columnar aerosol properties derived in summer and early autumn over a continental urban site in Warsaw, Poland. *Atmospheric Chemistry and Physics*, *19*(20), 13097–13128. https://doi.org/10.5194/acp-19-13097-2019

Weagle, C. L., Snider, G., Li, C., Van Donkelaar, A., Philip, S., Bissonnette, P., Burke, J., Jackson, J., Latimer, R., Stone, E., Abboud, I., Akoshile, C., Anh, N. X., Brook, J. R., Cohen, A., Dong, J., Gibson, M. D., Griffith, D., He, K. B., … Martin, R. V. (2018). Global Sources of Fine Particulate Matter: Interpretation of PM2.5 Chemical Composition Observed by SPARTAN using a Global Chemical Transport Model. *Environmental Science and Technology*, *52*(20), 11670–11681. https://doi.org/10.1021/acs.est.8b01658

Weingartner, E., Saathoff, H., Schnaiter, M., Streit, N., Bitnar, B., & Baltensperger, U. (2003). Absorption of light by soot particles: determination of the absorption coefficient by means of aethalometers. *Journal of Aerosol Science*, *34*(10), 1445–1463. https://doi.org/10.1016/S0021-8502(03)00359-8

Winiger, P., Andersson, A., Eckhardt, S., Stohl, A., & Gustafsson, O. (2016). The sources of atmospheric black carbon at a European gateway to the Arctic. *Nature Communications*, *7*. https://doi.org/10.1038/ncomms12776

Winiger, P., Barrett, T. E., Sheesley, R. J., Huang, L., Sharma, S., Barrie, L. A., Yttri, K. E., Evangeliou, N., Eckhardt, S., Stohl, A., Klimont, Z., Heyes, C., Semiletov, I. P., Dudarev, O. V., Charkin, A., Shakhova, N., Holmstrand, H., Andersson, A., & Gustafsson. (2019). Source apportionment of circum-Arctic atmospheric black carbon from isotopes and modeling. *Science Advances*, *5*(2). https://doi.org/10.1126/sciadv.aau8052

Winiwarter, W., Lindl, F., Zhang, S., Höglund-Isaksson, L., Kaltenegger, K., Wieser, L., Gomez Sanabria, A., Purohit, P., & Klimont, Z. (2024). *Anthropogenic emissions of CH4, N2O, F-gases and BC from GAINS, for EU-countries plus CH, NO, UK developed under the EYE-CLIMA project - March 2025 update*. https://doi.org/10.5281/zenodo.10886780

Winkler, P. (1988). The growth of atmospheric aerosol particles with relative humidity. *Physica Scripta*, *37*(2), 223–230. https://doi.org/10.1088/0031-8949/37/2/008

Witkowska, A., Lewandowska, A., & Falkowska, L. M. (2016). Parallel measurements of organic and elemental carbon dry (PM1, PM2.5) and wet (rain, snow, mixed) deposition into the Baltic Sea. *Marine Pollution Bulletin*, *104*(1–2), 303–312. https://doi.org/10.1016/j.marpolbul.2016.01.003

World Health Organization (WHO). (2021). *WHO global air quality guidelines. Particulate matter (PM2.5 and PM10), ozone, nitrogen dioxide, sulfur dioxide and carbon monoxide*. World Health Organization. https://apps.who.int/iris/handle/10665/345329

Xie, Y., Zeng, L., Hu, S., Wang, T., Du, Z., Tan, T., Xu, N., Chen, S., Mao, J.,

Xu, F., & Hu, M. (2025). Long-term trends of black carbon levels, sources, and radiative effects from 2013 to 2022 in Beijing, China. *Npj Clean Air*, *1*(1), 1–11. https://doi.org/10.1038/s44407-025-00010-z

Yang, A., Tan, Q., Rajapakshe, C., Chin, M., & Yu, H. (2022). Global premature mortality by dust and pollution PM2.5 estimated from aerosol reanalysis of the modern-era retrospective analysis for research and applications, version 2. *Frontiers in Environmental Science*, *10*(September), 1–18. https://doi.org/10.3389/fenvs.2022.975755

Yassin, M. F., Al-Shatti, L. A., & Al Rashidi, M. S. (2018). Assessment of the atmospheric mixing layer height and its effects on pollutant dispersion. *Environmental Monitoring and Assessment*, *190*(7), 372. https://doi.org/10.1007/s10661-018-6737-9

Yttri, K. E., Bäcklund, A., Conen, F., Eckhardt, S., Evangeliou, N., Fiebig, M., Kasper-Giebl, A., Gold, A., Gundersen, H., Myhre, C. L., Platt, S. M., Simpson, D., Surratt, J. D., Szidat, S., Rauber, M., Tørseth, K., Ytre-Eide, M. A., Zhang, Z., & Aas, W. (2024). Composition and sources of carbonaceous aerosol in the European Arctic at Zeppelin Observatory, Svalbard (2017 to 2020). *Atmospheric Chemistry and Physics*, *24*(4), 2731–2758. https://doi.org/10.5194/acp-24-2731-2024

Yuan, C. S., Chuang, H. L., Tseng, Y. L., Li, T. C., Soong, K. Y., & Cheng, W. H. (2024). Long-range transport and source apportionment of marine fine particles in the Taiwan Strait and South China Sea Intersection: Spatiotemporal variations and chemical fingerprints. *Atmospheric Environment*, *339*(October), 120867. https://doi.org/10.1016/j.atmosenv.2024.120867

Zgłobicki, W., & Baran-Zgłobicka, B. (2024). Air pollution in major Polish cities in the period 2005–2021: Intensity, effects and attempts to reduce it. *Environmental Research*, *240* (September 2023), 117497. https://doi.org/10.1016/j.envres.2023.117497

Zhang, G., Peng, X., Sun, W., Fu, Y., Yang, Y., Liu, D., Shi, Z., Tang, M., Wang, X., & Bi, X. (2024). Fog/cloud processing of atmospheric aerosols from a single particle perspective: A review of field observations. *Atmospheric Environment*, *329*(April), 120536. https://doi.org/10.1016/j.atmosenv.2024.120536

Zhang, Q., Jiang, X., Tong, D., Davis, S. J., Zhao, H., Geng, G., Feng, T., Zheng, B., Lu, Z., Streets, D. G., Ni, R., Brauer, M., Van Donkelaar, A., Martin, R. V., Huo, H., Liu, Z., Pan, D., Kan, H., Yan, Y., … Guan, D. (2017). Transboundary health impacts of transported global air pollution and international trade. *Nature*, *543*(7647), 705–709. https://doi.org/10.1038/nature21712

Zhu, C., Kanaya, Y., Takigawa, M., Ikeda, K., Tanimoto, H., Taketani, F., Miyakawa, T., Kobayashi, H., & Pisso, I. (2020). FLEXPART v10.1 simulation of source contributions to Arctic black carbon. *Atmospheric Chemistry and Physics*, *20*(3), 1641–1656. https://doi.org/10.5194/acp-20-1641-2020

Zhuang, B. L., Wang, T. J., Liu, J., Ma, Y., Yin, C. Q., Li, S., Xie, M., Han, Y., Zhu, J. L., Yang, X. Q., & Fu, C. B. (2015). Absorption coefficient of urban aerosol in Nanjing, west Yangtze River Delta, China. *Atmospheric*

Chemistry and Physics, *15*(23), 13633–13646. https://doi.org/10.5194/acp-15-13633-2015

Zotter, P., Herich, H., Gysel, M., El-Haddad, I., Zhang, Y., Močnik, G., Hüglin, C., Baltensperger, U., Szidat, S., & Prévôt, A. S. H. (2017). Evaluation of the absorption Ångström exponents for traffic and wood burning in the Aethalometer-based source apportionment using radiocarbon measurements of ambient aerosol. *Atmospheric Chemistry and Physics*, *17*(6), 4229–4249. https://doi.org/10.5194/acp-17-4229-2017

CURRICULUM VITAE

Agnė Minderytė

Education

2022–2026	*Joint Ph.D. studies* Natural sciences, Physics – N 002 Center for Physical Sciences and Technology & Vilnius University, Faculty of Physics
2020–2022	*Master's degree in physics* (Magna Cum Laude diploma) Vilnius University, Faculty of Physics
2016–2020	*Bachelor's degree in chemistry* Vilnius University, Faculty of Chemistry and Geosciences

Work experience

2023–2026	*Junior Researcher* Department of Environmental Research, Center for Physical Sciences and Technology
2020–2022	*Engineer* Department of Environmental Research, Center for Physical Sciences and Technology
2019–2020	*Technician* Department of Environmental Research, Center for Physical Sciences and Technology

Secondments

12–26 April, 2026	Institute of Geophysics, Faculty of Physics, University of Warsaw, Poland *The effect of extensive biomass burning events in urban environments of Vilnius and Warsaw*
7 April – 20 June, 2025	Institute of Geophysics, Faculty of Physics, University of Warsaw, Poland *The quantification of the city-produced and long-range transported black carbon in urban environments of Vilnius and Warsaw*
1 March – 31 May, 2023	Department of Design Sciences, Ergonomics and Aerosol Technology, Lund University, Lund, Sweden *Investigation of the long-range transport influence on wintertime submicron aerosol chemical composition across Hyltemossa and Preila*

GYVENIMO APRAŠYMAS

Agnė Minderytė

Išsilavinimas	
2022–2026	*Jungtinės doktorantūros studijos* Gamtos mokslai, fizika – N 002 Fizinių ir technologijos mokslų centras ir Vilniaus universitetas, Fizikos fakultetas
2020–2022	*Fizikos magistro diplomas* (Magna Cum Laude diplomas) Vilniaus universitetas, Fizikos fakultetas
2016–2020	*Chemijos bakalauro laipsnis* Vilniaus universitetas, Chemijos ir geomokslų fakultetas

Darbo patirtis	
2023–2026	*Jaunesnioji mokslo darbuotoja* Aplinkotyros skyrius, Fizinių ir technologijos mokslų centras
2020–2022	*Inžinierė* Aplinkotyros skyrius, Fizinių ir technologijos mokslų centras
2019–2020	*Technikė* Aplinkotyros skyrius, Fizinių ir technologijos mokslų centras

Stažuotės	
Balandžio 12–26 d., 2026	Geofizikos institutas, Fizikos fakultetas, Varšuvos universitetas, Lenkija *The effect of extensive biomass burning events in urban environments of Vilnius and Warsaw*
Balandžio 7 d. – Birželio 20 d. 2025	Geofizikos institutas, Fizikos fakultetas, Varšuvos universitetas, Lenkija *The quantification of the city-produced and long-range transported black carbon in urban environments of Vilnius and Warsaw*
Kovo 1 d. – Gegužės 31 d. 2023	Dizaino mokslų, ergonomikos ir aerozolio technologijų skyrius, Lundo universitetas, Švedija *Investigation of the long-range transport influence on wintertime submicron aerosol chemical composition across Hyltemossa and Preila*

ACKNOWLEDGEMENTS

This dissertation could not have been possible without the support and guidance of many. Although it is in the field of Natural Sciences, Physics, I feel the journey was more about the people involved than the physics itself.

Įžvalgus vadovės Steigvilės Byčenkienės žvilgsnis turėjo lemiamos reikšmės tam, kad ši disertacija įgytų svorį ir išvystų dienos šviesą. Jos palaikymo dėka tęsiau tyrimus mane dominančioje temoje nuo bakalauro studijų laikų, galėjau praplėsti savo įgūdžių ratą daugybės konferencijų ir stažuočių metu Lietuvoje ir užsienyje.

Mano akademinei kelionei neįkainojamą įtaką padarė Julija Pauraitė. Esu dėkinga už pirmąjį supažindinimą su aetalometru ir juodąja anglimi, nuo kurio prasidėjo mano susižavėjimas *aerozoliais*, pastūmėjimus keliauti ir mokytis, akiratį ir suvokimą plečiančias diskusijas, kurių pagrindu savo akademiniu keliu ėjau užtikrinčiau.

I am grateful to Iwona S. Stachlewska for her encouragement and support, and for showing the simplicity of being honest and fair. I have felt her knowledge and experience channelled to me throughout every moment of our discussions. The lessons I learnt from her go well beyond science to life.

I am grateful to Axel Eriksson, Adam Kristensson, and Erik Ahlberg at Lund University. I have learned a great deal during the three months I have been there. Axel, you are my example of how to stay curious and approach science with enthusiasm - an attitude I hope to maintain for a long time. Adam, your positivity is contagious, and I hope it endures for many years. In Erik, I see the meticulous eye that never overlooks the tiniest details.

Esu dėkinga visiems aplinkotyros skyriaus kolegoms už tai, kad buvo mano akademinės kelionės dalimi, o ypač Daliai Jasinevičienei, Linai Davulienei, Mehri Davtalab, Vadimui Dudoičiui ir Abdullah Khan. Esu dėkinga ilgametėms kabineto draugėms Audrei Kalinauskaitei ir Kamilei Kvedaravičienei, kurios man buvo ramybės ir išminties pavyzdys, o reikiant - gerų emocijų šaltinis. Dirbti komandoje kartu su jumis prie bendrų straipsnių – buvo tikras mokslinės kūrybos malonumas. Dėkoju Sonatai Pleskytei už palaikymą ir bendrystę doktorantūros kelionėje, suprastą ir atlieptą rūpestį smulkmenoms ir detalėms rašant disertaciją.

I wish to thank the Remote Sensing laboratory at the University of Warsaw: Lucja Janicka, Dominika Szczepanik, Afwan Hafiz, Maciej Karasewicz, Emeka A. Ugboma and Katarzyna Dyl. Thanks to your input, my time in Warsaw was both productive and genuinely enjoyable. For the FLEXPART results of the Vilnius-Warsaw study achieved during long evenings at the faculty, I thank F. Moritz Hey.

Thanks to John, Satabee, Céline, Lena, Silvia, and Ibrahim – my fellow PhDs at IKDC in Lund University. You made my lunch breaks, fikas and afterworks more enjoyable and showed how important and fun it is to have traditions at work.

Dėkoju Kristinai Plauškaitei-Šukienei ir Ievai Stirkei už pagalbą klaidžiojant doktorantūros prašymų ir dokumentų labirintuose.

Study No. 1 was based on results of the joint Lithuanian-Polish research project DAINA-2 grant "Importance of long range transport of BIOmass burning emissions to local Smog events in Urban Environments (BIOSURE)" supported by National Science Centre of Poland (Narodowe Centrum Nauki) (Grant no. 2020/38/L/ST10/00480) and the Research Council of Lithuania (Grant no. S-LL-21-7).

The FLEXPART model simulations for Study No. 2 were carried out within the project "Solutions for Sustainable Access to Atmospheric Research Facilities" (ATMO-ACCESS), supported by the EU Horizon 2020 Research and Innovation Programme (Grant Agreement no. 101008004).

The research was supported by the Research Council of Lithuania: funding for the research visit to the University of Warsaw (Poland) in 2026, support for participation in the European Aerosol Conference in Tampere (Finland) in 2024, and scholarships for academic achievements awarded in 2024 and 2025.

The Erasmus+ funding program of the European Commission supported my research visits at Lund University, Department of Design Sciences, in Sweden, in March – May 2023, and at the University of Warsaw, Faculty of Physics, in Poland, in April – June 2025.

Dėkoju Gabijai, Justinai, Kristijonui, Augustai, Augustei, Edvinui, Gretai, Gyčiui, Rūtai, Karolinai, Kamilei ir Vaivai, palaikiusiems mane ir stebėjusiems šią mano mokslinę kelionę. Buvote priežastimis džiaugtis laiku, kai atsigaudavau ir įsikvėpdavau.

Už meilę, kantrybę, mano dažnų darbo kelionių palaikymą ir gebėjimą visada matyti šviesą ateityje dėkoju Simui.

Galiausiai ir labiausiai ačiū mamai, tėčiui, Dominykai, Vytautui ir Danutei už besąlygišką palaikymą ir tikėjimą manimi labiau nei pati kartais tikėjau.

Vilniaus universiteto leidykla
Saulėtekio al. 9, III rūmai, LT-10222 Vilnius
El. p. info@leidykla.vu.lt, www.leidykla.vu.lt
bookshop.vu.lt, journals.vu.lt
Tiražas 30 egz.